

**PERFORMANCE OF A CIRCULAR CROSS-SECTION
MOORED FLOATING BREAKWATER**

by

WESLEY NEAL WHITESIDE

**B.Sc. in Mechanical Engineering
University of Alberta, 1992**

**A THESIS SUBMITTED IN PARTIAL FULFILLMENT OF
THE REQUIREMENTS FOR THE DEGREE OF
MASTER OF APPLIED SCIENCE**

in

**THE FACULTY OF GRADUATE STUDIES
DEPARTMENT OF CIVIL ENGINEERING**

**We accept this thesis as conforming
to the required standard**

THE UNIVERSITY OF BRITISH COLUMBIA

April, 1994

(c) Neal Whiteside, 1994

In presenting this thesis in partial fulfilment of the requirements for an advanced degree at the University of British Columbia, I agree that the Library shall make it freely available for reference and study. I further agree that permission for extensive copying of this thesis for scholarly purposes may be granted by the head of my department or by his or her representatives. It is understood that copying or publication of this thesis for financial gain shall not be allowed without my written permission.

(Signature)

Department of CIVIL ENGINEERING

The University of British Columbia
Vancouver, Canada

Date APRIL 28, 1994

TABLE OF CONTENTS

ABSTRACT	ii
LIST OF TABLES	vi
LIST OF FIGURES.....	vii
LIST OF SYMBOLS	x
ACKNOWLEDGEMENT	xii
CHAPTER 1: INTRODUCTION	1
1.1 Floating Breakwaters in Coastal Engineering.....	1
1.2 Floating Breakwater Designs in Use.....	2
1.3 Performance of Existing Floating Breakwaters	4
1.4 Motivation for Study	5
1.5 Organization of the Thesis	5
CHAPTER 2: SCOPE OF WORK.....	7
2.1 Attributes of Proposed Breakwater	8
2.2 Design Variables	9
2.3 Dimensional Analysis	11
CHAPTER 3: WAVE FLUME TESTING	15

3.1 Experimental Facilities and Measurement Equipment.....	15
3.2 Model Breakwater	16
3.3 Experimental Program and Procedures	17
CHAPTER 4: WAVE BASIN TESTING.....	19
4.1 Experimental Facilities and Measurement Equipment.....	19
4.2 Model Breakwater	20
4.3 Experimental Program and Procedures	21
CHAPTER 5: EXPERIMENTAL RESULTS.....	23
5.1 Breakwater System Characteristics	23
5.2 Breakwater Motions	27
5.2.1 Wave Flume Results and Observations.....	28
5.2.2 Wave Basin Observations	30
5.3 Wave Attenuation.....	30
5.4 Mooring Line Forces	32
5.5 Breakwater Internal Stresses	33
5.6 Comparison to Rectangular Caisson Results	33
CHAPTER 6: NUMERICAL MODEL.....	35
6.1 Hydrodynamic Analysis.....	35

6.1.1 Incident Potential.....	38
6.1.2 Scattered Potential.....	38
6.1.3 Forced Potentials and Body Motions	38
6.2 Mooring Analysis.....	39
6.3 Numerical Results	40
6.4 Comparison of Numerical and Experimental Results	43
CHAPTER 7: EVALUATION OF PERFORMANCE.....	45
7.1 General Conclusions	45
7.2 Performance of Numerical Model.....	46
7.3 Potential for Improvement and Further Study.....	47
BIBLIOGRAPHY	49

LIST OF TABLES

- 2.1 Comparison of Reynolds numbers between prototype and model states
- 3.1 Experimental program for wave flume tests
- 4.1 Experimental program and results for wave basin tests
- 5.1 Summary of experimental results from wave flume tests
- 5.2 Estimation of the natural frequencies in heave

LIST OF FIGURES

- 1.1 Cross-sections of typical bottom founded breakwaters, [25].
- 1.2 Floating tire breakwater, [7].
- 1.3 Equiport breakwater, [27].
- 1.4 Tethered float breakwaters, [14].
- 1.5 Log bundle floating breakwater, [4].
- 1.6 Various reflective floating breakwater cross-sectional geometries.
- 1.7 Comparison of transmissibility of rectangular caisson and tire breakwaters, [15].
- 1.8 Comparison of transmissibility of various caisson breakwater types, [3].
- 2.1 Definition of design parameters for proposed breakwater system.
- 2.2 Mooring line attachment point arrangements.
- 2.3 Importance of inertial and viscous effects, [24].
- 3.1 Experimental set-up used in wave flume tests.
- 3.2 Schematic layout of wave generation and data collection hardware.
- 3.3 Photograph of wave probes.
- 3.4 Photograph of a load cell.
- 3.5 Photograph of model breakwater used in wave flume tests.
- 4.1 Photograph of wave basin.
- 4.2 Experimental set-up used in wave basin tests.
- 4.3 Arrangement of strain gages.

- 4.4 Photograph of model breakwater used in wave basin tests.
- 5.1 Definition sketch for six degrees of freedom.
- 5.2 Response of a SDOF system to periodic forcing, [23].
- 5.3 Wave flume test results for base case with chain. (a) transmission coefficient, (b) motion amplitudes.
- 5.4 Wave flume test results for base case with nylon. (a) transmission coefficient, (b) motion amplitudes, (c) mooring line forces.
- 5.5 Wave flume test results showing the influence of wave steepness H/L for the case of nylon mooring lines. (a) transmission coefficient for $D/L = 0.116$ and 0.173 , (b) motion amplitudes for $D/L = 0.116$, (c) motion amplitudes for $D/L = 0.173$, (d) mooring line forces for $D/L = 0.116$ and 0.173 .
- 5.6 Wave flume test results showing the influence of relative draft h/D for the case of nylon mooring lines. (a) transmission coefficient, (b) surge RAO, (c) heave RAO, (d) roll RAO.
- 5.7 Wave flume test results showing the influence of line slackness s/s_0 for the case of chain mooring lines. (a) transmission coefficient, (b) surge RAO, (c) heave RAO, (d) roll RAO.
- 5.8 Wave flume test results showing the influence of mooring line attachment points on transmission coefficient. (a) chain mooring lines, (b) nylon mooring lines.
- 5.9 Wave basin test results showing the influence of the angle of wave incidence. (a) transmission coefficient, (b) mooring line forces, (c) horizontal bending moments, (d) vertical bending moments, (e) torsion.
- 5.10 Record of mooring line forces for wave flume test 2.5.
- 5.11 Comparison of transmission coefficients between rectangular and circular caisson breakwaters.
- 5.12 Comparison of observed breakwater motions; (a) surge, (b) heave, and (c) roll.

- 6.1 Numerical results for base case with chain mooring lines. (a) transmission coefficient, (b) motion amplitudes, (c) mooring line forces.
- 6.2 Numerical results for base case with nylon mooring lines. (a) transmission coefficient, (b) motion amplitudes, (c) mooring line forces.
- 6.3 Numerical results showing the influence of relative draft h/D for the case of chain mooring lines. (a) transmission coefficient, (b) surge RAO, (c) heave RAO, (d) roll RAO, (e) upwave mooring line force, (f) downwave mooring line force.
- 6.4 Numerical results showing the influence of wave steepness H/L for the case of chain mooring lines. (a) upwave mooring line force, (b) downwave mooring line force.
- 6.5 Numerical results showing the influence of line slackness s/s_0 for the case of chain mooring lines. (a) upwave mooring line force, (b) downwave mooring line force.
- 6.6 Numerical results showing the influence of mooring line attachment points for the case of chain mooring lines. (a) upwave mooring line force, (b) downwave mooring line force.
- 6.7 Wave flume test results compared with numerical results for base case with chain. (a) transmission coefficient, (b) surge RAO, (c) heave RAO, (d) roll RAO.
- 6.8 Wave flume test results compared with numerical results for base case with nylon. (a) transmission coefficient, (b) surge RAO, (c) heave RAO, (d) roll RAO.

LIST OF SYMBOLS

A	Cross-sectional area of mooring line
b	Horizontal spacing between adjacent mooring line attachment points
D	Breakwater diameter
d	Water depth
E'	Mooring line elasticity per unit length of breakwater (EA/b)
E	Young's modulus of mooring line
F	Mooring line pretension (at breakwater attachment point)
F'	Mooring line pretension per unit length of breakwater (F/b)
g	gravitational constant (9.81 m/s ²)
H	Wave height
H _i	Incident wave height
H _r	Reflected wave height
H _t	Transmitted wave height
h	Breakwater draft
I	Moment of inertia of breakwater
L	Wavelength
L _o	Deep water wavelength
M	Mass of breakwater
M _h	Horizontal bending moment induced in breakwater
M _t	Torsion induced in breakwater
M _v	Vertical bending moment induced in breakwater
m'	Mass of mooring line per unit length
m''	Mass of mooring line per unit length and per unit length of breakwater (m'/b)
\vec{n}	Normal vector to the body surface
S	Surface of the body
s	Unstretched length of mooring line
s _o	Distance between anchor point and attachment point on breakwater
T	Wave period
w'	Mooring line submerged weight per unit length of line
w''	Mooring line submerged weight per unit length of line and per unit length of breakwater (w'/b)
λ	horizontal span of mooring line

ν	kinematic viscosity of water
θ	incident wave direction
ρ	density of water
φ	partial potential (complex function of space only)
ϕ	total potential (function of space and time)
$\hat{\sigma}_j$	maximum mooring line tensions: $j = 1$, upwave line; $j = 2$, downwave line
$\bar{\xi}_1$	horizontal static offset of breakwater
$\hat{\xi}_i$	breakwater motion amplitudes: $i = 1$, sway; $i = 2$, heave; $i = 3$, roll

ACKNOWLEDGEMENT

The author would like to acknowledge and thank several individuals and institutions which were integral to the completion of this research. First, the guidance of his advisor, Dr. Michael Isaacson, has been critical to the progress of the research throughout and is deeply appreciated. As well, the financial and technical support from Hay & Co. Consultants Inc., in particular Mr. Bob Gardiner, who provided the original motivation for the research is gratefully acknowledged. The author would also like to thank several individuals within the Civil Engineering Department for help in completing the numerical and physical testing; Mr. Kurt Nielson for assisting with the assembly of physical models, Mr. Ron Dolling for assistance in providing instrumentation, Mr. Sundar Prasad for help in setting up data acquisition for the experiments, and Mr. John Baldwin for providing numerical results. The author would also like to thank his peers in the hydrotechnical engineering group for help during physical testing, in particular Mr. S.S. Bhat, Mr. A. Kennedy, and Mr. A. Phadke. Funding from the Natural Sciences and Engineering Research Council in the form of a scholarship is gratefully acknowledged.

CHAPTER 1 : INTRODUCTION

1.1 Floating Breakwaters in Coastal Engineering

Many marinas, fishing harbours, and aquaculture operations are partially protected from wave action by natural topographic features such as islands, shoals, and spits. Due to the minimal fetch and wind speeds required to generate water waves of a magnitude large enough to limit such operations, most such sites require additional protection. Therefore, the natural wave protection found at a site is often augmented by the construction of a breakwater. The term breakwater refers to a class of structures whose main function is attenuating wind or ship generated water waves.

The oldest and most common breakwaters are bottom-founded structures. Breakwaters such as the rubble-mound or caisson types (see Fig. 1.1) provide excellent harbour protection as transmission of waves occurs only by diffraction around the ends of the breakwater. However, as water depth increases the cost of a bottom-founded system can become prohibitive. Bottom-founded breakwaters also reduce water circulation in the protected area, possibly creating a sedimentation problem where dredging may be required to maintain navigable channels. Also, reduced flushing may lead to increased concentrations of pollutants within the protected area.

In some locations floating breakwaters have been used with good success in preference to traditional bottom-founded breakwaters, avoiding many of the problems outlined above. Sites where floating breakwaters may be preferable to traditional structures are characterized by a moderate wave climate sheltered from long period waves by surrounding land masses, and large tidal fluctuations and/or a steeply sloping seabed which would make a bottom founded structure very expensive. Floating breakwaters allow water circulation under the

structure reducing the siltation and pollution problems alluded to earlier. Floating breakwaters are also somewhat portable. This can be a tremendous advantage in situations where only temporary or seasonal protection is desired.

Due to the very nature of floating breakwaters, they become unfeasible as design wave periods increase beyond 5-6 seconds. For longer period and hence longer wavelength waves a floating breakwater will respond much like a ball in the ocean moving up and down in phase with the incoming waves. To be effective the breadth and/or depth of the breakwater must be of the same order of magnitude as the wavelengths of the incoming waves.

1.2 Floating Breakwater Designs in Use

A diverse variety of floating breakwaters have been developed and used, ranging from very simple schemes to complex and expensive designs. A report produced by the U.S. Navy [12] lists 52 different floating breakwater concepts for which either numerical or physical studies have been carried out. All of these structures use one or a combination of the following three basic mechanisms to reduce wave heights within the protected area:

- (i) wave reflection, a portion of the incident wave energy is reflected from the face of the breakwater as if it were a fixed obstacle;
- (ii) energy transformation, where incident wave energy excites breakwater motions forcing radiated waves which are out-of-phase with the incident wave forcing because of the response characteristics of the system;
- (iii) energy dissipation, where turbulence induced by either wave breaking or wave-structure interaction effects causes dissipation of incident wave energy.

The first two mechanisms can be modelled by ideal fluid theory and approximated by linear potential theory. The third mechanism is a result of viscous dissipation and nonlinear wave

breaking mechanisms, and as such can not be readily dealt with using ideal fluid theory. The diverse variety of breakwater types can be classified into two broad categories, pontoon breakwaters (which rely primarily on the first two mechanisms), and dissipative breakwaters.

Dissipative breakwaters rely primarily on wave-induced turbulence in order to dissipate wave energy and typically consist of flexible interconnected units. The most common breakwater of this type is a floating tire breakwater (Fig. 1.2). Other promising designs include equiport breakwaters (Fig. 1.3), tethered float breakwaters (Fig. 1.4), and flexible log rafts [12]. A dissipative floating breakwater has the advantage of not significantly increasing wave heights on the upwave side of the structure. This feature is advantageous for navigation in and out of marinas for instance. However in reviewing the literature, few systems of this type have been implemented compared to reflective breakwaters. This can be attributed to several disadvantages of dissipative breakwaters:

- (i) they require a large amount of material and space to be effective,
- (ii) high maintenance costs and/or a short service life,
- (iii) they may be aesthetically unappealing.

All that is required of a reflective floating system is sufficient size and inertia to reflect a significant portion of the incoming wave energy. Generally breakwaters of this type are rigid, wall-sided structures. Makeshift breakwaters of this type have been constructed from such diverse material as log bundles (see Fig. 1.5), partially submerged scrapped barges and rail cars, and even out-of-service floating bridges. These designs were economically feasible and hence successful due to the relatively low cost of the raw materials. However, as well as being perhaps aesthetically unappealing, it is not always possible to find such suitable inexpensive structures.

Many specially manufactured reflective floating breakwaters with different cross-sectional geometries and/or mooring arrangements have been put to use in harbours. Even more

designs have been either numerically or laboratory tested. Some of the common cross-sectional geometries found in the literature are shown in Fig. 1.6. The most common and simplest of these is the rectangular pontoon breakwater.

Two main types of restraint have been used; either mooring lines or piles. Piles have the advantage that they restrict surge and roll motions almost completely which should result in lower transmission coefficients. However, breakwaters with pile restraints have suffered from wear problems at the point of contact between the piles and the breakwater. This problem has resulted in higher initial design and manufacture costs and reduced service life and/or increased maintenance costs. As well, the design and installation of pile restraints can be complicated by poor soil conditions and/or the depth of the water at the site. For the foregoing reasons, mooring lines are the most common constraint used with floating breakwaters. The two most popular mooring line materials are steel chain and nylon cable. Chain mooring lines are usually slack to allow for tide fluctuations. Occasionally suspended weights are used somewhere along the length of the mooring line to increase the stiffness of the mooring system. Nylon cables have been installed pretensioned to ensure that the cable is in tension at all tide levels. This has been possible due to the relatively large elastic elongation these cables can withstand before failure.

1.3 Performance of Existing Floating Breakwaters

Figure 1.7 is reproduced from [12] and shows the transmission coefficients measured for various rectangular caissons breakwaters and floating tire breakwaters (here B is the breakwater width and L is the wavelength of incident waves). Clearly, the caisson breakwater types have better transmission characteristics.

Figure 1.8 shows the transmission characteristics measured for a variety of caisson breakwater types. The catamaran configuration performed best for these tests. These results

also examine the effectiveness of an intermediate skirt in reducing wave transmission. The results show that a substantial skirt (such as configuration no. 6) reduce wave transmission. However, the advantage of a skirt may be nullified by higher construction and maintenance costs due to more complex construction and larger internal stresses.

1.4 Motivation for Study

Although considerable expertise has been acquired with regard to their efficiency, construction, and maintenance, a truly satisfactory floating breakwater system has yet to be developed. It is hoped that the proposed circular-section breakwater may be an affordable alternative to existing floating breakwaters without some of the problems of existing designs.

Local concrete manufacturers presently have the capability of producing circular concrete pipe with cross sectional areas comparable to existing rectangular caisson type breakwaters. It is believed there is a potential for considerable cost savings by using circular concrete pipe in preference to rectangular cross sections because it has a simpler manufacturing procedure. As well, the nature of circular sections should preclude the development of significant torsion and corner stress concentrations that are induced by wave action on rectangular sections. As well, it may be possible to construct a long flexible breakwater by post-tensioning sections of the concrete pipe together.

1.5 Organization of the Thesis

The preceding sections described various types of breakwaters and introduced the circular cross-section floating breakwater concept. Chapter 2 defines the scope of work which the research encompasses and the goals of the research. As well, the design variables are defined. Chapters 3 and 4 describe the two and three dimensional physical testing respectively, including details concerning the facilities, measurement equipment, data

acquisition, the model breakwaters, and the testing programs. Chapter 5 gives the results of both the 2-D and 3-D physical modelling and the meaning of the results is discussed. Also in Chapter 5, a comparison is made between experimental results from this study and studies done with a rectangular caisson breakwater. Chapter 6 includes a description of the numerical model used in the research and a overview of the numerical results obtained. Chapter 7 summarizes some important conclusions about the breakwater system proposed and the performance of the numerical model. As well, improvements to the design are suggested and variables not examined are noted. Tables and figures follow the main text of the thesis.

CHAPTER 2: SCOPE OF WORK

A new floating breakwater concept based on a circular cross-section with a draft determined by the weight of fluid contained within the section has been proposed. Two and three dimensional laboratory model tests were completed in order to provide generic performance characteristics which could subsequently be applied to specific design situations. A numerical analysis of the breakwater based on linear potential theory was also used to obtain similar results. This allowed a comparison between results from numerical and physical modeling and an assessment of the accuracy of the numerical model.

Specific goals of the analytical and physical model studies of the circular cross-section floating breakwater were to:

- (i) evaluate the efficiency and practicality of the circular cross-section floating breakwater proposed compared to existing breakwaters;
- (ii) establish criteria with regards to mooring line forces and wall stresses to aid in the design of a floating breakwater of the type studied;
- (iii) better understand the role of design parameters in effecting the performance of floating breakwaters;
- (iv) identify potential improvements to the proposed breakwater;
- (v) evaluate the suitability of applying a linear potential theory model for the design of a floating breakwater.

2.1 Attributes of Proposed Breakwater

The proposed breakwater design consists of a large diameter concrete pipe ($D > 2\text{m}$) moored with either nylon cable or steel chain. A cross-sectional view of the proposed breakwater system defining the design parameters is shown in Fig. 2.1. The necessary buoyancy would be provided by a low density material such as extruded polystyrene sheet attached to the inside of the breakwater. The remainder of the volume inside the breakwater would be filled with water to add inertia to the system. The use of a low density material has two key advantages over using entrapped air for buoyancy: a secondary compartment which encloses the entrapped air does not have to be fabricated, and the breakwater does not have to be sealed to prevent sinking.

When designing the breakwater for a particular location, a suitable draft must be selected which is a compromise between excessive overtopping caused by too deep of a draft and the advantages of the added inertia at deeper drafts. One of the goals of this study is to provide data to aid the engineer in this design decision. The mooring lines chosen and their proposed configuration are similar to the mooring systems used for existing rectangular caisson breakwaters.

The prototype proposed breakwater consists of several sections of concrete pipe post-tensioned together at the installation site forming a long flexible breakwater. This feature allows the breakwater sections to be easily transported and also gives the design an advantage over present configurations which have gaps between breakwater sections. However, the present work concentrates on the performance of a single section of breakwater and does not address the design of connections between breakwater sections.

2.2 Design Variables

A complete listing of all the parameters considered when modelling the proposed breakwater is given in the list of symbols on pp. ix-x. To better understand the role of all of the relevant parameters and variables, it is useful to group the factors into the following categories:

- (i) independent wave parameters:
 - ρ , water density;
 - ν , dynamic viscosity;
 - g , gravitational acceleration;
 - H_i , incident wave height;
 - T , wave period;
 - d , water depth;
 - θ , incident wave angle.

- (ii) independent breakwater geometry parameters:
 - h , breakwater draft;
 - D , breakwater diameter.

- (iii) independent mooring line parameters:
 - w' , mooring line submerged weight per unit length of line;
 - s , unstretched length of mooring line;
 - s_0 , distance between anchor point and attachment point;
 - EA , mooring line elasticity;
 - b , mooring line spacing.

- (iv) dependent variables known by definition from above three categories:
- E' , mooring line elasticity per unit length (EA/b);
 - I , breakwater moment of inertia;
 - L , wavelength;
 - M , mass of breakwater.
- (v) dependent variables whose relationship to the independent variables is required:
- H_t , transmitted wave height;
 - M_h , horizontal bending moment induced in breakwater;
 - M_t , torsion induced in breakwater;
 - M_v , vertical bending moment induced in breakwater;
 - σ_j , mooring line forces: $j = 1$, upwave line; $j = 2$, downwave line;
 - ξ_i , breakwater motions: $i = 1$, sway; $i = 2$, heave; $i = 3$, roll.

The mooring line pretension, F , should be used as an alternate independent variable instead of the unstretched cable length, s , when a pretension is present in the mooring lines. However, pretensioning of the mooring lines is only seen as a possibility for nylon mooring lines since chain does not have enough elasticity to accommodate changes in the still water level due to tidal fluctuations. In fact, during model testing any initial pretension placed in the nylon lines disappeared after the breakwater was exposed to waves due to plastic elongation of the nylon cables and hence no testing was done with mooring lines in pretension. The ability of prototype-scale nylon lines to maintain pretension in field situations was not investigated in any of the literature reviewed.

In addition to the parameters considered above, the location of the mooring attachment points to the breakwater may also have an influence on the breakwater's response. In the present study, three arrangements (shown in Fig. 2.2) have been examined. These correspond to an

attachment point at the bottom of the breakwater, and a pair of attachment points subtending a 60° angle at the centre of the breakwater, with the mooring lines either uncrossed or crossed.

When considering three-dimensional conditions, two additional independent parameters become relevant, the overall breakwater length and the specific mooring line arrangement. Only one breakwater length and mooring line arrangement were considered in testing. The experimental setup for these parameters was similar to that of existing rectangular caisson breakwater installations. It is hoped therefore that actual field designs will not be sufficiently different in these two respects so as to significantly affect their performance.

2.3 Dimensional Analysis

As a preliminary to carrying out the laboratory tests and applying the numerical model, it is useful to carry out a dimensional analysis of the wave-breakwater interaction in order to:

- (i) identify the governing dimensionless groupings influencing the breakwater effectiveness and response;
- (ii) provide a basis for model scale selection;
- (iii) plan for the selection of the experimental test program.

There are a total of 14 independent variables, and on the basis of a 3 unit system (mass, length, and time), there should be 11 dimensionless groups influencing each dependent variable. For example, a dimensional analysis for the transmission coefficient, K_t , provides the following relationship:

$$(2.1) \quad K_t = \frac{H_t}{H_i} = f\left(\frac{D}{L}, \frac{h}{D}, \frac{d}{D}, \frac{H_i}{L}, \text{Re}, \frac{w''}{\rho g D}, \frac{E'}{\rho g D^2}, \frac{b}{D}, \frac{s_o}{d}, \frac{s}{s_o}, \theta\right)$$

where Re , the Reynolds number, is based on the maximum horizontal velocity of the water particles at the still water level as given by linear potential theory:

$$(2.2) \quad Re = U_{\max} \frac{D}{\nu} = \left(\frac{\pi H}{T} \cdot \frac{1}{\tanh kd} \right) \frac{D}{\nu}$$

Different functions with the same form as Eqn. 2.1 apply to the other dependent variables expressed in their non-dimensionalized forms. The non-dimensional groupings used for each of the remaining dependent variables are as follows:

$$(2.3) \quad K_r = \frac{H_r}{H_i}$$

$$(2.4) \quad RAO_i = \frac{\hat{\xi}_i}{H/2} \quad \text{for } i = 1 \text{ (surge), } i = 2 \text{ (heave)}$$

$$(2.5) \quad RAO_i = \frac{\hat{\xi}_i D}{H/2} \quad \text{for } i = 3 \text{ (roll)}$$

$$(2.6) \quad C_{Fj} = \frac{\hat{\sigma}_j}{\rho g H D b} \quad \text{for } j = 1 \text{ (upwave), } j = 2 \text{ (downwave)}$$

$$(2.7) \quad C_{Mh} = \frac{M_h}{\rho g H D b^2}, \quad C_{Mv} = \frac{M_v}{\rho g H D b^2}, \quad C_{Mt} = \frac{M_t}{\rho g H D b^2}$$

The significance of the dimensionless parameters in Eqn. 2.1 is as follows. D/L represents the breakwater size to wave length ratio and accounts for the influence of wave length or wave period on the breakwater response. h/D represents the relative draft of the breakwater, and is an indirect indication of the inertia of the breakwater. d/D represents the influence of water depth and is expected to be significant only for shallower water as d/D becomes smaller. H_i/L is the wave steepness, which should not significantly influence those parameters which vary linearly with wave height. As H_i/L and h/D increase and/or D/L decreases the propensity of the breakwater to overtopping increases. The remaining parameters, except for the Reynold's number, represent a characterization of the mooring line properties and configuration: b/D is the mooring line spacing ratio, $w''/\rho g D$ represents

the relative submerged weight of the mooring lines; $E'/\rho gD^2$ represents the relative elasticity of the mooring lines; and s_0/d and s/s_0 are dimensionless parameters describing the mooring line slope and slackness.

The Reynolds number which is an indication of viscous effects is not expected to influence the breakwater response strongly. In modeling the breakwater in physical tests it was not possible to match the Reynolds number and the other parameters concurrently. Hence, wave flume, wave basin, and prototype states do not have matching Re. The Reynolds number for several prototype scenarios and their corresponding model states are presented in Table 2.1. The Keulegan-Carpenter number, K, is an indicator of the importance of inertial and viscous effects and is defined as:

$$(2.8) \quad K = U_{\max} T / D$$

Figure 2.3 shows the relative importance of inertial (diffraction) and viscous (flow separation) effects as K and D/L vary. By comparing this figure with values of K and D/L from Table 2.1, it is concluded that inertial effects will be the dominant factor in determining the breakwaters response. This serves as a justification for the use of the potential theory model described in Chapter 6. For long period waves, D/L decreases and hence the importance of diffraction decreases.

Typical values of the dimensionless parameters may be estimated on the basis of prototype conditions corresponding to $D = 3.21$ m, $T = 2.0 - 6.0$ sec, and mooring lines made of 1 inch stud link anchor chain ($w' \approx 140$ N/m, $EA \approx 2 \times 10^8$ N) and 2 inch double-braided nylon rope ($w' \approx 2$ N/m, $EA \approx 2 \times 10^6$ N), and spaced 5 m apart. On this basis, typical values of the dimensionless parameters are as follows:

$$D/L \approx 0.1 - 0.5,$$

$$h/D \approx 0.6 - 1.0,$$

$$d/D \approx 2 - 20,$$

$$H/L \approx 0.01 - 0.1,$$

$$\lambda/d \approx 4,$$

$$s/s_0 \approx 1.00 - 1.06,$$

$$w''/\rho g D \approx 900 \times 10^{-6} \text{ for chain,}$$

$$E'/\rho g D^2 \approx 4000 \text{ for chain,}$$

$$w''/\rho g D \approx 130 \times 10^{-6} \text{ for nylon,}$$

$$E'/\rho g D^2 \approx 40 \text{ for nylon.}$$

On the basis of Eqn. 2.1, which corresponds to Froude scaling, the scale factors of the variables can be expressed in terms of the length scale factor, K_l , as follows. Note that the subscripts m and p denote variables corresponding to the model and prototype respectively.

$$(2.9) \quad \frac{D_m}{D_p} = \frac{H_m}{H_p} = \frac{d_m}{d_p} = \frac{h_m}{h_p} = \frac{\lambda_m}{\lambda_p} = \frac{s_m}{s_p} = K_l$$

$$(2.10) \quad \frac{T_m}{T_p} = \sqrt{K_l}$$

$$(2.11) \quad \frac{w'_m}{w'_p} = \frac{E'_m}{E'_p} = K_l^2$$

$$(2.12) \quad \frac{(EA)_m}{(EA)_p} = K_l^3$$

In a presentation of numerical results, it is convenient to present the results in the form of curves of transmission coefficient, response amplitude operators, and mooring line force coefficients as functions of D/L for given values of the other parameters (h/D , H/L , s/s_0 , and so on); and to examine the influence of each of these other parameters in turn on such curves.

In planning the physical and numerical experiments, it is not feasible to consider all ranges of each variable. Instead, one or more base cases were considered, and the influence of each variable was considered in turn.

CHAPTER 3: WAVE FLUME TESTING

3.1 Experimental Facilities and Measurement Equipment

The two-dimensional laboratory tests were carried out in the wave flume of the Hydraulics Laboratory in the Department of Civil Engineering at the University of British Columbia. The flume is 0.62 m wide and 20 m long from the wave paddle to the holding tank at the far end. The flume was operated with a water depth of 0.6 m. A 7 m long artificial beach consisting of plywood set at a 1:15 slope covered with artificial hair matting extends from the end of the tank. The beach combined with the holding tank at the end of the flume effectively absorb and dissipate wave energy preventing significant wave reflection. The flume is equipped with a computer controlled wave generator capable of producing regular and random waves. A one-tenth scale model of the proposed breakwater was centered 10.8 m down from the wave paddle. Figure 3.1 shows a sketch of the experimental set-up.

Figure 3.2 shows a schematic layout of the apparatus used for acquiring water surface elevation, force and motion records during the experiments. The main components are the video camera and recorder, wave probes, load cells, amplifiers, signal cables, analog-to-digital (A/D) converter, and computer. The latter is a Digital Equipment Corporation (DEC) VAXstation 3200 computer and was used to control the experiment. The GEDAP (Generalized Experiment control, Data acquisition and Analysis Package) library of software and associated RTC (Real Time Control) programs developed at the Hydraulics Laboratory of the National Research Council of Canada were used to control the wave generation and data acquisition processes. This system allowed simultaneous sampling of the wave probe and load cell signals. Data was recorded at a sampling frequency of 100 Hz so that spikes in the load cell records would not be lost.

Capacitance-type wave probes (see Fig. 3.3) were used for measurements of the water surface elevation. The wave probes exhibited a linearity better than 98.5% and a resolution better than 1 mm. Two sealed shear beam load cells (see Fig. 3.4) were placed in series with the mooring lines near the connection points with the breakwater in order to measure tensions in the upwave and downwave mooring lines. The load cells have a 50 lb (222 N) capacity with 99.5% linearity through their working range.

A Super VHS camera and recorder was used to record the motions of the breakwater in roll, surge and heave with respect to a grid placed on the side of the flume.

3.2 Model Breakwater

The prototype breakwater being proposed would be constructed of concrete pipe. Presently pipe diameters up to 3.5 m can be produced by local concrete manufacturers using existing equipment. Assuming a prototype diameter of 3.21 m, a 1:10 scale model was constructed for the two dimensional (2-D) tests. The scale chosen allowed for model tests at UBC's wave flume over the anticipated range of full scale wave periods and heights.

Figure 3.5 is a photograph of the model used. The model consists of a 321 mm diameter circular PVC cylinder of a width slightly narrower than that of the flume. The draft of the breakwater was altered by the addition of lead bars fixed inside the cylinder. Three ball bearings were connected to each end of the breakwater so the model could move freely along the sides of the flume. The bearings served the additional purpose of limiting undesirable pitch, yaw, and sway motions and reducing the necessary clearance between the breakwater and the sides of the flume thereby limiting the amount of wave energy diffracted.

The model breakwater was restrained by four mooring lines (two upwave and two downwave). The mooring line spacing of 0.3 m corresponds to a 1:16.7 scale ratio based on a typical prototype spacing of 5 m between adjacent mooring lines. Two different sets of

mooring lines were used during the tests, one modeling 1” (25 mm) stud link anchor chain, and the other modeling 2” (51 mm) double-braided nylon cable. Several connection points on the breakwater enabled tests to be carried out with the mooring lines connected at the bottom of the breakwater; and at the sides of the breakwater as shown in Fig. 2.2. All tests were conducted with a water depth of 0.6 m.

3.3 Experimental Program and Procedures

All wave flume tests were performed with monochromatic regular wave conditions. A total of 70 tests were performed with varying wave conditions and breakwater characteristics. A summary of the experimental program devised for the wave flume tests is shown in Table 3.1. The parameters varied in the experimental program included wave period, wave height, breakwater draft, and mooring line type, slackness, and connection points. Parameters held constant were water depth and breakwater diameter. The testing program was divided into sets of trials which focus on the effects of the variation of one of the design variables. For example, tests 4.1 to 4.16 focus on the effect of breakwater draft on breakwater efficiency and motions. The experimental program was organized to achieve two purposes; (i) to gain a better physical understanding of the effect of each parameter on the breakwater’s performance, and (ii) to enable the evaluation and calibration of the numerical model.

Originally the following parameters were to be measured in each test:

H_i	incident wave height
H_r	reflected wave height
H_t	transmitted wave height,
$\bar{\xi}_1$	horizontal static offset of breakwater,
$\hat{\xi}_i$	breakwater motion amplitudes (surge, heave, and roll),
$\hat{\sigma}_j$	maximum mooring line tensions (upwave and downwave).

The incident and reflected wave height were to be interpolated from three wave elevation records taken from wave probes placed upstream of the breakwater. The analysis was to be carried out using the GEDAP analysis program REFLM. After the first set of tests it was apparent that REFLM would not give reliable results given the short duration of the tests. Hence the reflected wave height was not measured for the remainder of the tests. Wave heights were obtained from water elevation records using the GEDAP program ZCA (Zero Crossing Analysis). The incident wave height was measured in calibration tests with the model removed from the water. An average transmitted wave height was calculated from three wave elevation records obtained by wave probes downwave of the breakwater.

Due to the limited length of the flume, after a time a partial standing wave would set-up between the wave paddle and the breakwater. This condition was especially pronounced in trials with short period waves where significant wave reflections from the breakwater were present. To avoid contaminating the results, the duration analyzed for each test was limited accordingly.

As described earlier, the breakwater motions were measured from VCR records of the tests, with a grid placed in the field of view. The accuracy of the video record in assessing breakwater motions is estimated to be ± 0.5 cm, allowing for constraints of resolution, frame speed, and undesirable pitch, yaw, and sway motions. The load cells used to measure mooring line tension were calibrated by hanging weights from the load cells. The calibration curves were very linear and consistent indicating good accuracy. Using 10 volts DC excitation and amplifying the signal 1000x, it was possible to obtain a signal resolution of better than 0.5 N.

To determine the natural periods of the wave flume model, the breakwater model was given initial displacements in the surge, heave, and roll directions in turn and the resulting oscillations were recorded with an accelerometer fixed to the breakwater.

CHAPTER 4: WAVE BASIN TESTING

4.1 Experimental Facilities and Measurement Equipment

The wave basin used for the testing shown in Fig. 4.1 has dimensions 13.7 m long by 4.5 m wide and 0.55 m deep. A variable speed, electrically driven flap-type wave generator at one end of the basin is capable of producing uniform long-crested waves with periods ranging from 0.4 to 2.0 s. The wave period and height have to be set manually by setting the speed control and altering the stroke of the wave paddle, respectively. A 1:3.5 slope, permeable beach consisting of a timber frame covered with 1" artificial hair matting was constructed at the opposite end of the wave basin to reduce wave reflection. Two movable dividing walls were constructed to isolate the breakwater so accurate readings of the transmitted and incident wave heights could be obtained. The dividing walls were also covered with artificial hair matting.

Figure 4.2 shows a sketch of the experimental set-up. The same capacitance-type wave probes and load cells described in Chapter 3 were used again for measurements of water surface elevation and mooring line tension, respectively. Two wave probes were used to measure the incident wave height and one to measure transmitted wave height.

In addition, the model breakwater was machined and instrumented with three strain gage bridges to measure vertical bending moment, horizontal bending moment, and torsion in the walls of the breakwater. Each of the three bridges was designed so it would only sense moments in the desired direction (either horizontal bending, vertical bending, or torsion) and ignore moments in other directions and any axial tension or compression. The strain gage bridges were installed at the midpoint between two mooring lines to capture the maximum moments. The arrangement of the strain gage bridges is shown in Fig. 4.3.

A Super VHS camera was used to record breakwater motions for all tests. Unlike the wave flume testing, the video record was only used to gain a qualitative understanding of the breakwater motions.

4.2 Model Breakwater

A 15.1 cm diameter aluminum tube 1.98 m long was used as a model breakwater (see Fig. 4.4) corresponding to a 1:21.3 scale based on a prototype diameter of 3.21 m. Aluminum was chosen as a material on which to mount the strain gages because of its uniform properties, machinability, and relatively low modulus of elasticity. The tubing had a nominal wall thickness of 1/8" (3.2 mm). The tube was machined down to 1/32" (0.8 mm) wall thickness where the strain gages were mounted to increase the output from the gages.

The model breakwater was ballasted with water and a made-to-fit insert made of styrofoam sheet was used for positive buoyancy. The ends of the breakwater were sealed, thereby eliminating any flow of air or water into the breakwater. This arrangement is a much better representation of the envisioned prototype ballasting than the 2-D model and hence should better represent the performance of the prototype breakwater. The relative draft of the breakwater, h/D , was not altered during the testing and was measured to be 0.735.

Six upwave mooring lines and six downwave mooring lines were used to restrain the breakwater. This corresponds to a 7.1 m/line prototype spacing. The six mooring lines on each side were connected uncrossed to three connection points on each side of the breakwater located 30° from the bottom. Mooring lines of light steel chain of the correct weight to imitate 1" (25 mm) stud link anchor chain were used. The mooring line slackness, s/s_0 , was 1.02 for all the wave basin tests.

4.3 Experimental Program and Procedures

The angle of incidence is defined as the angle between the breakwater axis and the incident wave crests. The angle of incidence was varied from 0° to 45° in the wave basin tests. Table 4.1 shows the testing program devised for three dimensional (3-D) testing. A total of 24 tests comprised of 4 sets of tests at different angles of incidence were performed. The six wave conditions tested in each set and the breakwater parameters other than angle of incidence were not varied from set to set, as far as possible.

Figure 4.5 is a photograph of the testing apparatus and breakwater model setup with an angle of incidence of 45° . The load cells and the strain gage bridges were given 10 volt excitation and their corresponding signals were boosted by a factor of 1000 with amplifiers.

Essentially the same data acquisition system as described in Sec. 3.1 was used for the wave basin tests as well, with the exception that the wave generator had to be activated and controlled manually as mentioned earlier. Eight channels of data were recorded by the data acquisition system at a sampling rate of 100 Hz. The data records tabulated for each test were:

$\eta_i(t)$	incident wave elevations (2 channels),
$\eta_t(t)$	transmitted wave elevation (1 channel),
$\sigma(t)$	mooring line tensions (2 channels),
$M_h(t), M_v(t), M_t(t)$	horizontal and vertical bending moments, and torsion induced in the breakwater (3 channels).

As in the wave flume testing, data was only analyzed over a limited duration to prevent the effects of wave reflection from affecting test results. As well any high frequency noise (greater than 10 Hz) was filtered out using the GEDAP program FILTA. A measure of the incident and transmitted wave energy for each test was calculated using two methods; zero-crossing analysis and spectral analysis. For the zero-crossing analysis, the average wave

height and period for a record were determined using the program ZCA. For the spectral analysis, the GEDAP program VSD was used with a filter bandwidth of 0.05 Hz and a cut-off frequency of 5 Hz to determine the record variance (proportional to H^2) and spectral peak frequency ($1/T$). The maximum mooring line tensions and induced moments for each test were determined by inspection of the individual records.

CHAPTER 5: EXPERIMENTAL RESULTS

This chapter summarizes the quantitative and qualitative experimental results obtained during wave flume and wave basin testing. As well, an attempt is made to explain the relevance of the results and the impact of the different dimensionless parameters on breakwater performance. Table 5.1 is a summary of experimental results for the wave flume test program and Table 4.1 contains results from the wave basin test program.

When analyzing the data it was assumed that the response of the breakwater would be periodic and of the same frequency as the incident waves. However, the inherent nonlinearities in the problem (particularly the nonlinear moorings) did result in some variance from cycle to cycle in the recorded quantities (partially non-periodic response) which combined with the limited length of the tests is responsible for some scatter in the data.

5.1 Breakwater System Characteristics

The natural frequencies of a floating breakwater are of interest because the amplitudes of the motions are expected to increase as the frequency of the incident waves approach one of the natural frequencies. If the breakwater is considered a 3-D rigid body then it should have six natural frequencies and six mode shapes corresponding to its six degrees of freedom: surge, heave, sway, roll, yaw, and pitch as defined in Fig. 5.1. Modelling the breakwater as a two-dimensional body eliminates three degrees of freedom (DOFs) leaving only the surge, heave, and roll DOFs and hence the system should have only three natural frequencies and mode shapes.

In a rigorous sense, to have well defined natural frequencies requires that the system has both constant inertia and linear stiffness. For the system studied, neither of these assumptions is

strictly satisfied. First, the mooring lines do not provide linear stiffnesses as there is generally some slack in the lines. As well, the vertical stiffness created by buoyancy forces varies as the floating breakwater is displaced from its equilibrium position. Finally, the added mass which contributes to the inertia varies with the frequency of excitation. However, by exciting the floating breakwater with displacements of similar amplitude as those experienced during testing, estimates of the natural frequencies may be made.

It is useful to discuss the type of results that may be expected. First, by examining the two-dimensional model, the following results concerning its three mode shapes can be deduced. Since the model can move freely in the heave direction without eliciting motion in the roll and surge directions, the heave degree of freedom is uncoupled from the other two degrees of freedom. Therefore, heaving motion without roll or surge will constitute one of the modes. However, a displacement in the surge direction will result in a rolling motion as well unless a restraining moment is applied to the breakwater. The coupling of the roll and surge modes results from the mooring line not being connected to the centre of the breakwater cylinder. However, the coupling of the surge and roll motions is not very strong. Therefore, one mode that is predominantly roll and another mode which is predominantly surge should be expected. For convenience, these modes will be referred to as the roll mode and surge mode respectively, although they are actually coupled modes. The same reasoning can be extended to the 3-D model with its extra degrees of freedom. The sway, yaw, and pitch motions are not coupled to the heave, surge, and roll motions.

Two types of restoring forces are present: mooring line forces and buoyancy / gravity forces. Because of the mooring lines' slackness, the magnitude of the hydrodynamic forces should generally be much larger than the mooring line forces. Therefore, it is expected that motions which are restored by hydrodynamic forces should have larger spring constants and hence lower natural periods (i.e. the natural period of the heave mode should be lower than the natural frequency in surge).

As a precursor to measuring the natural frequencies, the heave and roll natural frequencies were calculated ignoring mooring line stiffness for both the 2-D and 3-D models. The calculation method for both heave and roll motions is based on the hydrodynamic stiffness induced by buoyancy and gravitational forces.

For the heave mode, the inertia to motion is the sum of the mass of the body and the added mass predicted by potential theory. For a system with a free surface, the added mass for heave has a dependence on the frequency of oscillation as shown by Vugts [26]. Results from [26] were extrapolated to give rough estimates of the added mass in heave for circular cylinders with h/D ratios differing from 0.5 (see Table 5.2). Using these approximate values for the added mass, the predicted natural periods in heave for the 2-D and 3-D models were 1.01 s and 0.84 s respectively. The natural periods differ because of differences in scale size and relative draft. The natural periods for the 2-D and 3-D models can be translated into values for the prototype breakwater by applying the appropriate scale factor. For prototype scale breakwaters ($D = 3.21$ m) with draft ratios (h/D) of 0.579 and 0.735, the corresponding natural periods in heave would be 3.2 s and 3.9 s, respectively.

The restoring force for roll motion is caused by the eccentricity of the centre of gravity from the centre of the cylinder. The moment of inertia of the cylinder in roll was the only inertia component considered. Theoretically, a circular cylinder in roll should have no added mass. The natural periods in roll predicted for the 2-D and 3-D models were 0.72 s and 2.46 s. The 3-D model had such a long natural period in roll because its centre of gravity was very close to the centre of the cylinder and hence had a small spring constant. The 2-D model's internal configuration and moment of inertia were not a good approximation to those of the proposed breakwater, hence its roll response may not be indicative of the performance of the proposed prototype breakwater. However, the 3-D model was weighted properly so its roll response should approximate that of the prototype very well. The proposed prototype breakwater

should therefore have a natural period in roll of 11.4 s, much higher than the exciting period of incoming waves (less than 6 s).

The natural frequencies of the 2-D model were measured by exciting the model in each of its three DOFs and measuring the motion in the primary direction with an accelerometer. The resulting motions were recorded and converted to provide frequency spectra. When excited in heave, a natural period of 0.97 s was recorded, corresponding well with the estimate of 1.01 s. When excited in the roll DOF, frequency peaks corresponding to the heave ($T = 0.97$ s) and surge ($T = 3$ s) modes were detected. The natural frequency of the roll mode, which was expected to be 1.39 Hz ($T = 0.72$ s), could not be isolated. The most feasible explanation for this discrepancy is that the natural period in roll was close to the natural period in heave and could not be distinguished. The natural period for surge motions varied from 3 s to 5 s depending on the mooring line properties particularly the amount of slack in the lines.

For the 3-D model, wave elevation records were used to obtain a plot of the response in the frequency domain. A natural period of 0.83 s was recorded for the heave mode which compares well with the predicted value of 0.84 s. A natural period of 3.4 s was recorded for the surge mode (with $s/s_0 = 1.02$). A natural frequency could not be obtained for the roll mode since the rolling motion did not induce wave propagation. The other natural frequencies were heavily damped, approaching critical damping and records of sufficient length to obtain a reliable frequency spectrum could not be obtained. However, it was observed that the sway, pitch, and yaw modes had natural periods of comparable length to the natural period in surge (3.4 s).

For the 2-D model, both the heave and roll modes are very important to the response of the breakwater since their natural periods fall in the operating range of the breakwater ($T = 0.97$ s corresponds to $D/L = 0.22$). Hence it should be expected that the heave and roll motions will peak around $D/L = 0.22$ for the 2-D model.

For the 3-D model, which more truly represents the actual breakwater, the roll mode is not as important since its natural period in roll is considerably higher (approximately 2.46 s). The heave mode can therefore be expected to be the dominant mode since its natural frequency is still in the operating range of the breakwater ($T = 0.83$ s corresponds to $D/L = 0.141$).

5.2 Breakwater Motions

The importance of the breakwater motions is mainly due to their role in the transmission of waves past the breakwater. Incoming waves force heave, surge and other motions of the breakwater which in turn create a radiation velocity potential which results in wave generation downwave from the breakwater. As well, the breakwater motions induce the tensions in the mooring lines.

A body moving in the heave and surge directions in phase with incident waves (i.e. has same circular or elliptical orbit as surrounding water particles) will not deter the propagation of waves past the body. This situation will arise when the body length is much smaller than the wavelength of the waves (D/L small). If however, the motion of the body is of a smaller amplitude or out-of-phase from the water particle orbits then part of the wave energy will be reflected and there should be a net reduction in wave height on the downwave side of the breakwater. Ideally, the breakwater would have sufficient inertia to behave like a fixed body and wave transmission would occur only by overtopping of the breakwater and transmission of energy under the breakwater.

Some understanding of the situation can be gained by considering the response of a single degree of freedom (SDOF) system. A SDOF system's motion under periodic forcing is determined by the magnitude of the forcing and the frequency as shown in Fig. 5.2. Four parameters, δ_{st} (the static deflection produced by the magnitude of the force), ω (frequency of the forcing), ω_n (the natural frequency of the system), and ζ (the degree of damping) will

determine the amplitude and phase of the system's response. A drastic reduction in amplitude and increase in phase shift occurs when the frequency of forcing is greater than the natural frequency. For the case of a floating breakwater, the preceding statement suggests that if the frequency of the incident waves is greater than the natural frequencies of the breakwater then wave transmission will be notably reduced.

The situation under consideration is somewhat complicated by the additional degrees of freedom and the fact that the forcing is not independent of the motion. A more detailed mathematical description of the problem is given in Chapter 6. However, the SDOF system can still be useful in visualizing the response of the breakwater.

5.2.1 Wave Flume Results and Observations

Figure 5.3(b) shows the amplitude of the breakwater motions measured with the breakwater secured by chain mooring lines. The data points on the graph correspond to test conditions 1.1 to 1.8 and 7.1 to 7.5 as summarized in Table 5.1. For comparison purposes the amplitudes of motion are non-dimensionalized by the wave height. For $D/L \leq 0.15$, surge and heave motions are of approximately the same amplitude as the amplitude of orbit of a water particle at the water's surface ($\hat{\xi}_1, \hat{\xi}_2 \cong H/2$). As well, the video record shows that the motions for these conditions were essentially in-phase with the incident wave train. There was little roll for these conditions because there was sufficient mooring line slack to allow the centre of gravity to move freely within its orbit. Under these conditions, little or no reflection of the incoming waves should be expected. At about $D/L \cong 0.23$, the breakwater appears to undergo resonance in heave. At this frequency the orbit of the centre of gravity is nearly elliptical with the major axis inclined about 15° clockwise from the z-axis. The heave amplitude is about 50% greater than the amplitude of the incident waves, whereas the surge amplitude is considerably less than the amplitude of incident waves. As well, the breakwater's motion is almost completely out-of-phase with the incident wave train. For

tests performed at $D/L > 0.23$, motions decreased dramatically as D/L increased and the motions continued to be out-of-phase with the incident waves.

Figure 5.4(b) is a graph of the breakwater motions for essentially the same conditions except the breakwater is constrained by nylon mooring lines. This data corresponds to tests 2.1 to 2.8 and 8.1 to 8.5. At $D/L \cong 0.10$, the breakwater appears to undergo resonance in a surge/roll mode. This resonant condition was not present with the chain mooring lines, and is almost certainly due to the added stiffness from the taut nylon lines. However the breakwater's motion was still fundamentally in-phase with the excitation. At larger D/L , the breakwater's response is essentially the same as with chain mooring lines but with one exception. At the heave resonance condition ($D/L \cong 0.23$), the roll response is significantly less. This also may be due to the taut mooring lines causing some shifting of the surge and roll mode shapes.

Figures 5.5(b) and 5.5(c) show the effect of wave height on the non-dimensional motions. Figure 5.5(b) is based on test results from 3.1 to 3.4 and Fig. 5.5(c) on 3.5 to 3.8. These figures show that there is little or no dependence of the non-dimensionalized motions on the incident wave height (i.e. the actual motions have a nearly linear dependence on wave height).

Figures 5.6(b), 5.6(c) and 5.6(d) show the effect of relative draft on the surge, heave, and roll motions, respectively. These figures were compiled from the results of tests 4.1 to 4.16. In general, the results indicate that the motions decrease as the relative draft and inertia increase, as expected. A few exceptions to this general trend are present in Fig. 5.6(c) and are associated with resonant peaks in the heave response at different drafts.

Figures 5.7(b), 5.7(c) and 5.7(d) were taken from the results of tests 6.1 to 6.8 and show the response of the breakwater with chain mooring lines for different degrees of slack present in the lines. Less slack in the mooring lines tended to result in decreased heave and surge

motions. As well, the roll response increased. Since the mooring lines are fastened at the bottom of the breakwater, larger moments were induced by the increased rigidity of the bottom of the cylinder resulting in greater roll motions. The increased roll motions allow the breakwater's centre of gravity to move in a larger orbit.

5.2.2 Wave Basin Observations

As alluded to earlier, the 3-D tests essentially consisted of the same six tests within the range $0.1 \leq D/L \leq 0.6$ repeated for four different angles of incidence. Yaw, pitch, and sway motions were expected for angles of incidence other than zero. As the angle of incidence was increased, the net amount of breakwater motion decreased markedly. Rolling motion in particular was much less for $\theta \neq 0^\circ$.

Pitch and yaw motions were especially noticeable for the longer period waves (when $\theta \neq 0^\circ$). When combined with the surge and heave motions, the pitch and yaw motions allowed the breakwater's orbit to nearly match the orbit of the water particles along most of the length of the breakwater for these long period waves. No noticeable sway oscillations were detected for any of the tests.

5.3 Wave Attenuation

Wave energy can pass a floating breakwater and contribute to the transmitted wave height by three means: energy transmitted under the breakwater, energy transmitted over the breakwater (overtopping), and by transferring energy through the breakwater via breakwater motions. In the model tests, a fourth mechanism, diffraction between the ends of the breakwater and the walls of the flume or wave barriers existed. Diffraction was limited by keeping this gap as small as possible. At field breakwater sites, diffraction will occur around the ends of the breakwater arrays and through gaps between breakwaters (if gaps exist).

However, diffraction considerations are not included in the calculation of wave transmission characteristics here.

The breakwater model was observed to use all three of the wave protection mechanisms listed in Sec. 1.2 (wave reflection, out-of-phase damping, and turbulence) to varying degrees. The most prevalent mechanism for short period waves ($D/L \geq 0.30$) was wave reflection. Out-of-phase motion and turbulence were more pronounced for waves of comparable period to the breakwater's natural period in heave ($D/L \approx 0.20 - 0.25$). Waves with longer periods tended to transmit nearly completely past the breakwater.

Figures 5.3(a) and 5.4(a) show the transmission coefficients for chain and nylon mooring lines respectively. Both figures show that the breakwater is ineffective for D/L (relative diameters) less than 0.20. A distinct decrease in transmission coefficient occurs as the relative diameter parameter increases from 0.15 to 0.20. Still, wave transmission remains quite large (between 40% and 60%) for relative diameters ranging from 0.20 to 0.50.

Figure 5.5(a) shows the variance of the transmission coefficient caused by altering the wave steepness for two wave periods. The figure shows that the wave steepness does not significantly effect the transmission coefficient.

Figure 5.6(a) shows the effect of relative draft on wave transmission. In general wave transmission was somewhat better for relative drafts varying from 0.55 to 0.70. Relative drafts greater than 0.70 give rise to excessive overtopping, which results in higher transmission coefficients even though breakwater motions were reduced by the increased inertia.

Figure 5.7(a) shows the influence of line slackness on wave transmission. It was expected that a decreased line slackness would decrease the wave transmission. However, the results are non-conclusive, probably due to the effect of the mooring line slackness on the natural periods and the breakwater motions. Decreasing the wave slackness, increases the effect of

the nonlinearities in the mooring response making it difficult to define the net effect on the system. Figures 5.8(a)-(b) show the effect of the attachment point on the transmission coefficient. The uncrossed arrangement shown in Fig. 2.2 gave marginally better results. In general, the overall performance of the breakwater was insensitive to variations in the mooring line parameters.

Figure 5.9(a) shows the wave transmission coefficients recorded for the wave basin tests. The figure shows wave transmission improves dramatically as the angle of incidence is increased. When the angle of incidence is significantly different from 0° , wave crests and troughs are hitting the breakwater at the same instant along the length of the breakwater inducing forces in opposite directions. The net result is that breakwater motions are reduced and hence greater wave reflection and lower wave transmission is achieved.

5.4 Mooring Line Forces

Records of the mooring line tension for both nylon and chain lines showed the forces in the mooring lines were typically close to zero for a portion of the cycle with one sharp spike per cycle when the line became taut. As well, the peak mooring line force often varied considerably from cycle-to-cycle. These two observations indicate that the mooring lines' behavior was very nonlinear. Figure 5.10 shows typical mooring line forces experienced by the load cells as recorded during test 2.5 of the wave flume experiments.

Figure 5.4(c) shows the mooring line forces measured for the base case with nylon moorings non-dimensionalized as defined by Eqn. 2.6. The mooring line forces decreased with increasing D/L , corresponding with the decreased breakwater motions.

Figure 5.5(d) shows the influence of wave height on the maximum forces experienced with nylon moorings. The graph shows that the maximum mooring line forces at a particular D/L value increase linearly with the wave height .

Figure 5.9(b) shows the influence of wave angle on the forces measured with chain mooring lines. Here too, with chain moorings, the breakwater forces decrease dramatically as D/L increases. Mooring line forces are much less for wave angles other than zero.

5.5 Breakwater Internal Stresses

Figures 5.9(c)-(e) show the bending moments and torsion (non-dimensionalized as defined by Eqn. 2.7) experienced by the wave basin model at different angles of incidence. There is considerable scatter in the data due to the difficulty in obtaining stress measurements of the magnitude experienced during testing. However, horizontal and vertical bending moments tended to decrease with increasing D/L (shorter periods) and increasing angle of incidence. No significant torsion was induced in the breakwater for any of the conditions tested.

5.6 Comparison to Rectangular Caisson Results

Results from Byres [4], Nece and Skjelbriia [17], and Nelson and Broderick [18] for a rectangular caisson breakwater are compared here to results obtained for the circular cross-section breakwater. The rectangular caisson breakwater considered in the studies cited had a width to depth ratio of 3.2:1 and was moored by chain lines. The test results from Byres were obtained for monochromatic regular waves produced in a wave basin. Results from Nece and Skjelbreia were for ship-generated waves approaching at various angles of incidence (from 0 to 36 degrees). Results from Nelson and Broderick were for the same breakwater, but with wind-generated waves. Nelson and Broderick used the average wave height and period calculated from a spectral analysis of 8.5 minute records.

The researchers cited above used the parameter, ka , as an indication of the breakwater's relative size, where k is the wave number and a is the half width. In order to compare these

results to results for a circular-section, an effective diameter, D' , is defined for the rectangular caisson. D' is defined by equating the cross-sectional perimeter, P , of the rectangular and circular sections:

$$(5.1) \quad \begin{aligned} P &= \pi D' && \text{(for circular section)} \\ &= 2w + 2d && \text{(for rectangular section)} \end{aligned}$$

For a rectangular section with a width to depth ratio of 3:2:1 the conversion $D'/L = 0.266ka$ results. The comparison was based on equivalent perimeters since the magnitude of the perimeter is proportional to the amount of concrete needed to form the walls.

Figure 5.11 compares the wave transmission characteristics observed for the circular cross-section floating breakwater to the transmission coefficients reported for a rectangular caisson breakwater in the above studies. Figure 5.12 compares the motion response of the circular cross-section breakwater to motions observed by Byres for a rectangular caisson breakwater.

Figure 5.11 shows that the circular and rectangular cross-sections perform similarly as the frequency of forcing is increased. Both geometries are ineffective for values of D/L less than about 0.20 to 0.25. Because of the scatter in the data, no definitive conclusion can be drawn as to which cross-section performs better, although transmission coefficients for the rectangular cross-section generally seem to be slightly lower.

Figure 5.12 shows that heave and roll motions were nearly equivalent for both cross-sections. A resonance peak in the surge mode is present at $D/L \approx 0.27$ for the rectangular caisson. This resonant peak was not observed for the circular cross-section and also surge motions were considerably less for large values of D/L . These discrepancies could be due to differences in mooring line properties between the two studies. As well, Byres reported concerns about the accuracy of some of his motion measurements.

CHAPTER 6: NUMERICAL MODEL

The numerical model used is based on two component analyses: a hydrodynamic analysis which treats the problem of normal or oblique incident waves interacting with the breakwater and is based on two-dimensional wave diffraction theory; and a mooring analysis, which provides the mooring line configurations, mooring line tensions and anchor forces. These are summarized in Sec. 6.1 and Sec. 6.2, respectively. The hydrodynamic analysis for a 2-D floating body given in Sec. 6.1 is well documented by authors such as Chan and Hirt [5] and Sarkaya and Isaacson [24]. The mooring analysis is that used by Isaacson [10] to quantify the effect of nonlinear moorings on the floating body's response.

6.1 Hydrodynamic Analysis

The flow about a long floating breakwater caused by incoming waves can be studied as the two-dimensional problem of a rigid floating body exposed to an incident wave train (see Fig 2.1 for definition of variables). If certain conditions of linearity are met, it is possible to represent irregular ocean waves as the superposition of linear regular waves of different frequencies. It can be shown that the resulting flow about the breakwater can be described as the sum of the solutions to the simpler problem of linear waves incident on the breakwater. For simplicity, the problem will be stated only for waves approaching perpendicular to the breakwater. However the theory can be extended to the three-dimensional problem of oblique incident waves.

In defining the problem in the above manner it is implicitly assumed that the fluid is inviscid and the flow is irrotational so that the velocity field can be described in terms of a velocity potential, ϕ . The horizontal and vertical velocities (u and w) are then given by:

$$(6.1) \quad u = \frac{\partial \phi}{\partial x} ; \quad w = \frac{\partial \phi}{\partial z}$$

The continuity condition (conservation of mass) then reduces to Laplace's equation:

$$(6.2) \quad \frac{\partial^2 \phi}{\partial x^2} + \frac{\partial^2 \phi}{\partial z^2} = 0$$

The linearized boundary conditions for the problem are zero vertical velocity at the seabed which is assumed to be horizontal (Eqn. 6.3), the combined linear free surface condition (Eqn. 6.4), and the body-fluid interface condition requiring no flow through the rigid body (Eqn. 6.5).

$$(6.3) \quad \frac{\partial \phi}{\partial z} = 0 \quad \text{at } z = -d;$$

$$(6.4) \quad \frac{\partial^2 \phi}{\partial t^2} = -g \frac{\partial \phi}{\partial z} \quad \text{at } z = 0, \text{ where } t \text{ is time;}$$

$$(6.5) \quad \frac{\partial \phi}{\partial n} = V_n \quad \text{on the surface of the cylinder;}$$

where V_n is the velocity of the body normal to its surface and n is the direction normal to the body surface. In addition to the boundary conditions, a radiation condition must be imposed to obtain a unique solution to the problem. The radiation condition requires that the disturbed portion of the flow away from the body must represent waves with the same period as the incident forcing traveling outward from the body.

The method of solution adopted is to split the problem into: (i) a diffraction problem of waves incident upon a fixed body, and (ii) a radiation problem of forced oscillations of a body in calm water. The two problems are coupled by finding the forces acting on the fixed body of the diffraction problem and applying these as the exciting forces in the radiation problem. The total potential is expressed as the summation of an incident potential, ϕ_w ; a

scattered or diffracted potential, ϕ_s ; and forced potentials; ϕ_{f1} , ϕ_{f2} , ϕ_{f3} , caused by the heave, sway, and roll motions, respectively.

$$(6.6) \quad \phi = \phi_w + \phi_s + \phi_{f1} + \phi_{f2} + \phi_{f3}$$

The governing equations and boundary conditions presented earlier must now be stated in terms of these potentials. The scattered and forced potentials represent the disturbed portion of the flow and as such must each satisfy the two-dimensional radiation condition which requires these potentials, denoted as ϕ , vary as:

$$(6.7) \quad \phi \propto e^{-ik|x|} \quad \text{as } |x| \rightarrow \infty$$

To further simplify the problem, the incident, scattered, and forced potentials are decomposed using the knowledge that these potentials are oscillatory in time. As well, the incident and scattered potentials should be proportional to the amplitude of the incident waves, while the forced potentials will be proportional to the amplitudes of heave, sway, and roll motions; $\hat{\xi}_1, \hat{\xi}_2, \hat{\xi}_3$, respectively. Hence the following forms for the potentials can be derived:

$$(6.8) \quad \phi_w + \phi_s = \text{Re}\{A(\phi_w + \phi_s)e^{i\omega x}\}$$

$$\phi_{fj} = \text{Re}\{\xi_j \phi_{fj} e^{i\omega x}\} \quad \text{for } j = 1, 2, 3$$

where the ξ_j are complex amplitude coefficients for the harmonic motions of the three body motions. The partial potentials; $\phi_w, \phi_s, \phi_{f1}, \phi_{f2}, \phi_{f3}$, defined by the above equations are complex functions of position (x,y) that represent the magnitude and phase of the potentials with respect to the incident flow. The boundary conditions, radiation condition, and Laplace's equation stated earlier may now be expressed in terms of the partial potentials.

6.1.1 Incident Potential

The incident potential is defined as the flow existing in the absence of the breakwater. For regular waves approaching perpendicular to the breakwater the incident potential is:

$$(6.9) \quad \phi_w = \frac{\pi H}{kT} \left(\frac{\cosh k(z+d)}{\sinh(kd)} \right) \sin(kx - \omega t)$$

6.1.2 Scattered Potential

The scattered potential is a result of the diffraction created by the presence of the body. It is independent of the body motions and the boundary conditions are therefore defined with the body fixed. The boundary condition on the corresponding fixed body surface is:

$$(6.10) \quad \frac{\partial \phi_s}{\partial n} + \frac{\partial \phi_w}{\partial n} = 0 \quad \text{on the surface of the cylinder}$$

Other conditions on the scattered potential are the same as for the incident potential. Namely, no vertical velocity at the seabed, and the combined free surface condition at the still water level must be satisfied for ϕ_s . In addition, the radiation condition (Eqn. 6.7) must be satisfied. Solution of the diffraction problem stated in this manner can be achieved using various methods. The two most popular methods are a “wave source” method as outlined by Sarpkaya and Isaacson [24] and a finite element method described by Newton [21].

6.1.3 Forced Potentials and Body Motions

In order for the total potential to satisfy Eqn. 6.5, the forced potentials must satisfy the boundary condition:

$$(6.11) \quad \frac{\partial \phi_{f1}}{\partial n} + \frac{\partial \phi_{f2}}{\partial n} + \frac{\partial \phi_{f3}}{\partial n} = V_n \quad \text{on the surface of the cylinder.}$$

Eqn. 6.11 can be broken down into three separate equations with each forced potential satisfying the portion of the normal velocity due to motion in that mode. The forced potentials must also satisfy the other boundary conditions and Laplace's equation. By expressing the problem in terms of partial potentials, the solution can be found using wave source methods as in the case of the diffraction problem, except that the body boundary condition is changed appropriately. Once this is accomplished the only remaining unknowns are the complex motion amplitudes, ξ_j 's.

Using the known partial potentials and carrying out suitable integrations, the unsteady Bernoulli equation may be used to develop an expression for the hydraulic force components. These can in turn be expressed in terms of; added mass components proportional to the body accelerations, damping components proportional to body velocities, and exciting forces associated with the diffraction problem. Once the forces are split up in this manner, it is possible to set up a complex matrix equation for the harmonic response of the floating body being forced at an angular frequency, ω .

$$(6.12) \quad (-\omega^2([m] + [\mu]) - i\omega[\lambda] + ([k] + [k^{(h)}]))\{\xi\} = \{f^{(e)}\}$$

where $[\mu]$ contains added mass coefficients, $[\lambda]$ contains damping coefficients, and $\{f^{(e)}\}$ is the vector of the exciting forces. Additional terms in the matrix equation are; the body mass matrix, $[m]$; the linearized mooring stiffnesses, $[k]$; and the hydrodynamic stiffnesses, $[k^{(h)}]$. A complex matrix inversion procedure can be used to solve Eqn. 6.12 for the magnitude and phase of the motions of the body. Once the solution is found the total potential can be found using Eqns. 6.6 and 6.8, and hence the problem is solved. As well, then quantities such as mooring line forces and the velocities and accelerations of the body can be calculated as needed.

6.2 Mooring Analysis

The hydrodynamic analysis indicated above is carried out in conjunction with a mooring analysis. For a specified three-dimensional mooring configuration and mooring line properties, the corresponding computer program first carries out a static analysis to obtain the equilibrium profiles of the moorings and the mooring line forces in the absence of environmental loads due to wind, waves and currents. This mooring analysis is repeated for a set of unit displacements of the breakwater in order to provide the effective stiffness components of the breakwater for application to the hydrodynamic model. At this stage, the hydrodynamic analysis is carried out with these stiffnesses included in the equations of motion as indicated by Eqn. 6.12. This provides the breakwater motions and the wave drift force in the presence of the moorings (assumed to behave with linear stiffnesses). The mooring analysis is then repeated with the steady environmental loads, including wind drag, current drag and the wave drift force, now assumed to be present, and this involves a balance between these forces and the mooring forces acting on the breakwater. This provides the steady offset of the breakwater. Finally, the oscillatory breakwater motions which have been calculated by the hydrodynamic analysis are now used to provide the extreme displacements of the mooring line connection points, and the mooring analysis is carried out under these conditions to obtain the maximum forces in the mooring line connections, the anchor forces and mooring line tensions.

6.3 Numerical Results

The numerical model has been applied to a series of conditions varying the dimensionless parameters in a manner similar to the wave flume tests. Results plotted in Figs. 6.1 (chain mooring) and 6.2 (nylon mooring) correspond to the following base case:

Breakwater geometry:	$D = 3 \text{ m}$
	$h = 2.25 \text{ m}$
Wave climate:	$T = 3 - 6 \text{ s (varied)}$

H = up to 2 m (H/L constant)

d = 15 m

Mooring parameters:

b = 5 m

λ = 60 m

n = 1

attachment point on bottom (as in Fig. 2.2)

Mooring line parameters:

chain *nylon*

w' (N/m) = 140 20

EA (N) = 2×10^8 2×10^6

s/s₀ = 1.05 1.01

In addition, the centres of gravity and buoyancy are taken to be 0.95 m and 1.0 m, respectively, below the water surface; and the roll radius of gyration is taken as 0.87 m. The above conditions correspond to the following dimensionless parameters:

$d/D = 5$

$\lambda/d = 4$

$H/L = 0.035$

$h/D = 0.75$

$D/L = \text{up to } 0.4$

chain *nylon*

$w''/\rho g D =$ 890×10^{-6} 130×10^{-6}

$E'/\rho g D^2 =$ 4000 40

s/s₀ = 1.05 1.01

The results obtained can therefore be applied to a range of alternative prototype conditions with similar dimensionless parameters.

Figures 6.1 and 6.2 show the transmission coefficient, motion amplitudes and mooring line forces (in N) as functions of D/L for the base case with chain mooring lines and with nylon mooring lines, respectively. The differences in the wave transmission and motion amplitudes between the two sets of data is very minor, suggesting that mooring properties play only a minor role in the breakwater's response. Both figures show that the breakwater experiences resonance in the heave mode at approximately $D/L = 0.15$. The resonant peak occurs at a lower D/L (as compared to $D/L = 0.22$ from experiments) because of the higher relative draft which effectively reduces the buoyancy force. The wave transmission predicted for both base cases is between 75 and 100% for all values of D/L except for $D/L = 0.15$ where it is very low.

The maximum mooring line tensions predicted by the numerical model for the chain moorings are much higher than for the nylon lines. This corresponds with the physical reality. By virtue of the nylon moorings being in constant tension, the momentum of the breakwater is absorbed throughout the cycle. As opposed to the chain moorings, which tend to experience high snapping forces over a short fraction of the cycle.

The influence of breakwater draft, wave steepness, mooring line slackness, and mooring line attachment points are further examined by altering the following parameters individually in subsequent sets of numerical tests, as shown below:

$h/D = 0.67, 0.75, 1.0$ (chain mooring base case, see Fig. 6.3)

$H/L = 0.0175, 0.035, 0.070$ (chain mooring base case, see Fig. 6.4)

$s/s_0 = 1.05, 1.10$ (chain mooring base case, see Fig. 6.5)

attachment points : bottom, crossed, uncrossed (chain mooring, see Fig. 6.6)

Figures 6.3(a)-(f) show the transmission coefficient, motion amplitudes and mooring line forces as functions of D/L predicted for three values of relative draft, h/D . From the figures, we can see that the natural frequency predicted in heave increases (higher D/L) as the relative

draft decreases, as expected. For $h/D = 0.67$, the resonant condition is at D/L of about 0.19, and for a $h/D = 0.75$ at $D/L = 0.15$. For $h/D = 1.0$, no resonant peak is evident which agrees with theory since the breakwater has no positive buoyancy.

Figures 6.4(a)-(b) show the upwave and downwave mooring line forces as functions of D/L for three values of wave steepness H/L . The non-dimensionalized wave transmission and motion amplitudes predicted by the numerical model were independent of H/L and so are not shown.

Figures 6.5(a)-(b) show the upwave and downwave mooring line forces as functions of D/L for two values of line slackness, s/s_0 for the base case with chain mooring lines. The figure indicates that mooring line forces increase dramatically as the line slackness is decreased.

Figures 6.6(a)-(b) plot the mooring line forces as functions of D/L , showing the influence of attachment points for the base case with chain mooring lines. The numerical model does not predict any variance in forces due to changing the attachment points.

6.4 Comparison of Numerical and Experimental Results

Figure 6.7(a)-(d) shows the numerical results compared to experimental findings for wave flume test conditions 1.1 to 1.8 (chain mooring lines, $s/s_0=1.06$). Figure 6.8(a)-(d) are a similar set of graphs comparing numerical and experimental results for flume test conditions 2.1 to 2.8 (nylon mooring lines).

In general, there is good agreement between the numerical model and experimental data. The two sets of data indicate the same trends at approximately the same values of D/L . The numerical model tends to overestimate the wave transmission for D/L values greater than 0.15. This effect may be due to an underestimation of damping effects caused by viscous action which becomes more important at higher frequencies. As well, the numerical model

tends to underestimate surge response, most likely due to an overestimation of the mooring line stiffness.

CHAPTER 7: EVALUATION OF PERFORMANCE

7.1 General Conclusions

As a result of the physical and numerical testing of a circular-section floating breakwater, a better understanding of the role of the governing variables was gained. Some of the most important points are summarized here:

- (i) The relative size of the floating breakwater, D/L , is a dominant parameter in determining the efficiency of the breakwater. As D/L increases, wave transmission decreases. To be effective, a circular floating breakwater should have a diameter of at least one quarter of the wavelength of the design waves ($D/L \geq 0.25$).
- (ii) The relative draft, h/D , is directly related to the natural frequency in heave. As h/D approaches 1, the natural frequency in heave approaches zero. Ideally the breakwater should be operated at a D/L value which corresponds to a forcing frequency greater than the natural frequency so that response will be out-of-phase from the forcing. A local minimum in the wave transmission curve was observed when D/L was equal to the natural frequency of the breakwater in heave.
- (iii) The breakwater motions decrease as h/D increases (due to increased inertia) but overtopping may occur resulting in higher transmission coefficients. A h/D value of 0.6 - 0.7 performed best in testing (optimum h/D would depend on the D/L and H_j/L values present in the wave climate of the location).
- (iv) Wave steepness, H_j/L , did not greatly effect the non-dimensionalized results.

- (v) An increase in the slack in the mooring lines will tend to result in somewhat increased breakwater motions and wave transmission but greatly reduced mooring line forces. It was found to be very difficult to maintain line pretension in nylon lines. The choice of mooring line does not appear to significantly affect the overall performance of the breakwater. This conclusion is supported by Cox [6].
- (vi) Positioning the mooring lines in an uncrossed arrangement seemed to reduce roll motion and result in slightly better wave transmission.
- (vii) The efficiency of the breakwater increases dramatically for incoming waves approaching obliquely ($\theta \neq 0^\circ$). As well, mooring line forces and breakwater motions were reduced. This conclusion contradicts Nece and Skjelbreia [17] who concluded that the angle of incidence did not affect wave transmission. However, the results obtained clearly show that wave transmission is reduced for $\theta \neq 0^\circ$.
- (viii) Horizontal and vertical bending moments induced in the breakwater walls will be an order of magnitude larger than any torsional moments.
- (ix) The wave transmission past the circular cross-section breakwater for a particular wave period was comparable to that of a rectangular breakwater of equivalent size. The amplitudes of the surge, heave, and roll motions of the circular and rectangular sections were also very similar.

7.2 Performance of Numerical Model

The numerical model based on linear potential theory and linearized mooring stiffnesses provided results which corresponded approximately with the physical results for most of the

conditions examined. The numerical model does not properly model the extremely nonlinear mooring forces. As well, the model does not truly reflect the viscous behaviour of the fluid. These two pitfalls (particularly the nonlinear moorings) prevent the numerical model from providing more accurate results, particularly concerning the prediction of peak mooring line forces. However, as a whole the numerical model provides a good approximation of the response of the breakwater.

7.3 Potential for Improvement and Further Study

From a study of related literature on similar floating breakwater designs, it becomes apparent that there are several modifications to the design proposed which may improve the overall performance of the breakwater. However most of these modifications would complicate the fabrication of the breakwater and it is difficult to determine without further study whether these modifications would be economically efficient.

During the tests, it was noted that the breakwater's surge motion was basically unconstricted for small displacements. A way of introducing pretension in to the mooring lines would be helpful in reducing surge motions. One method of achieving this goal is to include hanging weights on the mooring lines, as has been done for the breakwater at West Point, Washington [17]. The use of nylon cables in pretension is a good solution theoretically, but may be problematic because of the tendency of the cables to undergo plastic elongation over time.

Vertical barriers extending from the bottom of the breakwater (skirts) as shown in Fig. 1.8 on a rectangular caisson would certainly reduce wave transmission by decreasing wave transmission underneath the breakwater, increasing added mass in roll and surge, and introducing considerable turbulence. However they would also most likely introduce considerable internal stresses and increase mooring line forces. Horizontal barriers

extending from the sides of the breakwater may also be beneficial by virtue of increasing the added mass in heave and roll and increasing turbulent dissipation.

Results from the wave basin (3-D tests) suggest the possibility of a breakwater designed such that incident waves are always oblique to the breakwater's axis. One method of achieving this would be to arrange short lengths of breakwater connected in a zig-zag pattern. The obvious disadvantages of this type of system would be the increased lengths of breakwater required to protect an equivalent length of harbor and the difficulty of designing the connections between breakwater units.

Finally, it should be noted that the breakwater was only tested with regular periodic waves, not with random waves. On the basis of linear potential theory, superposition of the breakwater's response in regular waves can be used to predict response to a specified wave spectrum. However, linear potential theory does not account for effects such as nonlinearities associated with the moorings or with turbulent dissipation. Therefore, it would be useful to test the breakwater in irregular wave conditions to determine its effectiveness and compare results with predictions based on a superposition of regular wave test results or the numerical model.

BIBLIOGRAPHY

- [1] ASCE Ports and Harbors Task Committee, 1992. Progress Report on Small Craft Harbors, *Proc. Ports '92*, ASCE, Seattle WA, Vol. 2.
- [2] Bai, K. J. and R. Yeung, 1974. Numerical Solutions to Free Surface Problems. *10th Symposium on Naval Hydrodynamics*, Cambridge MA, pp. 609-647.
- [3] Blumberg, G. P. and R. J. Cox, 1988. Floating Breakwater Physical Model Testing for Marina Applications, *Bulletin of the Permanent International Association of Navigational Congresses*, No. 63, pp. 5-13.
- [4] Byres, R. D., 1988. *Floating Breakwaters in British Columbia*. M.A.Sc. Thesis, Dept. of Civil Engineering, University of British Columbia, Vancouver BC.
- [5] Chan, R. K. and Hirt, C. W. 1974. Two Dimensional Calculations of the Motion of Floating Bodies. *10th Symposium on Naval Hydrodynamics*, Cambridge MA, pp. 667-683.
- [6] Cox, J. C., 1989. Design of a Floating Breakwater for Charleston Harbor, South Carolina, *Proc. Ports '89*, ASCE, Boston MA, pp. 411-420.
- [7] Giles, M. L. and R. M. Sorenson, 1979. Determination of Mooring Loads and Wave Transmission for a Floating Tire Breakwater, *Proc. Coastal Structures '79*, ASCE, Alexandria VA, Vol. 2, pp. 1069-1086.
- [8] Greenhow, M. and Y. Li, 1987. Added masses for circular cylinders near or penetrating fluid boundaries - review, extension and application to water-entry - exit and slamming, *Ocean Engineering*, Vol. 14, No. 4, pp. 325-348.
- [9] Isaacson, M., 1993. Hydrodynamic Coefficients of Floating Breakwaters, *Proc. 1993 Annual Conference of the Canadian Society for Civil Engineering*, Fredericton NB, Vol. 1, pp. 485-494.
- [10] Isaacson, M., 1993. Wave Effects on Floating Breakwaters, *Proc. 1993 Canadian Coastal Conference*, CC-SEA, Vancouver BC, Vol. 1, pp. 53-65.

- [11] Isaacson, M. and O. Nwogu, 1987. Directional Wave Effects on Long Structures, *Journal of Offshore Mechanics and Arctic Engineering*, ASME, Vol. 109, No. 2, pp. 126-132.
- [12] Jones, D. B., 1971. *Transportable Breakwaters - A Survey of Concepts*, Technical Report R-727, Naval Civil Engineering Laboratory, U. S. Navy.
- [13] Kim, C. H., 1969. Hydrodynamic Forces and Moments on Heaving, Swaying, and Rolling Cylinders on Water of Finite Depth. *Journal of Ship Research*, Vol. 13, pp. 137-154.
- [14] McCartney, B. L., 1985. Floating Breakwater Design, *Journal of Waterway, Port, Coastal, and Ocean Engineering*, Vol. 111, No. 2, pp. 304-317.
- [15] McLaren, W. L., 1981. Preparation of Floating Breakwater Manual, *Proc. 2nd Conference on Floating Breakwaters*, University of Washington, Seattle WA, pp. 22-47.
- [16] Muschell, J. E. and J. H. Schlak, 1989. Floating Breakwater for Small Recreational Harbors, *Proc. Ports '89*, ASCE, Boston MA, pp. 44-53.
- [17] Nece, R. E. and N. K. Skjelbreia, 1984. Ship wave attenuation tests of a prototype floating breakwater. *Proc. Coastal Engineering 1984*, pp. 2514-2529.
- [18] Nelson, E. E. and L. L. Broderick, 1984. Floating breakwater prototype test program. *Proc. 41st Meeting of the Coastal Engineering Research Board*, U.S. Army Coastal Engineering Research Center.
- [19] Newman, J. N. 1977. *Marine Hydrodynamics*. M.I.T. Press, Mass., pp. 285-311.
- [20] Newman, J. N. 1962. The Exciting Forces on Fixed Bodies in Waves. *Journal of Ship Research*, Vol. 6, pp. 10-17.
- [21] Newton, R. E. 1975. Finite Element Analysis of Two Dimensional Added Mass and Damping. *Finite Elements in Fluids - Vol. 1*, editors. R. H. Gallagher, J. T. Oden, C. Taylor, and O. C. Zieniewicz, John Wiley, New York NY, pp. 219-232.

- [22] Ofuya, A. O., 1968. *On Floating Breakwaters*, Queen's University, Civil Engineering Report No. 60.
- [23] Rao, S. S., 1990. *Mechanical Vibrations*, 2nd ed., Addison-Wesley Publishing, Reading, MA.
- [24] Sarpkaya, T. and M. Isaacson, 1981. *Mechanics of Wave Forces on Offshore Structures*, Van Nostrand Reinhold, New York NY.
- [25] Van Damme, L. V., D. J. Vandebossche and G. Gyselynck, 1985. The Zeebrugge Breakwaters, *Developments in Breakwaters: Proc. Breakwaters '85*, ICE, London, England, pp. 285-286.
- [26] Vugts, J. H., 1968. The Hydrodynamic Coefficients for Swaying, Heaving and Rolling Cylinders in a Free Surface, *International Shipbuilding Progress*, Vol. 15, pp. 251-276.
- [27] Werner, G., 1988. Experiences with Floating Breakwaters, a literature review, *Bulletin of the Permanent International Association of Navigational Congresses*, No. 63, pp. 23-30.

Table 2.1 Comparison of Reynold's numbers between prototype and model states

Non-dimensional Parameters				Keulegan			Prototype			Wave Flume Model (KI=1/10)			Wave Basin Model (KI=1/21)		
D/L	H/L	d/L	Carpenter No.	T (s)	H (m)	Re	T (s)	H (m)	Re	T (s)	H (m)	Re			
0.514	0.080	0.961	0.489	2.00	0.50	1.93E+06	0.63	0.05	6.10E+04	0.43	0.023	1.96E+04			
0.230	0.057	0.431	0.790	3.00	0.80	2.08E+06	0.95	0.08	6.56E+04	0.65	0.037	2.11E+04			
0.139	0.035	0.259	0.845	4.00	0.80	1.67E+06	1.26	0.08	5.27E+04	0.86	0.037	1.69E+04			
0.100	0.031	0.186	1.187	5.00	1.00	1.87E+06	1.58	0.10	5.92E+04	1.08	0.047	1.90E+04			
0.079	0.024	0.147	1.346	6.00	1.00	1.77E+06	1.90	0.10	5.59E+04	1.30	0.047	1.80E+04			

Table 3.1 Experimental Program for wave flume tests

TEST NO.	Breakwater Specifications				Wave Characteristics		
	Draft (h/D)	Mooring Material	Connection Pt.	Slackness s/so	Period T (s)	D/L	Hi (m)
1.1	0.579	Chain	Bottom	1.060	0.79	0.329	0.060
1.2	0.579	Chain	Bottom	1.060	0.95	0.230	0.087
1.3	0.579	Chain	Bottom	1.060	1.11	0.174	0.122
1.4	0.579	Chain	Bottom	1.060	1.27	0.139	0.123
1.5	0.579	Chain	Bottom	1.060	1.42	0.116	0.121
1.6	0.579	Chain	Bottom	1.060	1.58	0.100	0.129
1.7	0.579	Chain	Bottom	1.060	1.74	0.088	0.119
1.8	0.579	Chain	Bottom	1.060	1.90	0.079	0.137
2.1	0.579	Nylon	Bottom	1.000	0.79	0.329	0.060
2.2	0.579	Nylon	Bottom	1.000	0.95	0.230	0.098
2.3	0.579	Nylon	Bottom	1.000	1.11	0.174	0.132
2.4	0.579	Nylon	Bottom	1.000	1.27	0.139	0.136
2.5	0.579	Nylon	Bottom	1.000	1.42	0.116	0.131
2.6	0.579	Nylon	Bottom	1.000	1.58	0.100	0.129
2.7	0.579	Nylon	Bottom	1.000	1.74	0.088	0.119
2.8	0.579	Nylon	Bottom	1.000	1.90	0.079	0.137
3.1	0.579	Nylon	Bottom	1.000	1.11	0.174	0.063
3.2	0.579	Nylon	Bottom	1.000	1.11	0.174	0.084
3.3	0.579	Nylon	Bottom	1.000	1.11	0.174	0.106
3.4	0.579	Nylon	Bottom	1.000	1.11	0.174	0.132
3.5	0.579	Nylon	Bottom	1.000	1.42	0.116	0.062
3.6	0.579	Nylon	Bottom	1.000	1.42	0.116	0.081
3.7	0.579	Nylon	Bottom	1.000	1.42	0.116	0.102
3.8	0.579	Nylon	Bottom	1.000	1.42	0.116	0.132
4.1	0.579	Nylon	Bottom	1.000	0.95	0.230	0.098
4.2	0.579	Nylon	Bottom	1.000	1.11	0.174	0.132
4.3	0.579	Nylon	Bottom	1.000	1.27	0.139	0.136
4.4	0.579	Nylon	Bottom	1.000	1.42	0.116	0.131
4.5	0.657	Nylon	Bottom	1.000	0.95	0.230	0.098
4.6	0.657	Nylon	Bottom	1.000	1.11	0.174	0.132
4.7	0.657	Nylon	Bottom	1.000	1.27	0.139	0.136
4.8	0.657	Nylon	Bottom	1.000	1.42	0.116	0.131
4.9	0.738	Nylon	Bottom	1.000	0.95	0.230	0.098
4.10	0.738	Nylon	Bottom	1.000	1.11	0.174	0.132
4.11	0.738	Nylon	Bottom	1.000	1.27	0.139	0.136
4.12	0.738	Nylon	Bottom	1.000	1.42	0.116	0.131
4.13	0.832	Nylon	Bottom	1.000	0.95	0.230	0.098
4.14	0.832	Nylon	Bottom	1.000	1.11	0.174	0.132
4.15	0.832	Nylon	Bottom	1.000	1.27	0.139	0.136
4.16	0.832	Nylon	Bottom	1.000	1.42	0.116	0.131
5.1	0.579	Nylon	Bottom	1.000	1.11	0.174	0.132
5.2	0.579	Nylon	Bottom	1.000	1.42	0.116	0.131
5.3	0.579	Nylon	Crossed	1.000	1.11	0.174	0.132
5.4	0.579	Nylon	Crossed	1.000	1.42	0.116	0.131
5.5	0.579	Nylon	Uncrossed	1.000	1.11	0.174	0.132
5.6	0.579	Nylon	Uncrossed	1.000	1.42	0.116	0.131

Table 3.1 Experimental Program for wave flume tests (cont.)

TEST NO.	Breakwater Specifications				Wave Characteristics			
	Draft (h/D)	Mooring Material	Connection Pt.	Slackness s/so	Period T (s)	D/L	Hi (m)	Hi/L
6.1	0.579	Chain	Bottom	1.060	1.11	0.174	0.122	0.066
6.2	0.579	Chain	Bottom	1.060	1.42	0.116	0.121	0.044
6.3	0.579	Chain	Bottom	1.020	1.11	0.174	0.132	0.071
6.4	0.579	Chain	Bottom	1.020	1.42	0.116	0.131	0.047
6.5	0.579	Chain	Bottom	1.000	1.11	0.174	0.132	0.071
6.6	0.579	Chain	Bottom	1.000	1.42	0.116	0.131	0.047
6.7	0.579	Chain	Bottom	1.041	1.11	0.174	0.132	0.071
6.8	0.579	Chain	Bottom	1.041	1.42	0.116	0.131	0.047
7.1	0.579	Chain	Bottom	1.046	0.63	0.518	0.051	0.081
7.2	0.579	Chain	Bottom	1.046	0.71	0.408	0.056	0.072
7.3	0.579	Chain	Bottom	1.046	0.79	0.330	0.065	0.067
7.4	0.579	Chain	Bottom	1.046	0.95	0.230	0.099	0.071
7.5	0.579	Chain	Bottom	1.046	1.11	0.173	0.130	0.070
8.1	0.579	Nylon	Bottom	1.000	0.63	0.518	0.051	0.081
8.2	0.579	Nylon	Bottom	1.000	0.71	0.408	0.056	0.072
8.3	0.579	Nylon	Bottom	1.000	0.79	0.330	0.065	0.067
8.4	0.579	Nylon	Bottom	1.000	0.95	0.230	0.099	0.071
8.5	0.579	Nylon	Bottom	1.000	1.11	0.173	0.130	0.070
9.1	0.579	Chain	Uncrossed	1.047	0.63	0.518	0.051	0.081
9.2	0.579	Chain	Uncrossed	1.047	0.79	0.330	0.065	0.067
9.3	0.579	Chain	Uncrossed	1.047	0.95	0.230	0.099	0.071
9.4	0.579	Chain	Crossed	1.046	0.63	0.518	0.051	0.081
9.5	0.579	Chain	Crossed	1.046	0.79	0.330	0.065	0.067
9.6	0.579	Chain	Crossed	1.046	0.95	0.230	0.099	0.071

Table 4.1 Experimental program and results for wave basin tests

TEST NO.	Angle of Incidence (deg)	Wave Characteristics				Mooring Forces Cf	Breakwater Wall Forces		
		Tp (s)	D/L	Hi (m)	Kt (%)		Horiz. Bending Cm	Vert. Bending Cm	Torsion Cm
1.1	0	0.411	0.573	0.0129	28.10%	0.0079	0.131	0.155	0.020
1.2	0	0.516	0.364	0.0419	60.13%	0.0053	0.067	0.063	0.010
1.3	0	0.652	0.228	0.0452	84.34%	0.0290	0.112	0.113	0.009
1.4	0	0.780	0.160	0.0442	78.86%	0.0465	0.105	0.094	0.010
1.5	0	0.863	0.132	0.0437	86.05%	0.0750	0.111	0.113	0.012
1.6	0	1.068	0.092	0.0524	86.55%	0.0674	0.072	0.072	0.046
2.1	15	0.413	0.567	0.0251	9.04%	0.0024	0.040	0.097	0.017
2.2	15	0.520	0.358	0.0380	19.87%	0.0024	0.109	0.159	0.018
2.3	15	0.655	0.226	0.0511	42.09%	0.0071	0.141	0.177	0.014
2.4	15	0.751	0.172	0.0521	70.46%	0.0104	0.126	0.130	0.011
2.5	15	0.872	0.130	0.0475	62.48%	0.0210	0.112	0.120	0.009
2.6	15	1.085	0.089	0.0609	67.89%	0.0866	0.091	0.082	0.046
3.1	30	0.414	0.563	0.0205	18.31%	0.0037	0.043	0.075	0.019
3.2	30	0.521	0.356	0.0460	31.18%	0.0017	0.062	0.101	0.014
3.3	30	0.653	0.227	0.0522	27.14%	0.0036	0.100	0.123	0.011
3.4	30	0.749	0.173	0.0416	56.19%	0.0096	0.238	0.253	0.016
3.5	30	0.864	0.132	0.0454	55.46%	0.0174	0.236	0.271	0.012
3.6	30	1.085	0.089	0.0637	71.73%	0.0291	0.131	0.140	0.011
4.1	45	0.412	0.570	0.0249	20.85%	0.0021	0.022	0.038	0.008
4.2	45	0.520	0.358	0.0459	14.59%	0.0023	0.040	0.035	0.012
4.3	45	0.651	0.228	0.0507	32.29%	0.0024	0.062	0.056	0.013
4.4	45	0.759	0.169	0.0580	21.95%	0.0034	0.128	0.121	0.010
4.5	45	0.868	0.130	0.0630	48.13%	0.0026	0.196	0.204	0.011
4.6	45	1.079	0.089	0.0529	86.48%	0.0088	0.207	0.236	0.016

Parameters held constant:

Draft, $h/D=0.735$
 Diameter, $D=0.151$ m
 Slackness, $s/s_0=1.02$
 Water Depth, $d=0.44$ m

Attachment point spacing:
 $n=2$, $b=0.66$ m
 Mass, $m=28.88$ kg

Table 5.1 Summary of experimental results from wave flume tests

TEST NO.	D/L	Kt (%)	Mooring Forces		Non-Dimensional Breakwater Motions			
			Cf		Surge RAO		Heave RAO	Roll RAO
			Upstream	Downstream	Offset/(H/2)	Amp/(H/2)	Amp/(H/2)	rads*D/H
1.1	0.329	69.7%	n/a	n/a	1.16	0.17	0.57	0.98
1.2	0.230	67.0%	n/a	n/a	0.73	0.71	1.69	1.13
1.3	0.174	92.3%	n/a	n/a	0.11	0.90	1.46	0.59
1.4	0.139	104.8%	n/a	n/a	0.13	1.11	1.26	0.70
1.5	0.116	101.1%	n/a	n/a	0.09	1.03	1.16	0.48
1.6	0.100	105.3%	n/a	n/a	0.07	1.15	1.07	0.35
1.7	0.088	102.7%	n/a	n/a	0.05	1.38	1.27	0.32
1.8	0.079	94.4%	n/a	n/a	0.05	1.36	1.01	0.21
2.1	0.329	47.9%	0.36	0.46	0.03	0.47	0.90	0.50
2.2	0.230	49.2%	0.45	0.38	0.04	0.50	1.32	0.70
2.3	0.174	81.6%	0.38	0.39	-0.10	0.77	1.08	0.79
2.4	0.139	80.4%	0.37	0.44	-0.05	0.90	1.02	0.86
2.5	0.116	90.4%	0.40	0.41	-0.13	1.15	1.03	1.28
2.6	0.100	81.8%	0.43	0.58	-0.16	1.49	1.09	1.59
2.7	0.088	114.0%	0.73	0.85	-0.21	1.88	1.28	1.84
2.8	0.079	99.5%	0.65	0.70	-0.15	1.71	1.27	1.90
3.1	0.174	83.8%	0.34	0.38	-0.06	0.74	1.07	0.74
3.2	0.174	81.3%	0.34	0.39	-0.01	0.72	1.09	0.76
3.3	0.174	79.9%	0.34	0.38	-0.01	0.68	1.08	0.78
3.4	0.174	81.3%	0.37	0.38	0.00	0.70	1.14	0.80
3.5	0.116	86.5%	0.29	0.49	-0.03	1.17	1.02	1.25
3.6	0.116	86.3%	0.31	0.51	-0.04	1.14	1.06	1.28
3.7	0.116	89.1%	0.31	0.49	-0.05	1.13	1.05	1.39
3.8	0.116	94.2%	0.33	0.49	-0.06	1.25	1.18	1.38
4.1	0.230	51.3%	0.45	0.38	0.04	0.50	1.32	0.70
4.2	0.174	77.7%	0.38	0.39	-0.10	0.77	1.08	0.79
4.3	0.139	77.3%	0.37	0.44	-0.05	0.90	1.02	0.86
4.4	0.116	94.8%	0.40	0.41	-0.13	1.15	1.03	1.28
4.5	0.230	70.9%	0.48	0.22	0.09	0.60	0.83	0.62
4.6	0.174	73.8%	0.52	0.36	0.02	0.77	1.31	1.00
4.7	0.139	81.5%	0.36	0.52	-0.01	0.82	1.21	0.81
4.8	0.116	93.5%	0.34	0.51	-0.07	1.02	1.20	1.12
4.9	0.230	90.0%	0.23	0.21	-0.03	0.53	0.28	0.59
4.10	0.174	81.8%	0.29	0.27	-0.02	0.61	0.56	0.71
4.11	0.139	86.9%	0.50	0.46	-0.03	0.79	1.43	0.86
4.12	0.116	92.0%	0.45	0.48	-0.08	0.87	1.23	1.02
4.13	0.230	91.5%	0.19	0.28	0.01	0.54	0.14	0.60
4.14	0.174	92.2%	0.23	0.31	-0.01	0.64	0.26	0.60
4.15	0.139	95.1%	0.32	0.36	-0.01	0.79	0.33	0.74
4.16	0.116	89.7%	0.39	0.34	0.01	0.92	0.58	0.81
5.1	0.174	82.3%	0.41	0.36	0.00	0.72	1.20	0.82
5.2	0.116	91.8%	0.30	0.59	-0.03	1.20	1.09	0.98
5.3	0.174	84.4%	0.34	0.24	0.06	0.73	1.13	0.75
5.4	0.116	95.8%	0.24	0.32	0.00	1.14	1.04	1.11
5.5	0.174	78.3%	0.69	0.57	-0.05	0.83	0.83	1.09
5.6	0.116	82.8%	0.75	0.75	-0.13	1.35	1.05	1.29

Table 5.1 Summary of experimental results from wave flume tests (cont.)

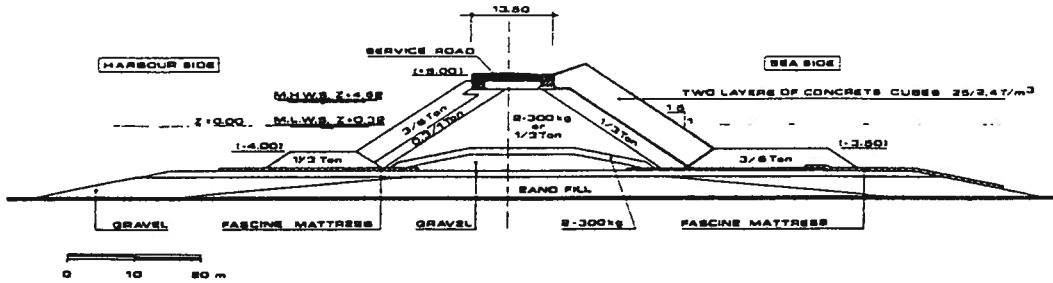
TEST NO.	D/L	Kt (%)	Mooring Forces		Non-Dimensional Breakwater Motions			
			Cf		Surge RAO		Heave RAO	Roll RAO
			Upstream	Downstream	Offset/(H/2)	Amp/(H/2)	Amp/(H/2)	rads*D/H
6.1	0.174	92.3%	n/a	n/a	0.11	0.90	1.46	0.59
6.2	0.116	101.1%	n/a	n/a	0.09	1.03	1.16	0.48
6.3	0.174	72.0%	1.57	1.65	0.05	0.48	1.18	0.77
6.4	0.116	87.6%	0.79	2.28	0.04	1.11	1.10	1.03
6.5	0.174	89.4%	1.32	1.46	0.00	0.69	0.78	0.82
6.6	0.116	95.2%	1.85	1.80	-0.02	0.99	0.76	1.27
6.7	0.174	81.6%	1.22	0.64	0.09	0.71	1.36	0.69
6.8	0.116	90.5%	0.96	1.41	0.03	1.03	1.08	0.66
7.1	0.518	30.7%	0.00	0.00	0.66	0.06	0.10	0.29
7.2	0.408	61.9%	0.00	0.00	0.43	0.14	0.32	0.64
7.3	0.330	61.4%	0.00	0.00	0.47	0.21	0.55	0.89
7.4	0.230	38.9%	0.60	0.06	0.50	0.38	1.46	1.07
7.5	0.173	76.8%	1.36	0.90	0.09	0.63	1.28	0.61
8.1	0.518	34.3%	0.00	0.11	-0.01	0.14	0.08	0.32
8.2	0.408	55.0%	0.05	0.15	-0.02	0.35	0.39	0.41
8.3	0.330	47.0%	0.20	0.21	0.01	0.47	0.74	0.51
8.4	0.230	52.7%	0.42	0.28	0.19	0.54	1.35	0.70
8.5	0.173	84.0%	0.42	0.36	0.00	0.69	1.11	0.79
9.1	0.518	36.6%	0.00	0.00	0.51	0.08	0.08	0.27
9.2	0.330	59.6%	0.00	0.00	0.67	0.29	0.57	0.91
9.3	0.230	46.0%	1.45	0.06	-0.09	0.95	1.43	1.29
9.4	0.518	32.5%	0.00	0.00	0.50	0.30	0.24	0.32
9.5	0.330	58.7%	0.00	0.00	0.47	0.26	0.55	0.79
9.6	0.230	39.3%	0.22	0.04	0.63	0.35	1.39	0.95

Table 5.2 Estimation of natural frequencies in heave

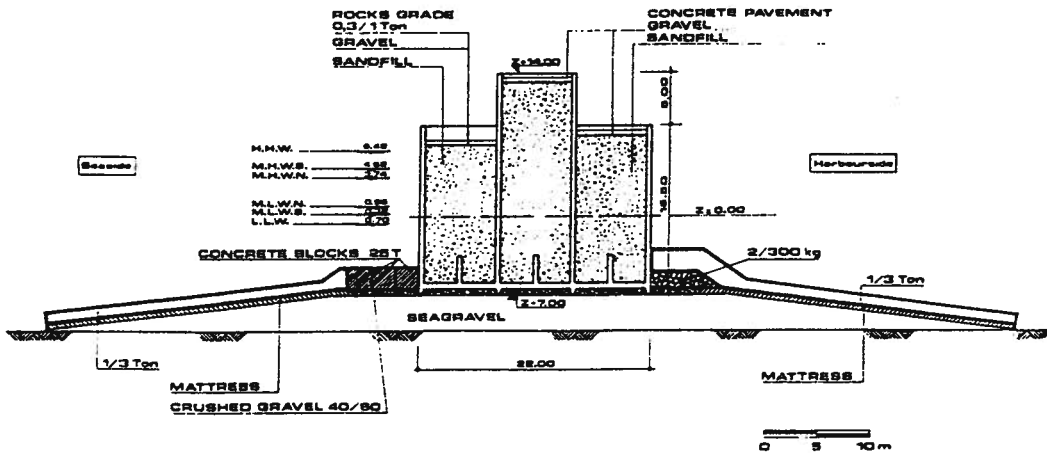
Draft Ratio h/D	Non-dim. stiffness k/ρglD	Non-dim. mass m/ρAl*	Added Mass † non-dim. by ρAl*	$\omega^2/(g/(\pi D/4))$	Natural Frequencies (Hz)		
					Prototype D=3.21 m	Kl=1:10 D=0.321 m	Kl=1:21.4 D=0.151m
0.500	1.000	0.500	0.325	1.212	0.346	1.093	1.594
0.550	0.995	0.564	0.366	1.070	0.325	1.027	1.497
0.579	0.987	0.600	0.390	0.997	0.313	0.991	1.445
0.650	0.954	0.688	0.447	0.840	0.288	0.910	1.327
0.700	0.917	0.748	0.486	0.743	0.271	0.856	1.248
0.735	0.883	0.788	0.512	0.679	0.259	0.818	1.193
0.800	0.800	0.858	0.557	0.565	0.236	0.746	1.088
0.850	0.714	0.906	0.589	0.478	0.217	0.686	1.001
0.900	0.600	0.948	0.616	0.384	0.194	0.615	0.897
0.950	0.436	0.981	0.638	0.269	0.163	0.515	0.751
1.000	0.000	1.000	0.650	0.000	0.000	0.000	0.000

*here ρ is water density, A is cross-sectional area of cylinder, l is length of cylinder

†added mass extrapolated from Vugts (1968)



(a) rubble mound breakwater



(b) caisson breakwater

Fig. 1.1 Cross-sections of typical bottom founded breakwaters, [25].

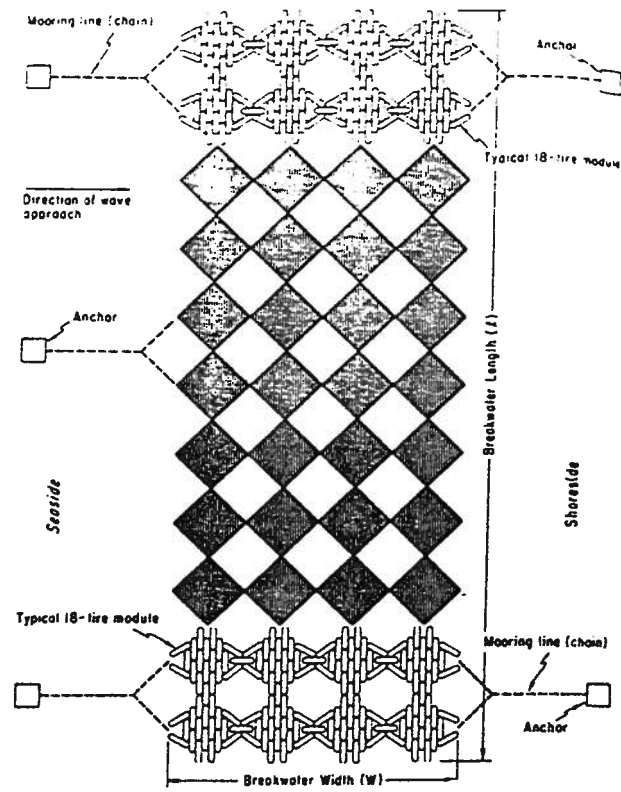


Fig. 1.2 Floating tire breakwater, [7].

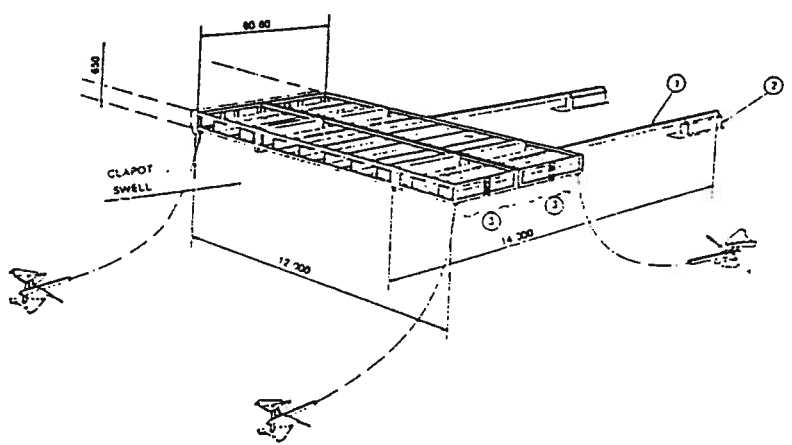


Fig. 1.3 Equiport breakwater, [27].

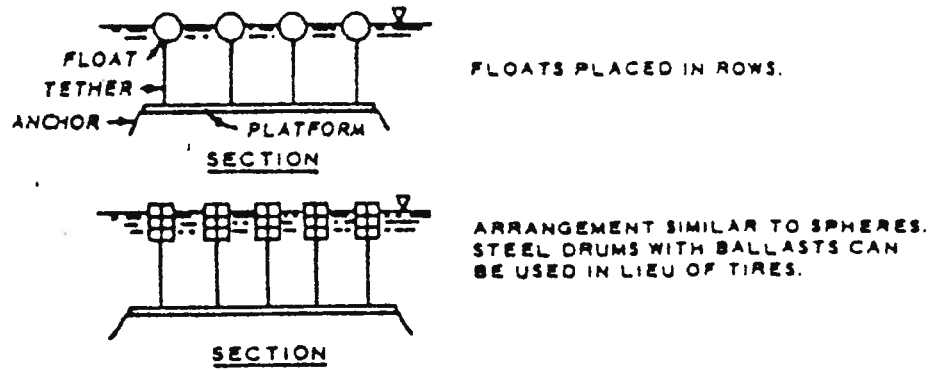


Fig. 1.4 Tethered float breakwaters, [14].

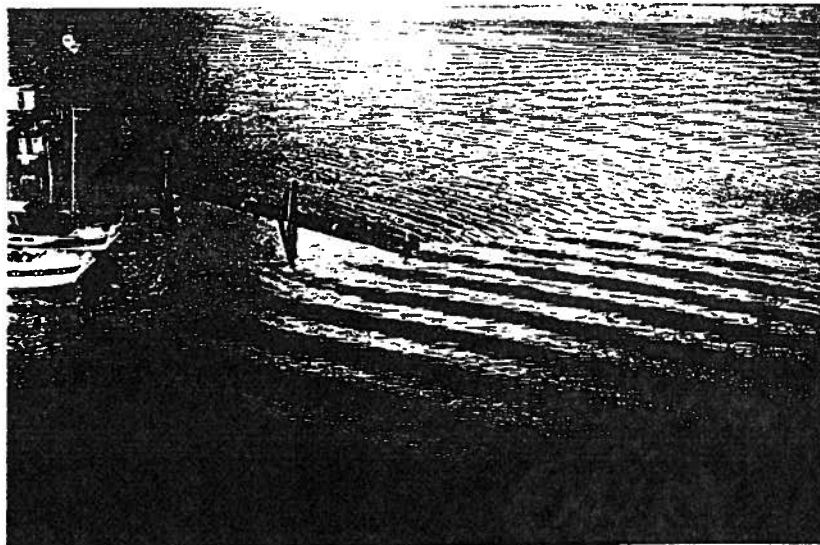


Fig. 1.5 Log bundle floating breakwater, [4].

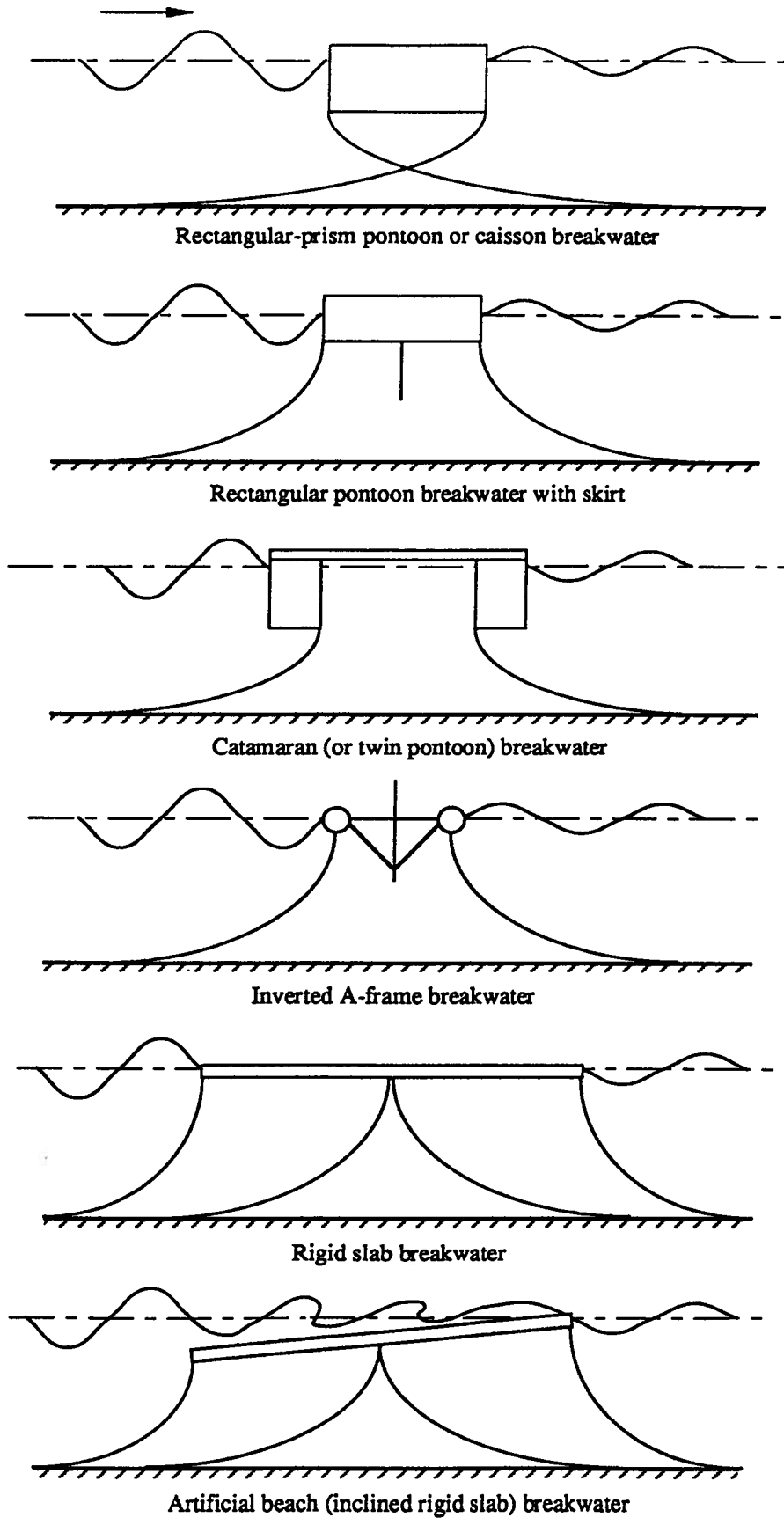
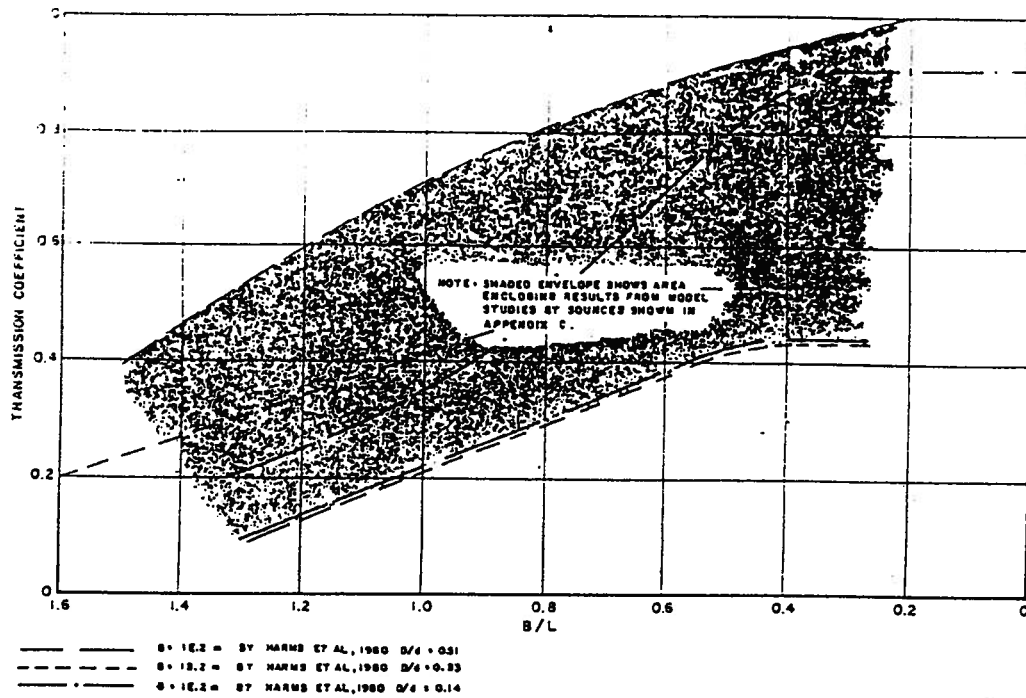
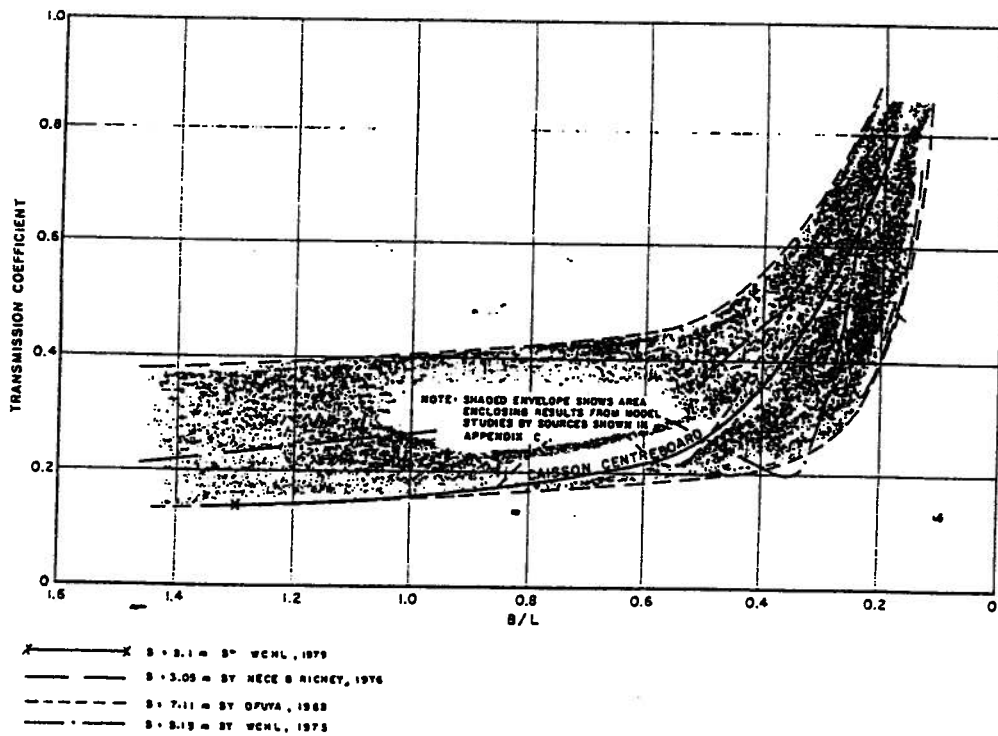


Fig. 1.6 Various reflective floating breakwater cross-sectional geometries.



(a) floating tire breakwaters



(b) floating rectangular caisson breakwaters

Fig. 1.7 Comparison of transmissibility of rectangular caisson and tire breakwaters, [12].

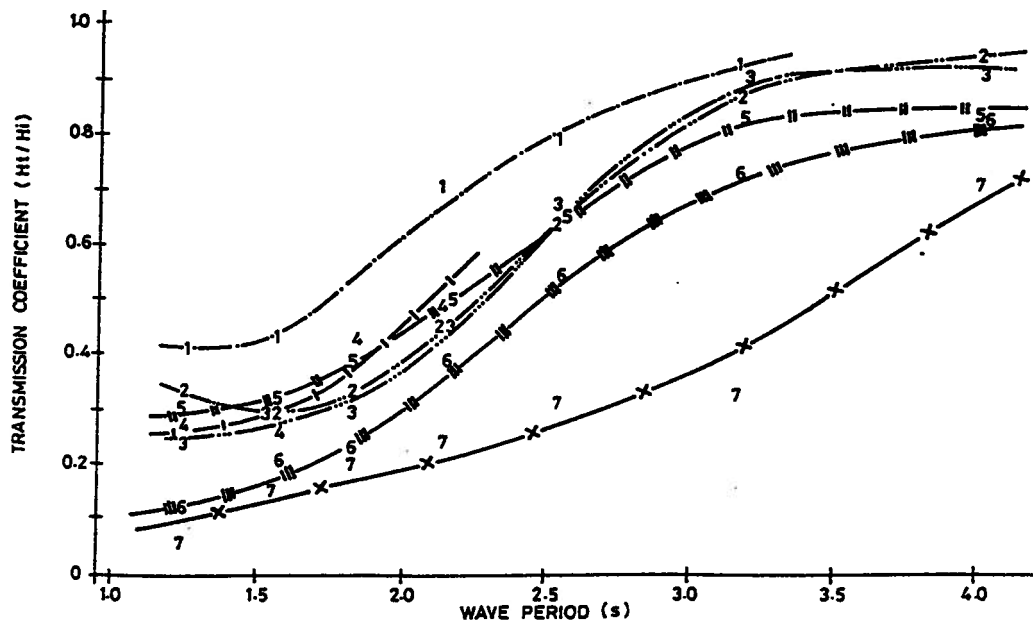
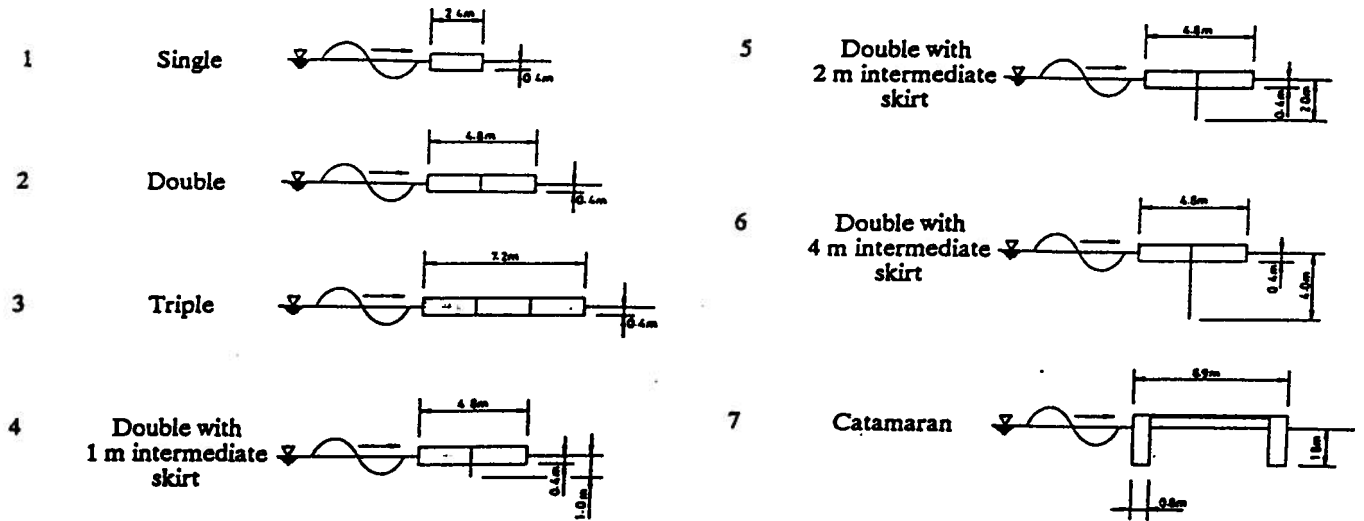


Fig. 1.8 Comparison of transmissibility of various caisson breakwater types, [3].

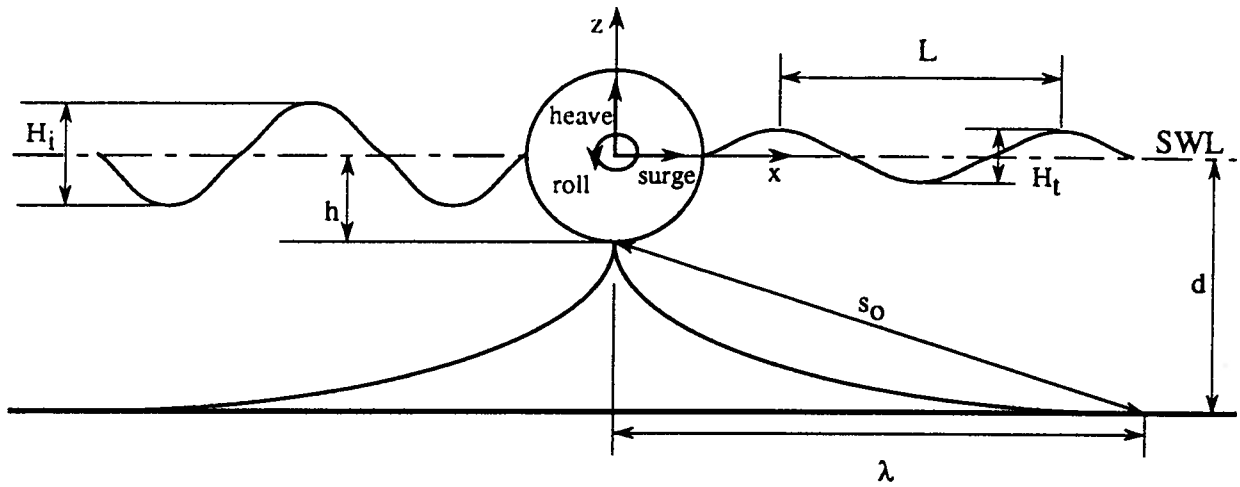


Fig. 2.1 Definition of design parameters for proposed breakwater system.

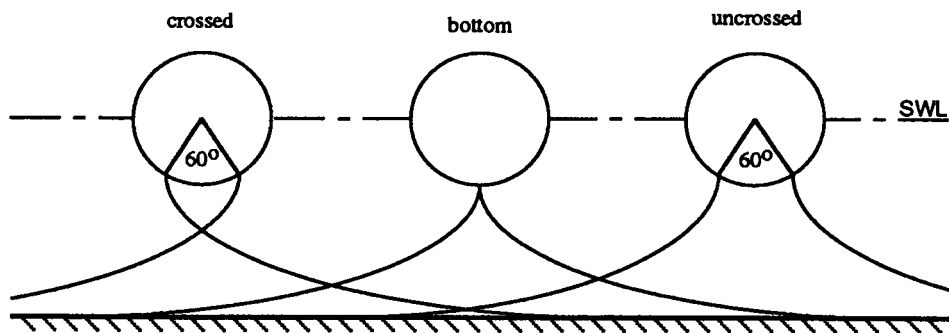


Fig. 2.2 Mooring line attachment point arrangements.

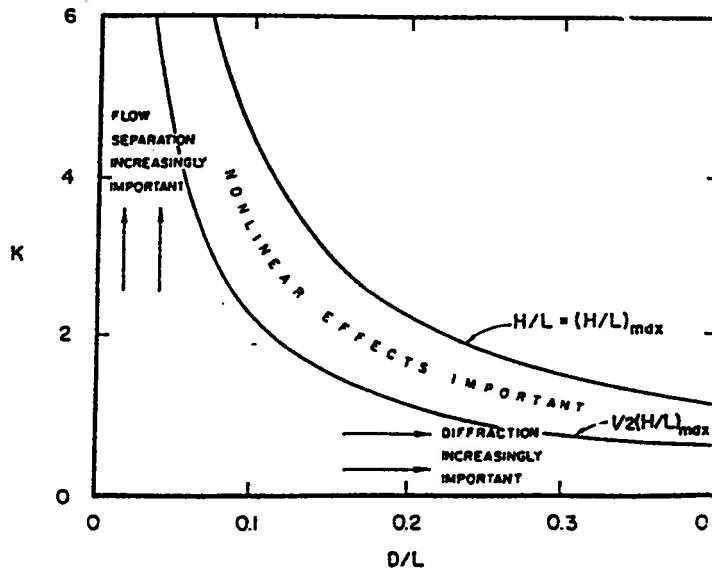


Fig. 2.3 Importance of inertial and viscous effects, [24].

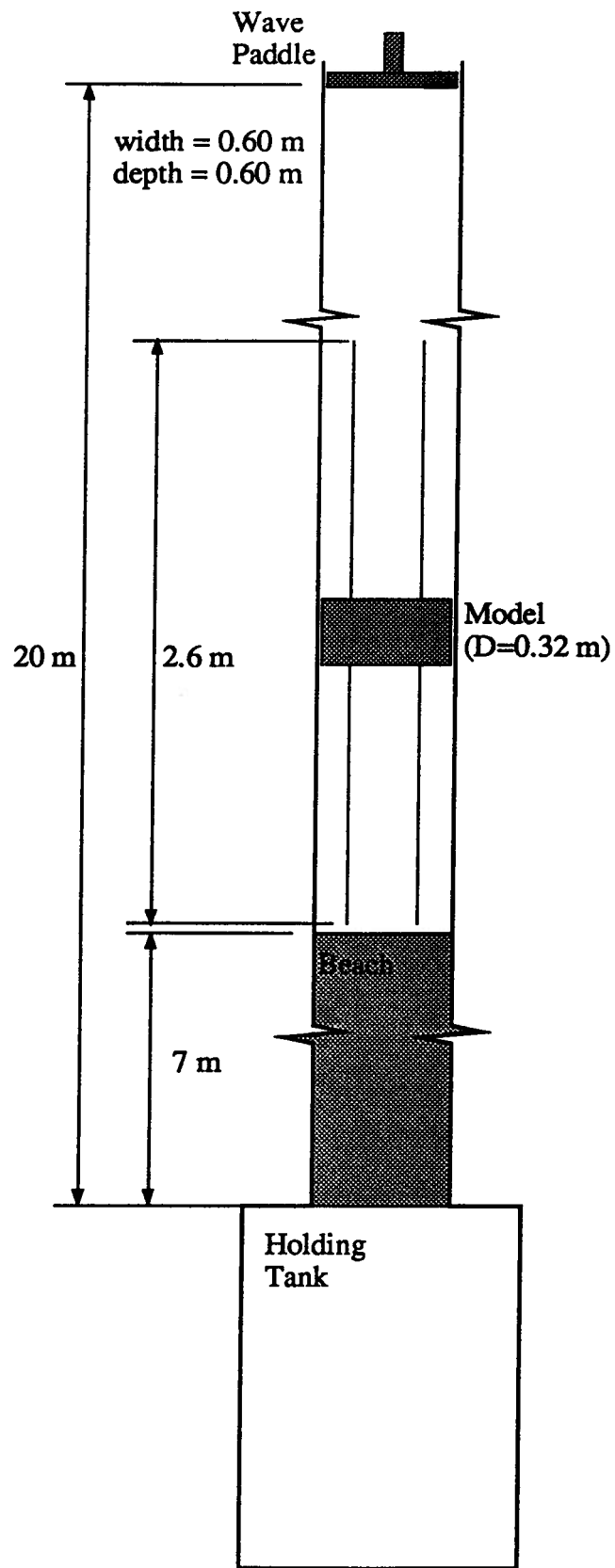


Fig. 3.1 Experimental set-up used in wave flume tests.

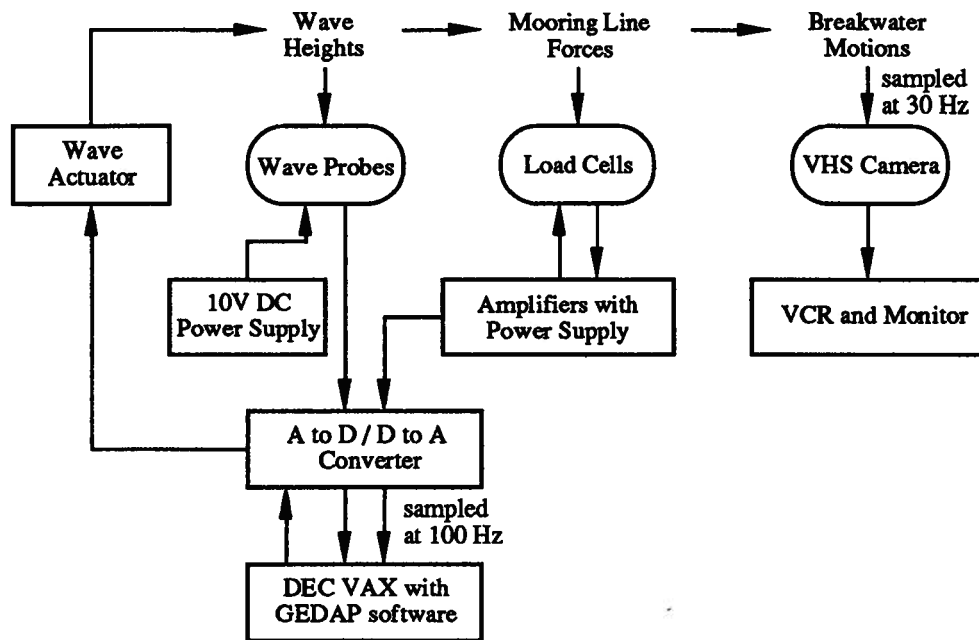


Fig. 3.2 Schematic layout of wave generation and data collection hardware.

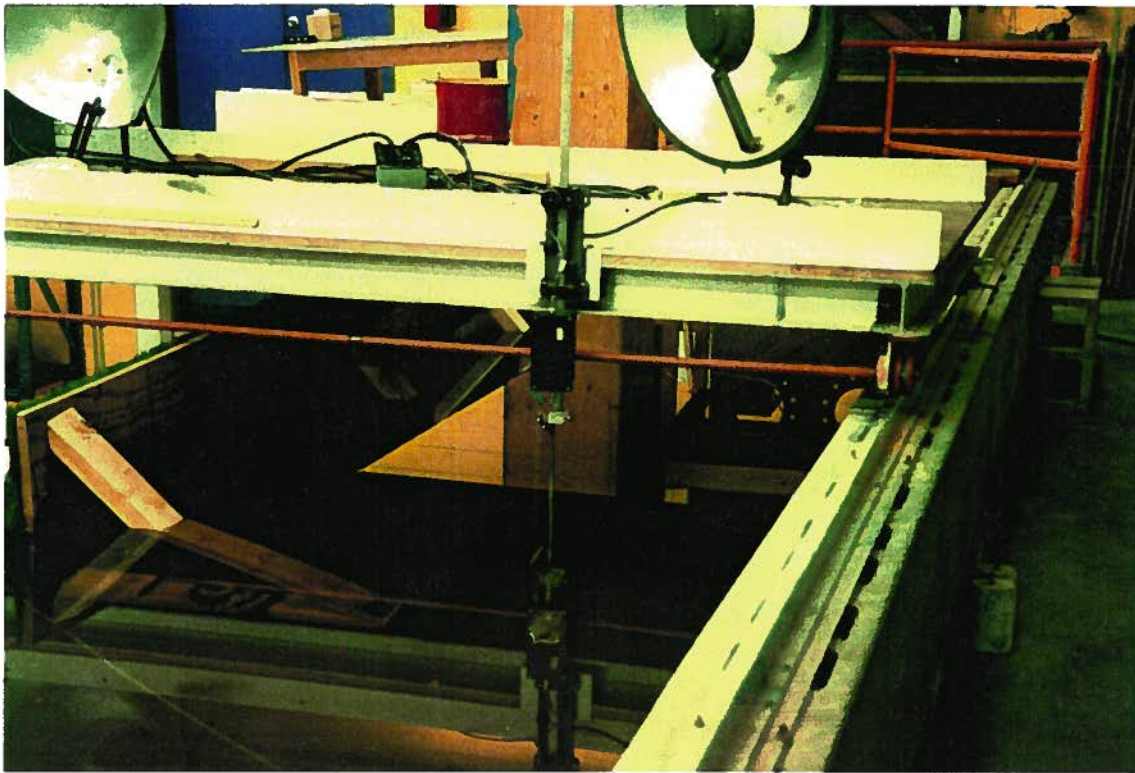


Fig. 3.3 Photograph of wave probes.

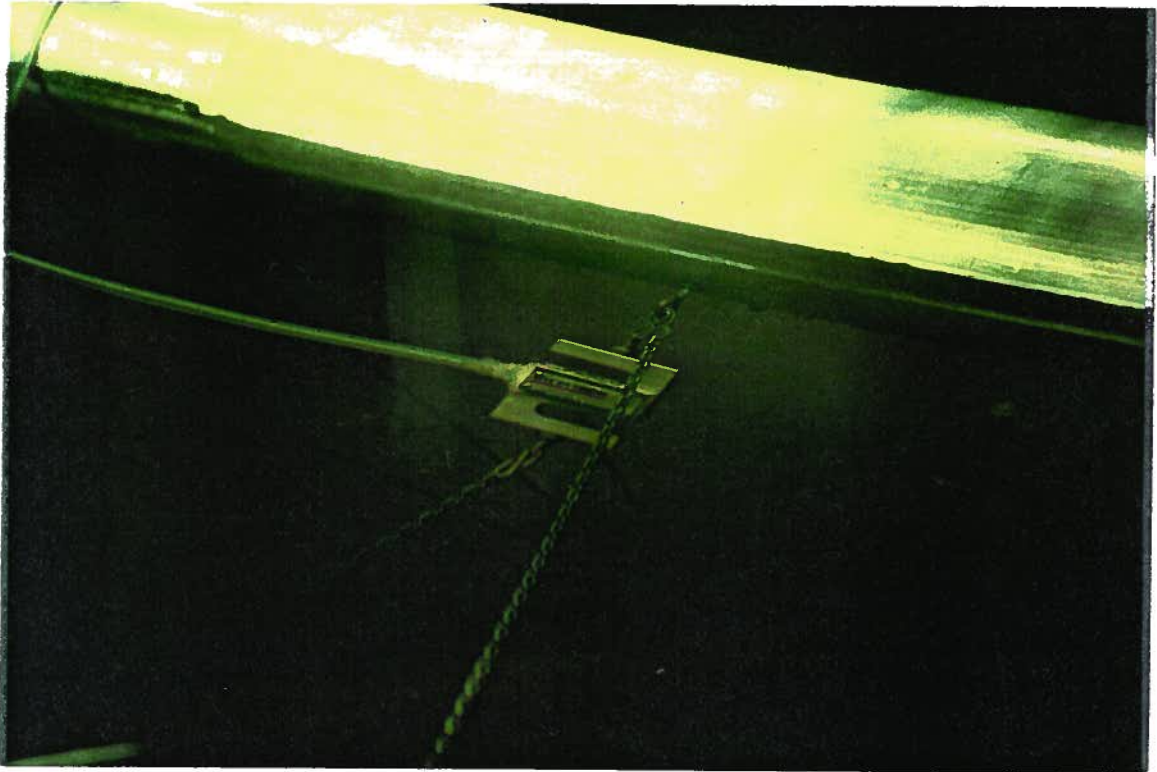


Fig. 3.4 Photograph of a load cell.

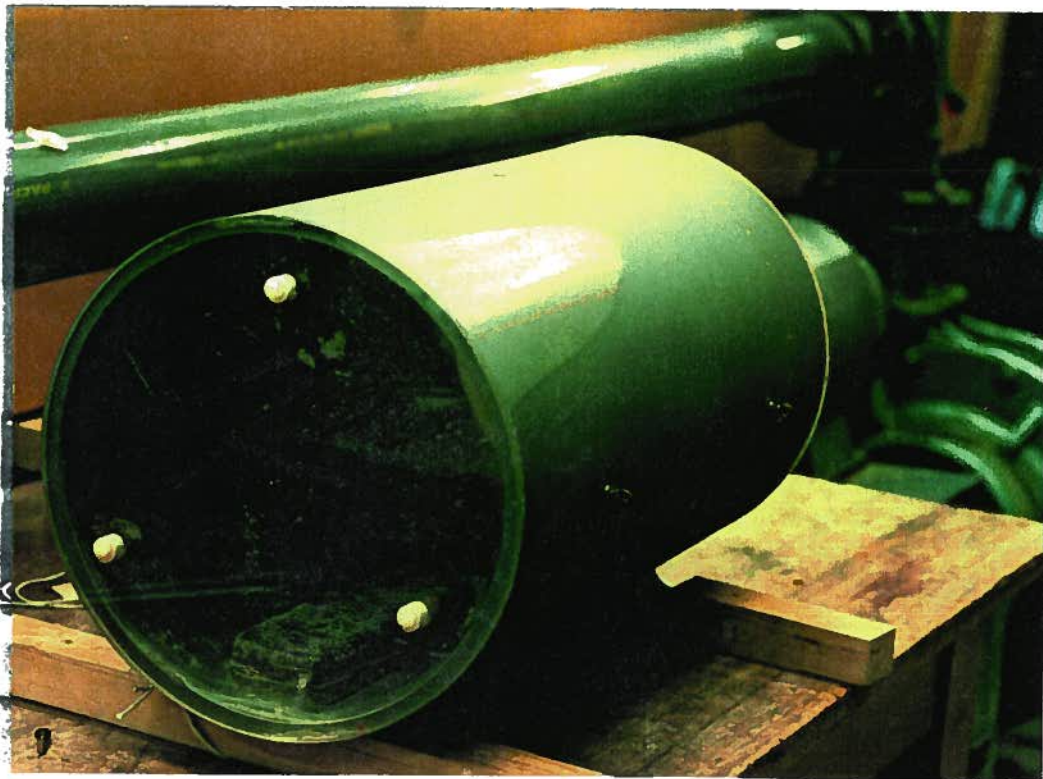


Fig. 3.5 Photograph of model breakwater used in wave flume tests.

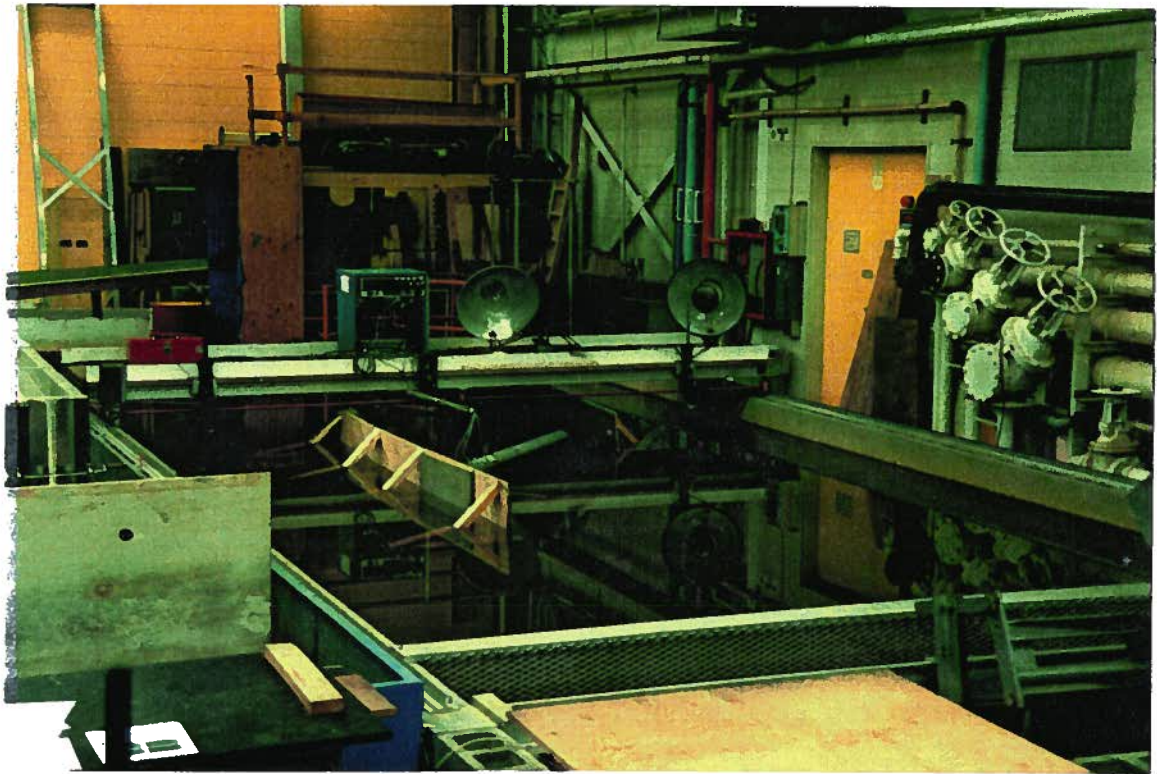


Fig. 4.1 Photograph of wave basin.

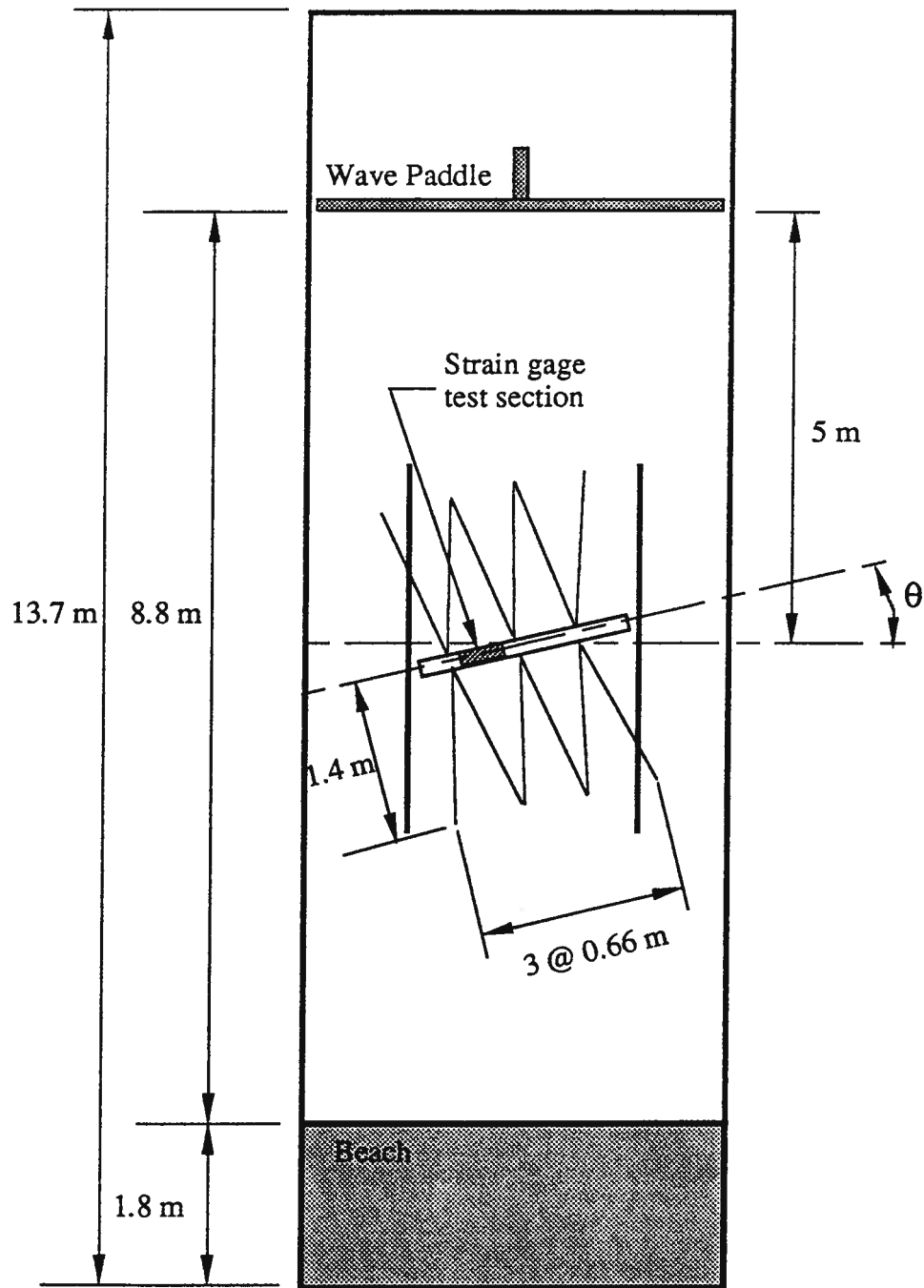


Fig. 4.2 Experimental set-up used in wave basin tests.

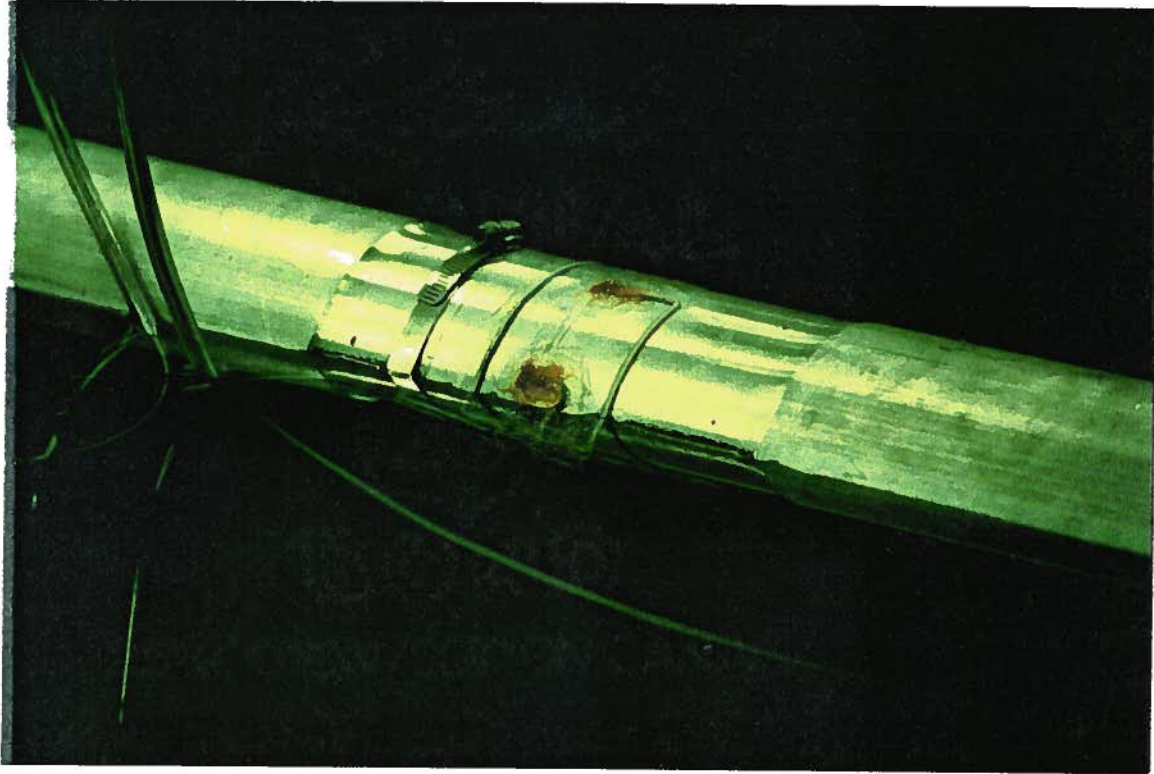


Fig. 4.3 Arrangement of strain gages.

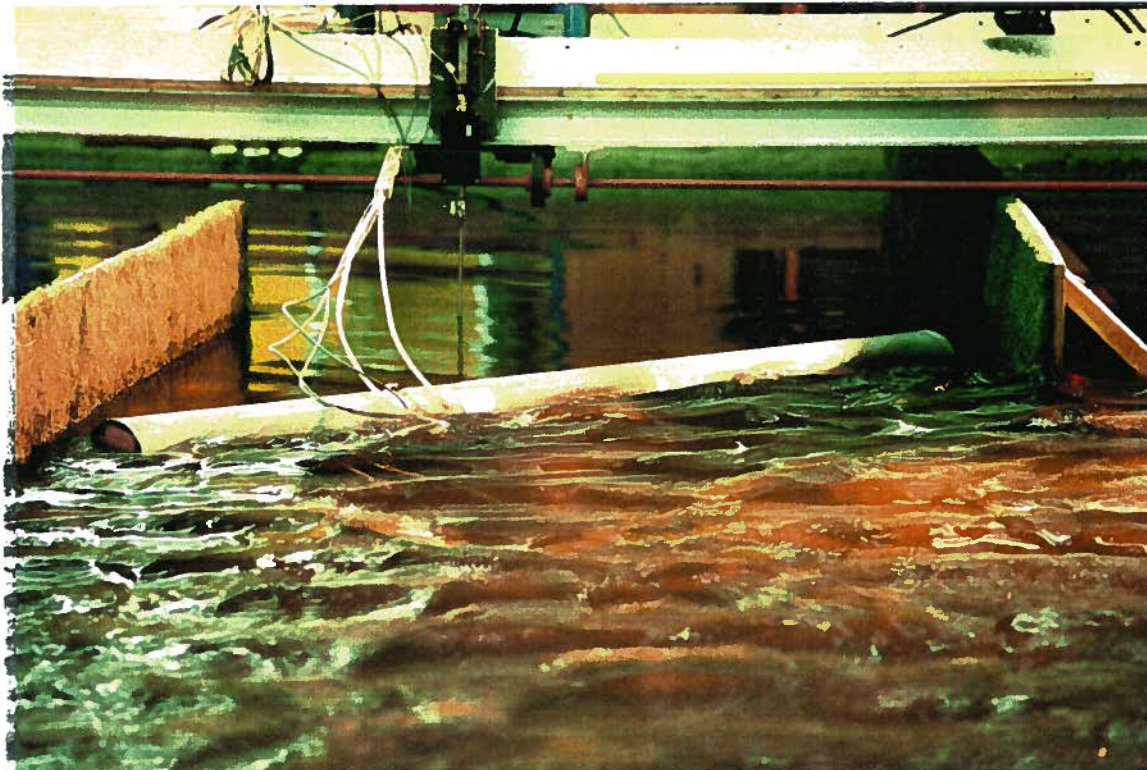


Fig. 4.4 Photograph of model breakwater used in wave basin tests.

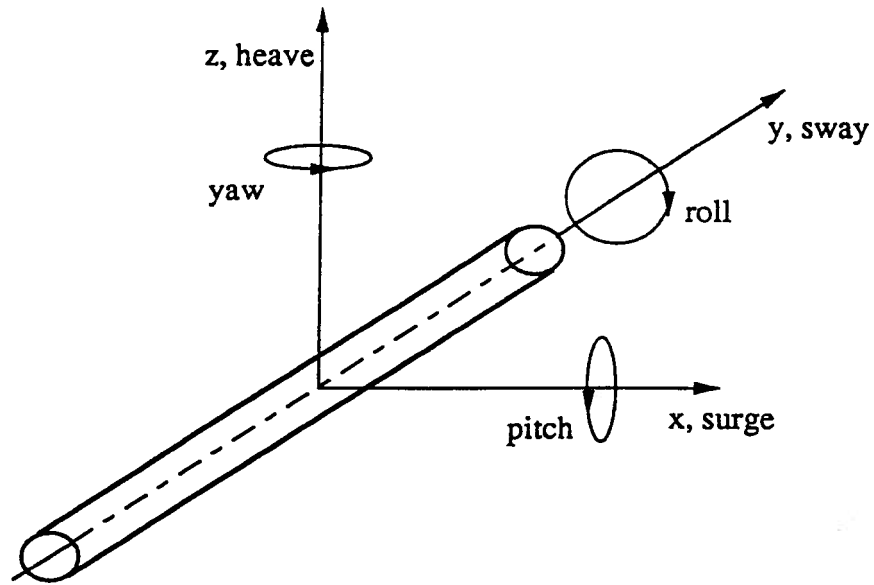


Fig. 5.1 Definition sketch for six degrees of freedom.

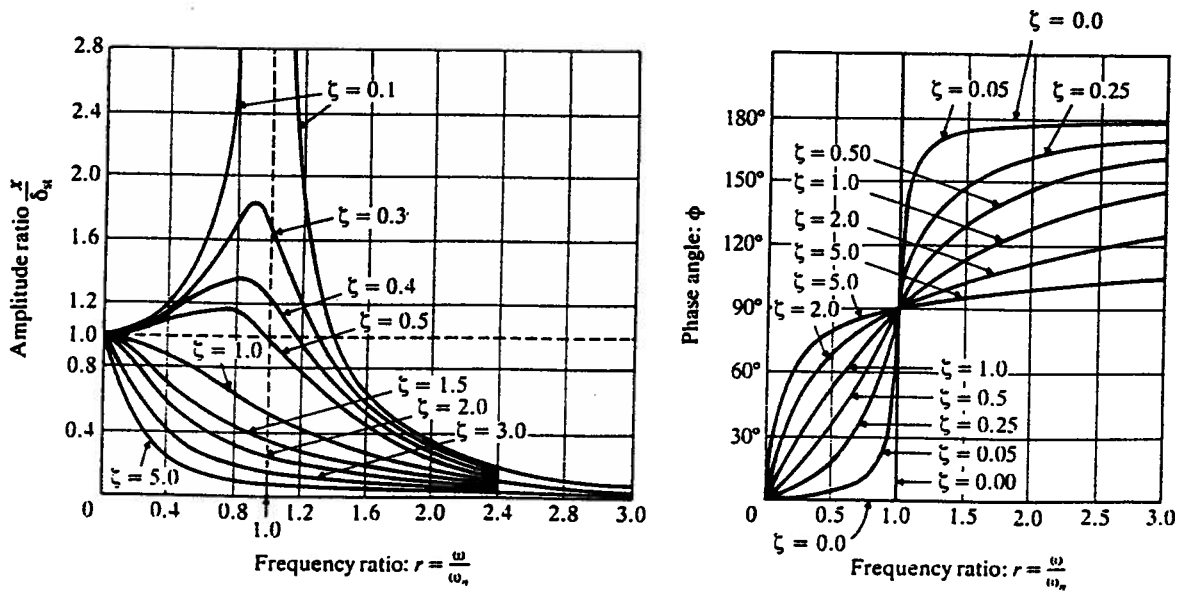


Fig. 5.2 Response of a SDOF system to periodic forcing, [23].

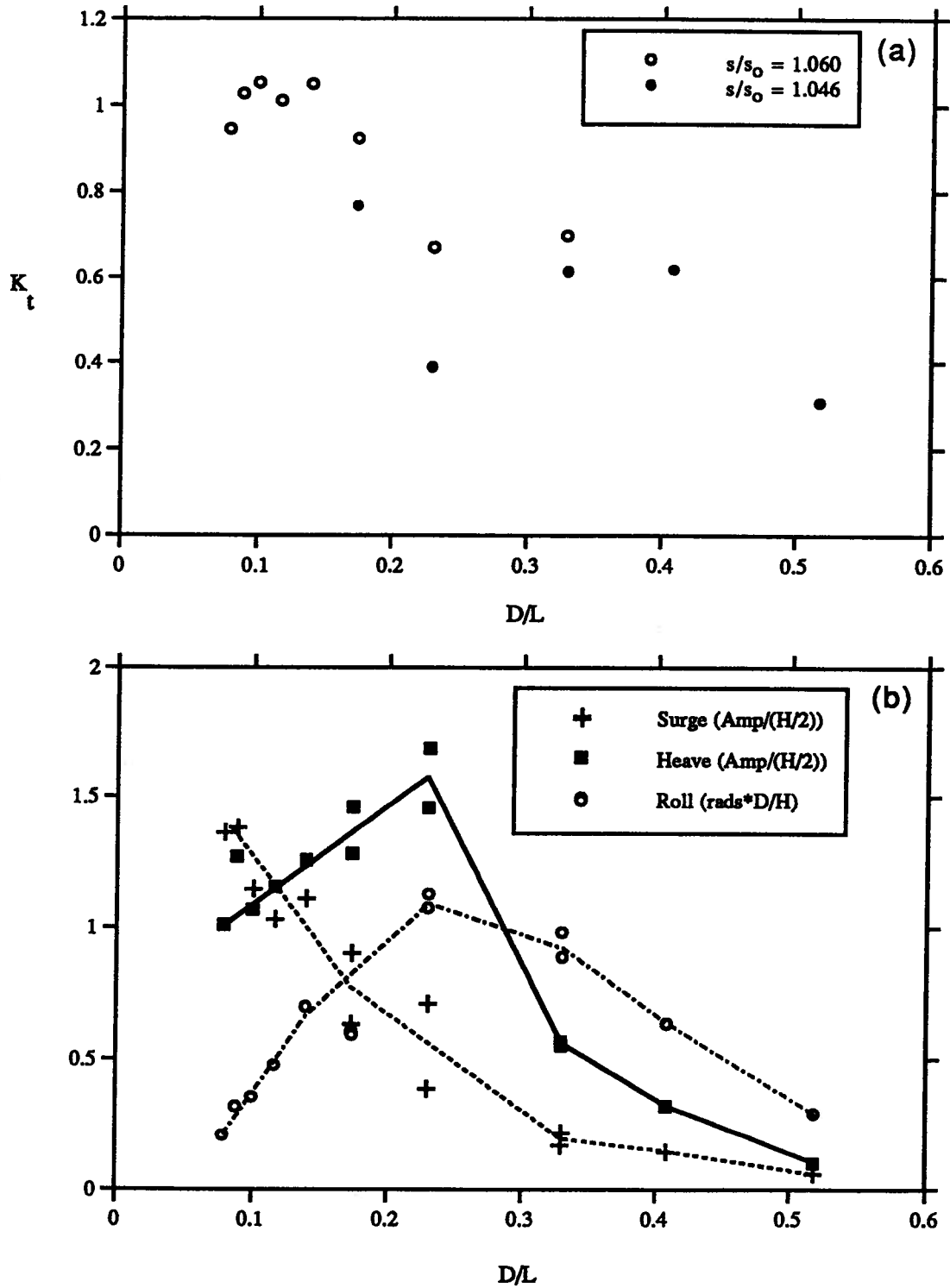


Fig. 5.3 Wave flume test results for base case with chain. (a) transmission coefficient, (b) motion amplitudes.

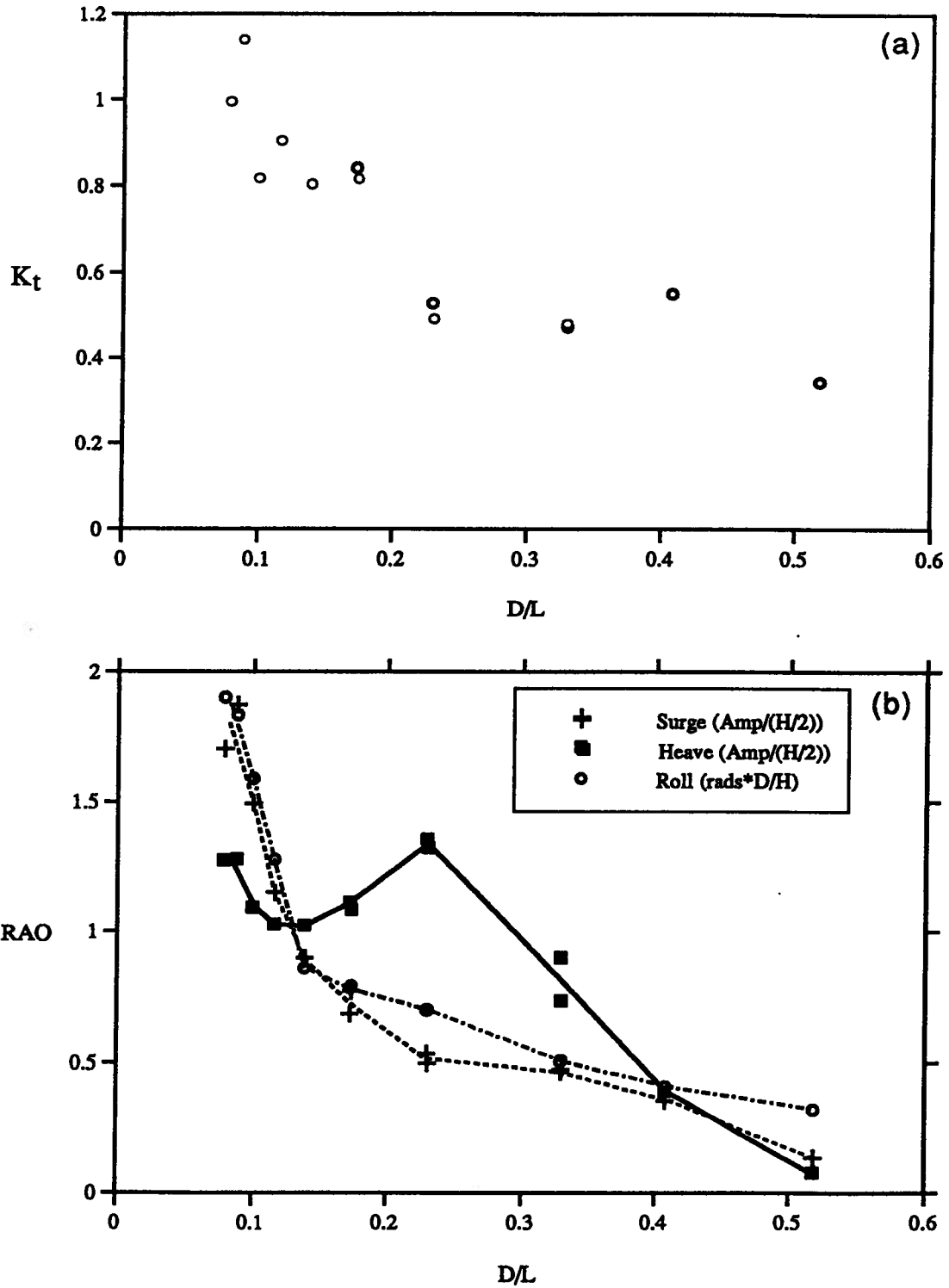


Fig. 5.4 Wave flume test results for base case with nylon moorings. (a) transmission coefficient, (b) motion amplitudes.

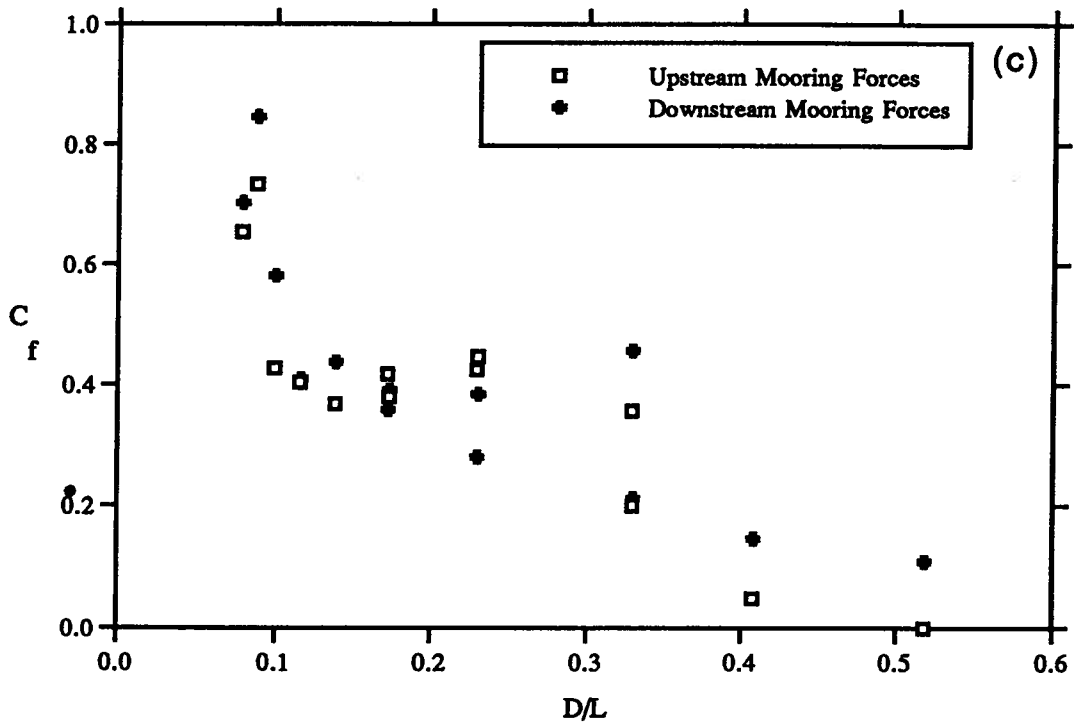


Fig. 5.4 Wave flume test results for base case with nylon moorings (cont.).
 (c) mooring line forces.

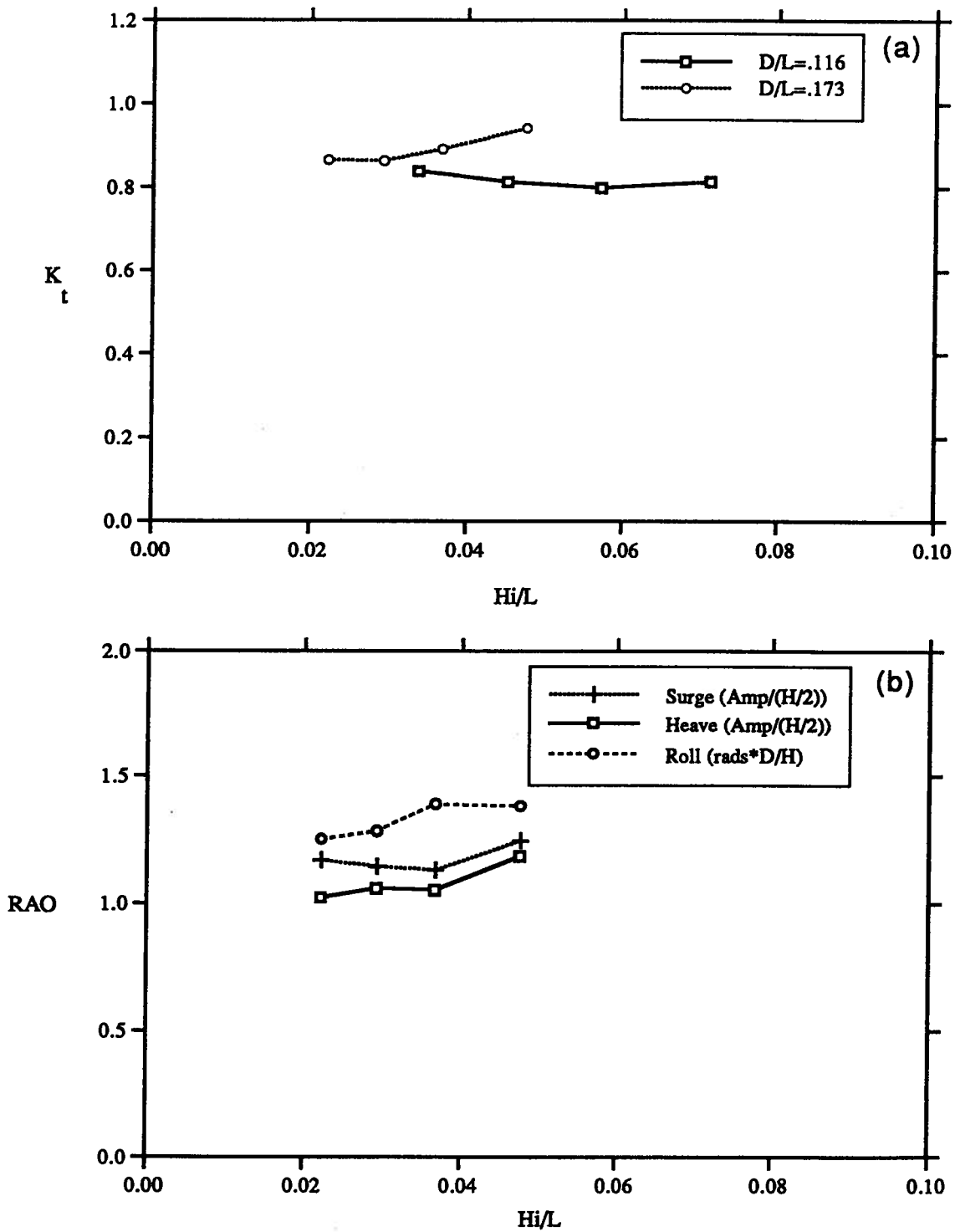


Fig. 5.5 Wave flume test results showing the influence of wave steepness H/L for the case of nylon mooring lines. (a) transmission coefficient for $D/L = 0.116$ and 0.173 , (b) motion amplitudes for $D/L = 0.116$.

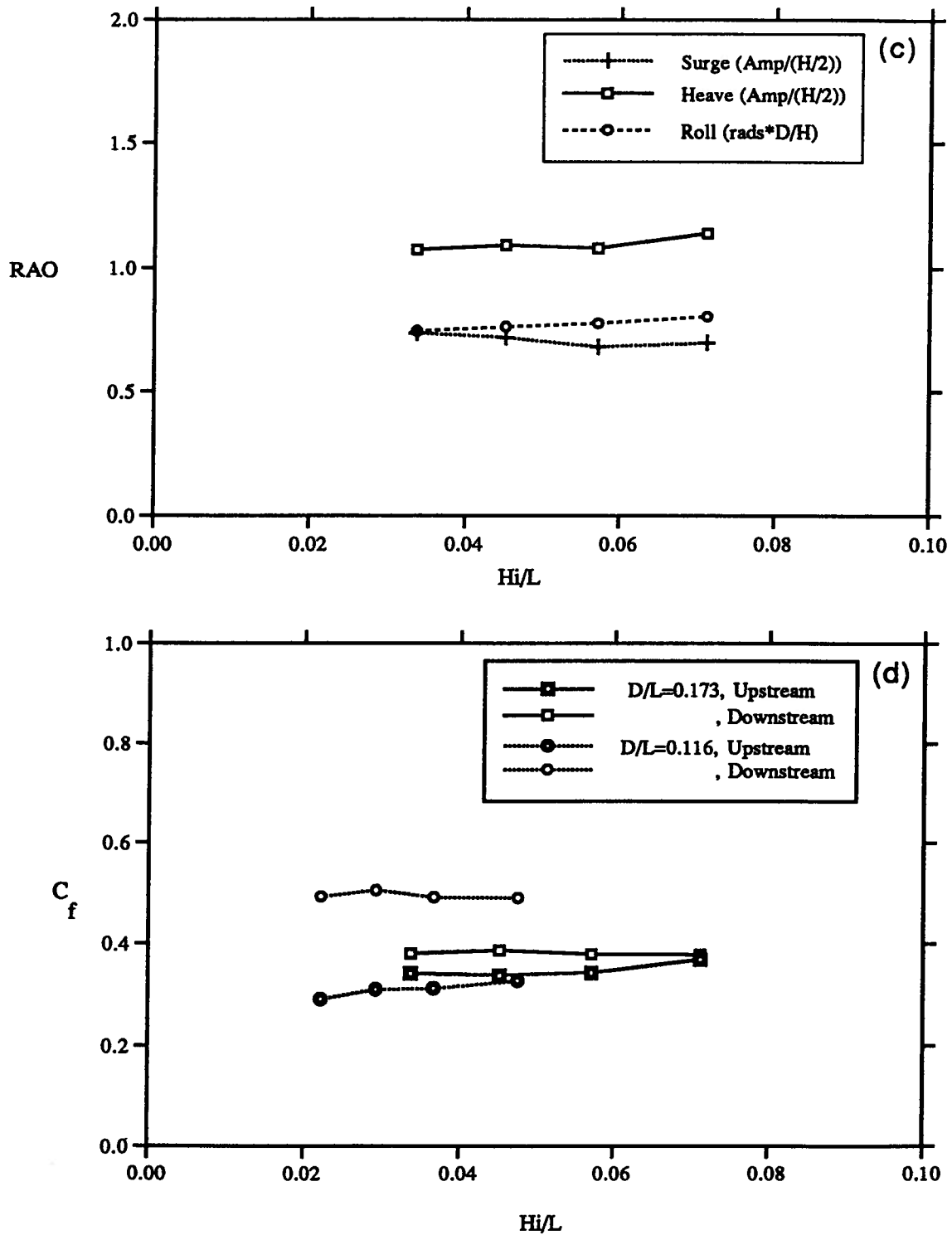


Fig. 5.5 Wave flume test results showing the influence of wave steepness H/L for the case of nylon mooring lines (cont.). (c) motion amplitudes for $D/L = 0.173$, (d) mooring line forces for $D/L = 0.116$ and 0.173 .

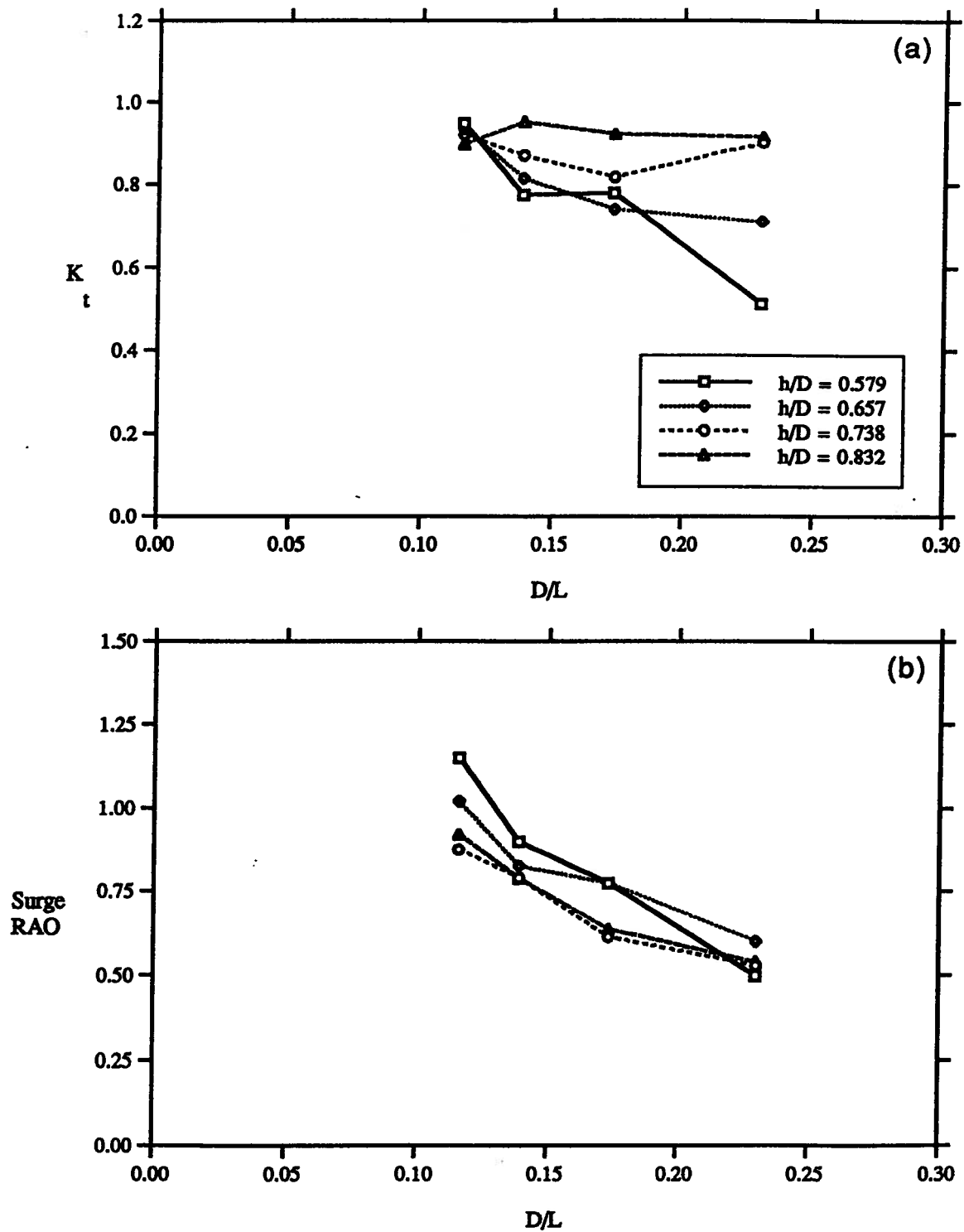


Fig. 5.6 Wave flume test results showing the influence of relative draft h/D for the case of nylon mooring lines. (a) transmission coefficient, (b) surge RAO.

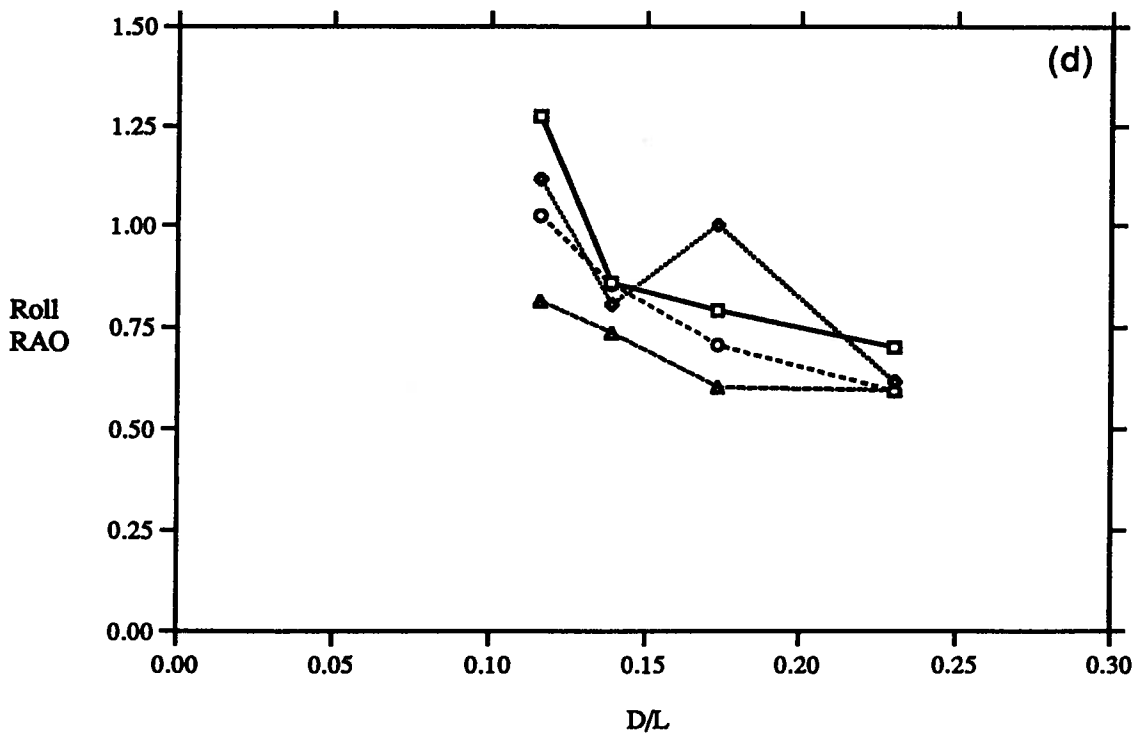
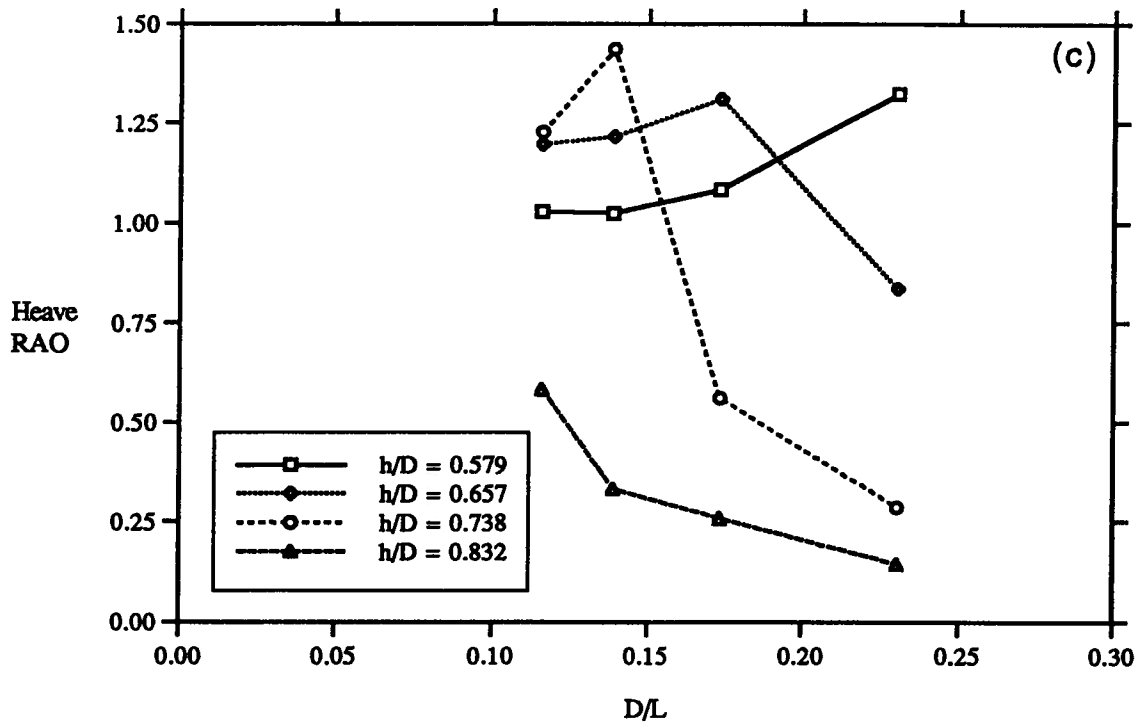


Fig. 5.6 Wave flume test results showing the influence of relative draft h/D for the case of nylon mooring lines (cont.). (c) heave RAO, (d) roll RAO.

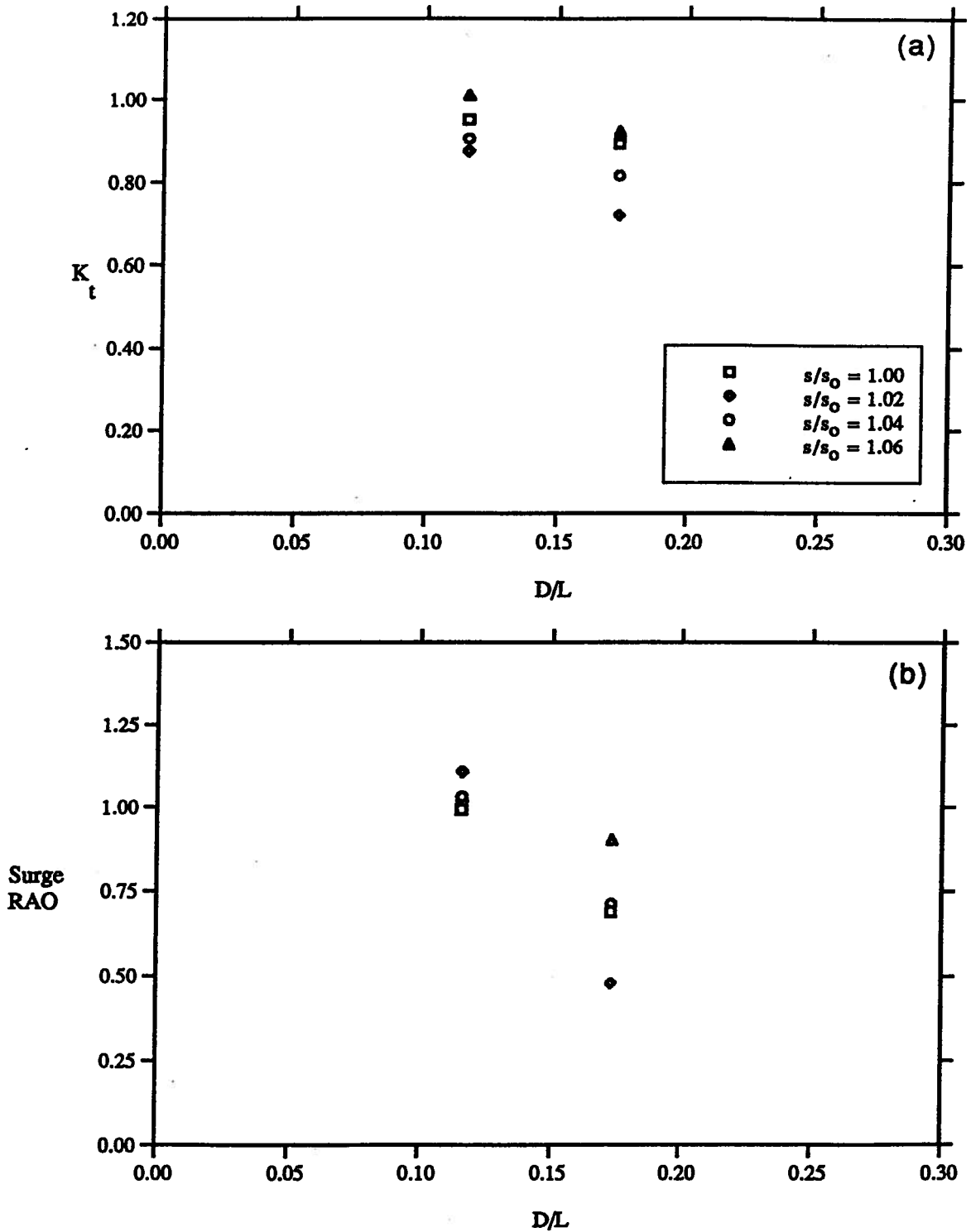


Fig. 5.7 Wave flume test results showing the influence of line slackness, s/s_0 for the case of chain mooring lines. (a) transmission coefficient, (b) surge RAO.

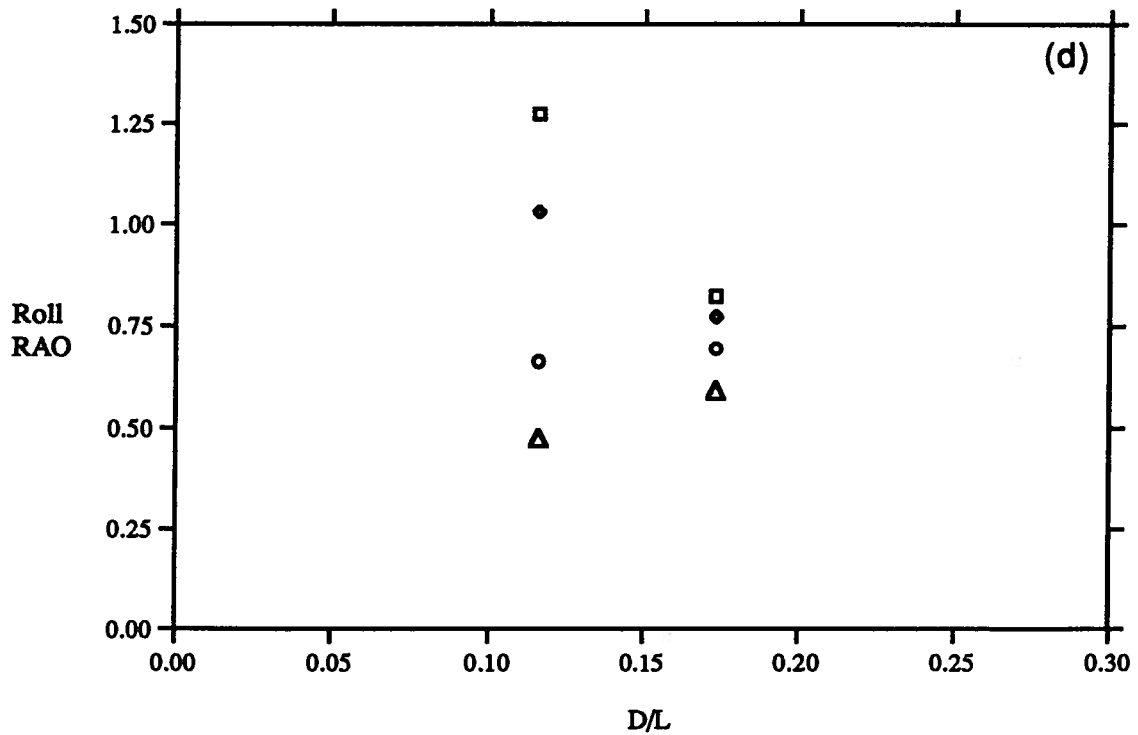
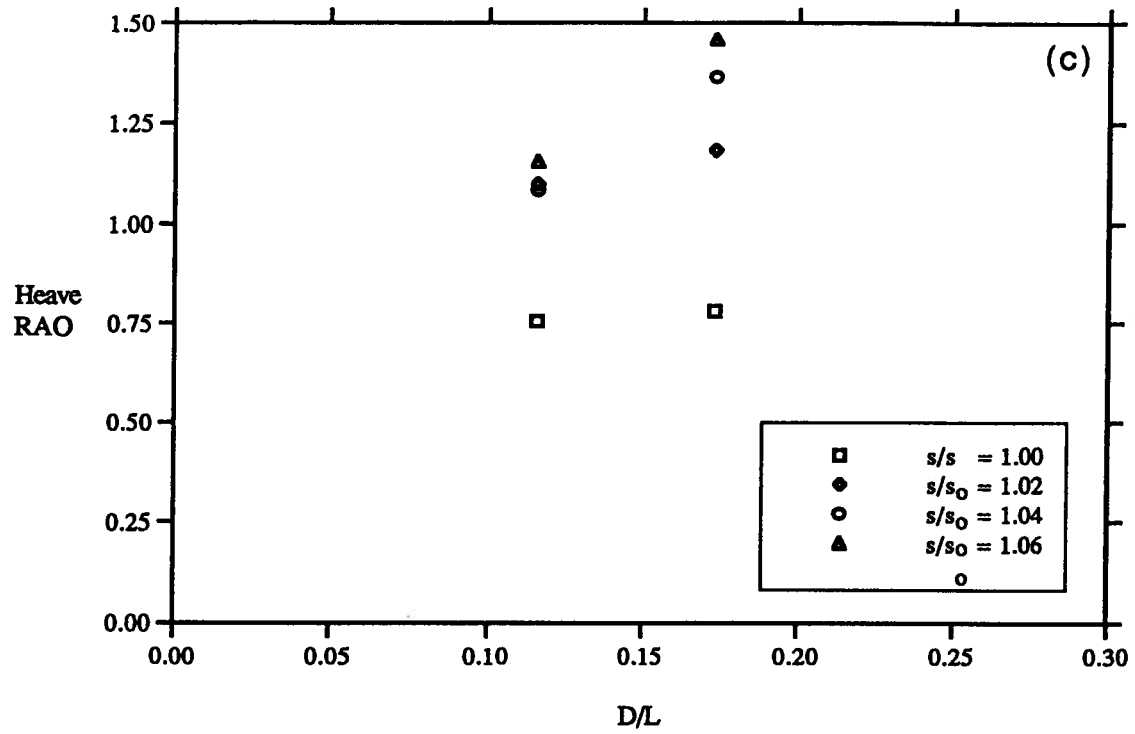


Fig. 5.7 Wave flume test results showing the influence of line slackness, s/s_0 for the case of chain mooring lines (cont.). (c) heave RAO, (d) roll RAO.

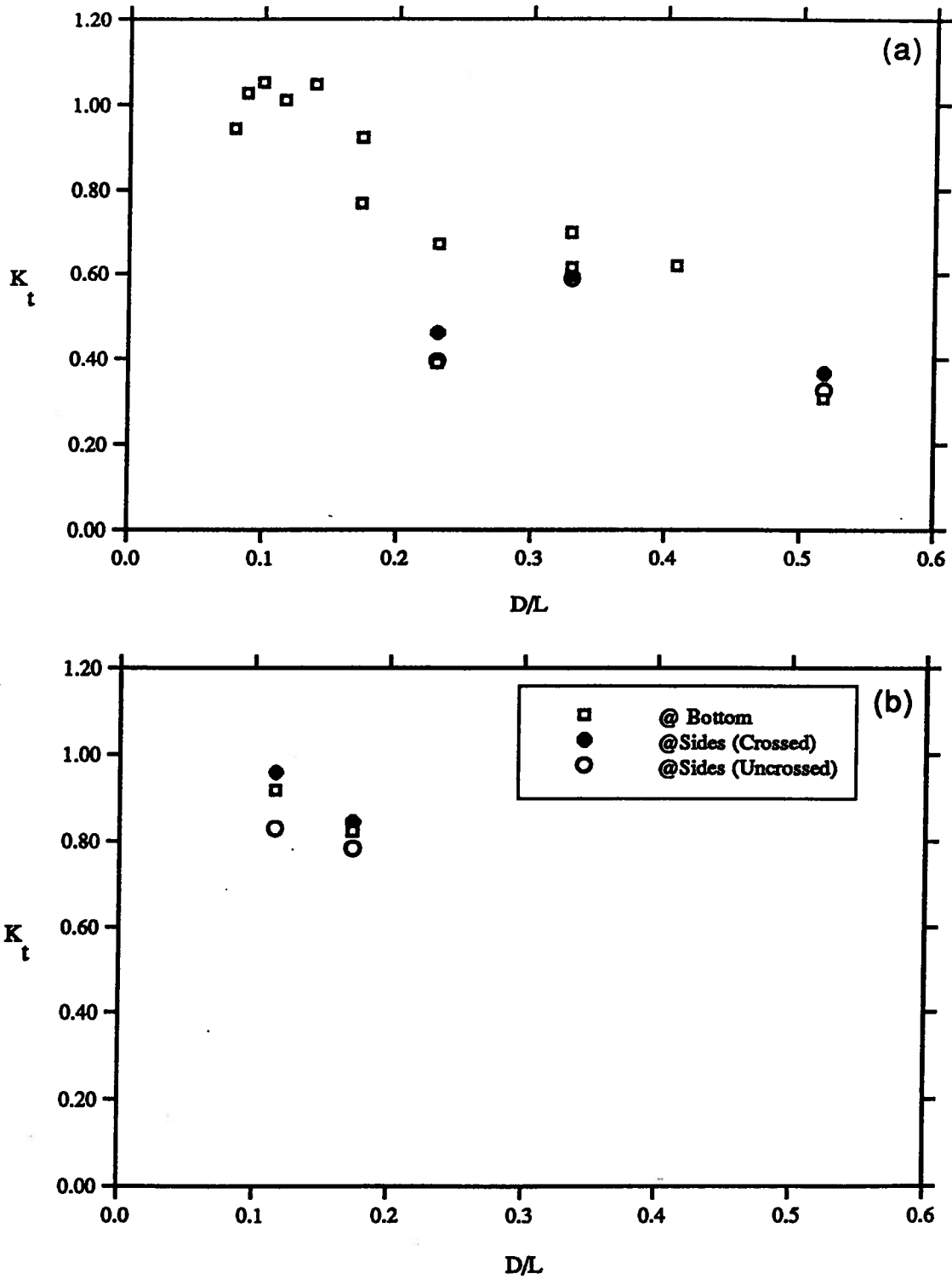


Fig. 5.8 Wave flume test results showing the influence of mooring line attachment points on transmission coefficient. (a) chain mooring lines, (b) nylon mooring lines.

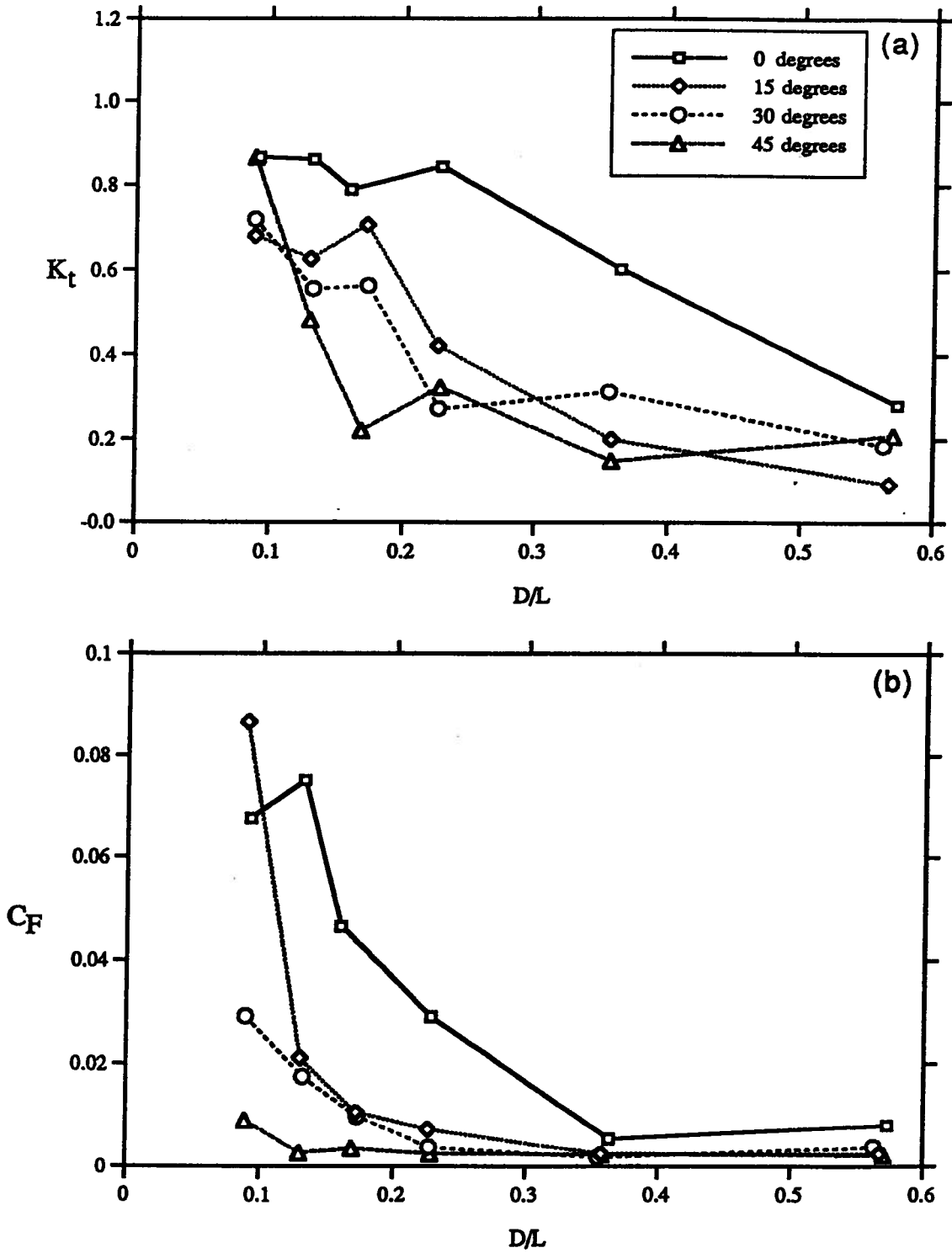


Fig. 5.9 Wave basin test results showing the influence of the angle of wave incidence. (a) transmission coefficient, (b) mooring line forces.

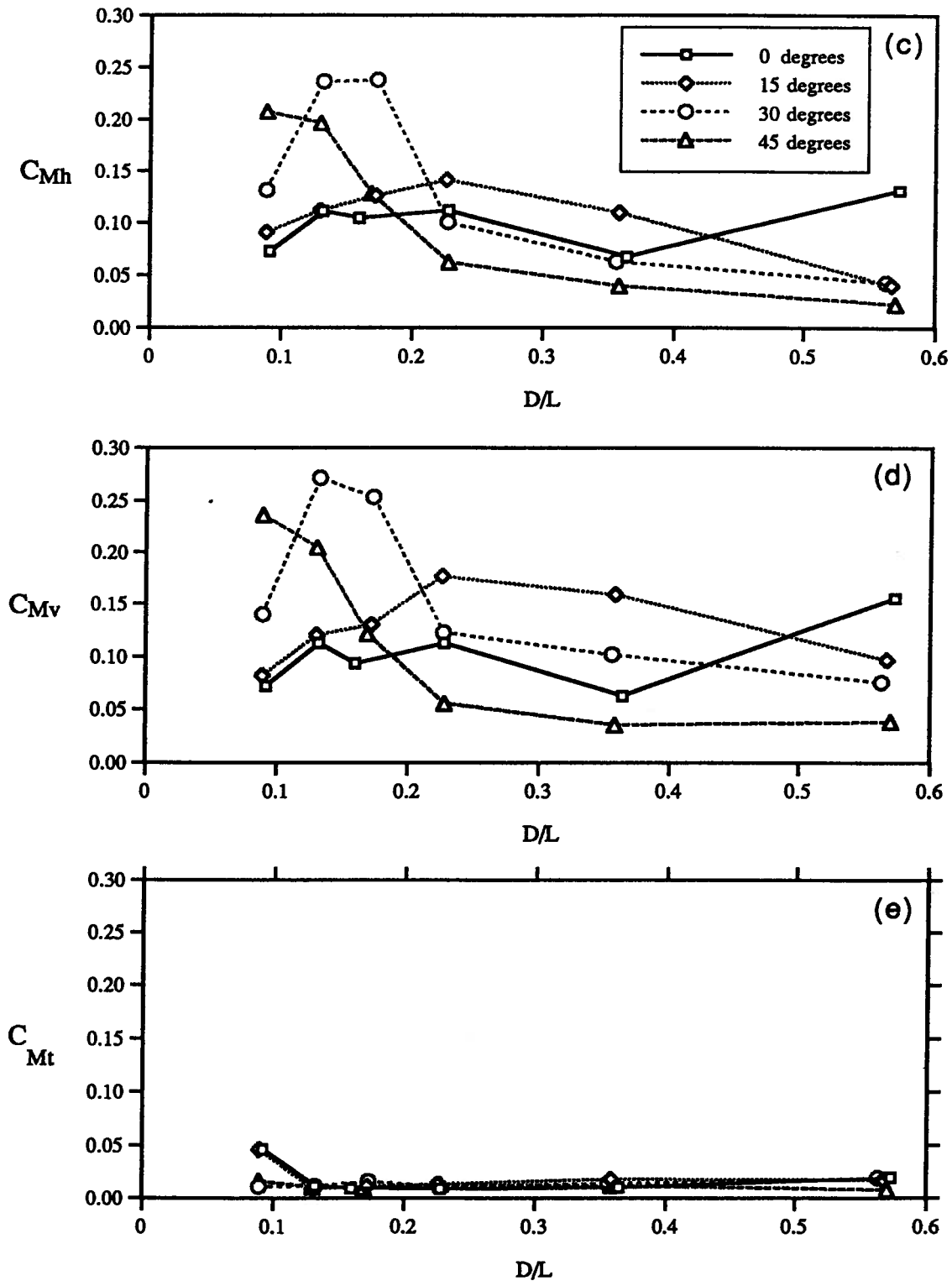


Fig. 5.9 Wave flume test results showing the influence of the angle of wave incidence (cont.). (c) horizontal bending moment, (d) vertical bending moment, (e) torsion.

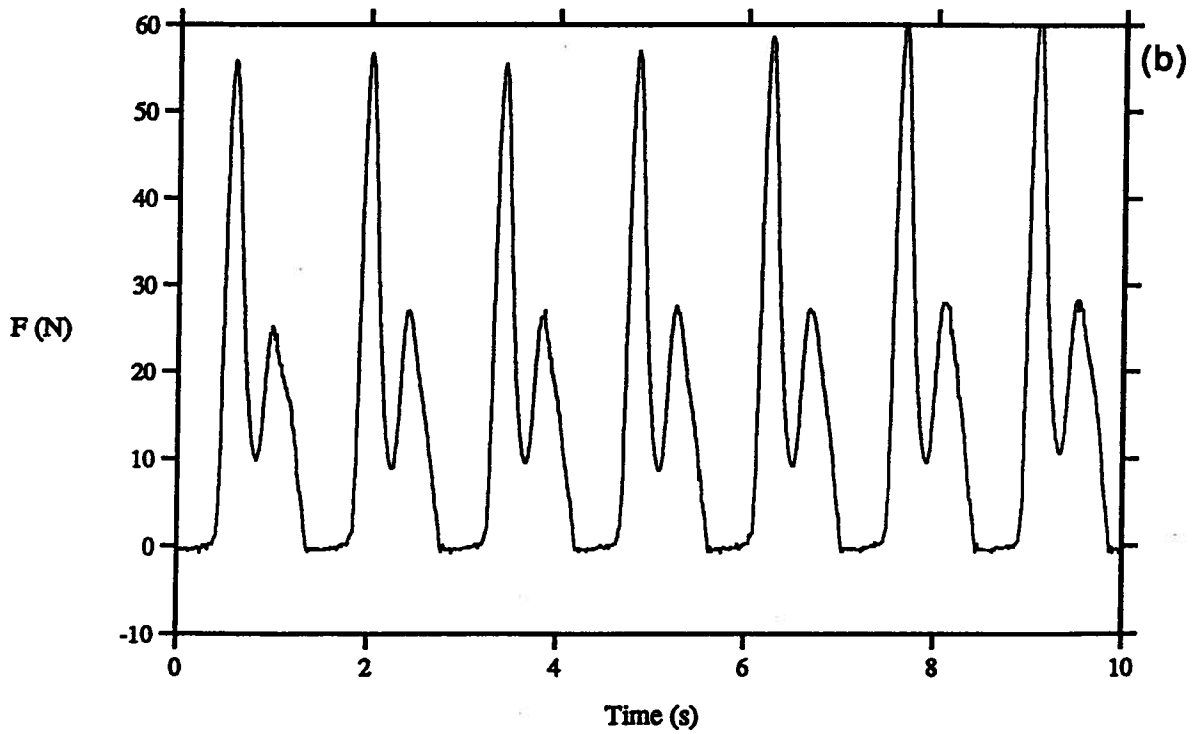
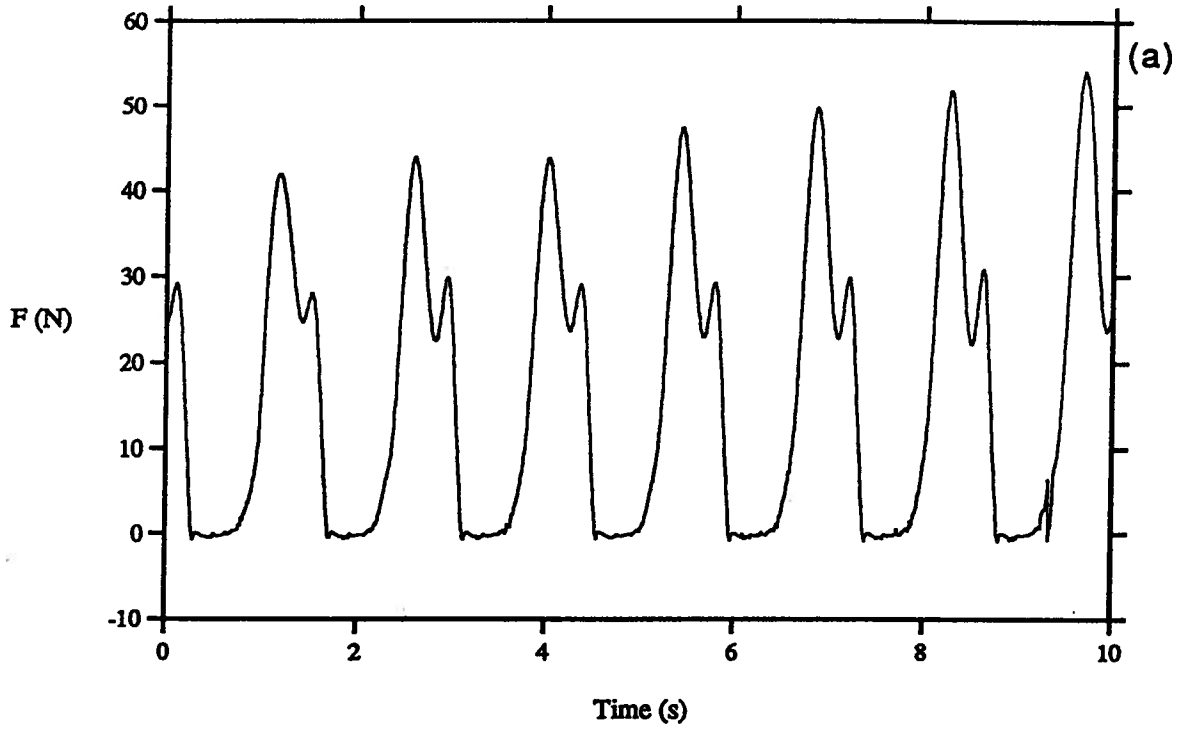


Fig. 5.10 Record of mooring line forces for wave flume test 2.5. (a) forces in upwave line, (b) forces in downwave line.

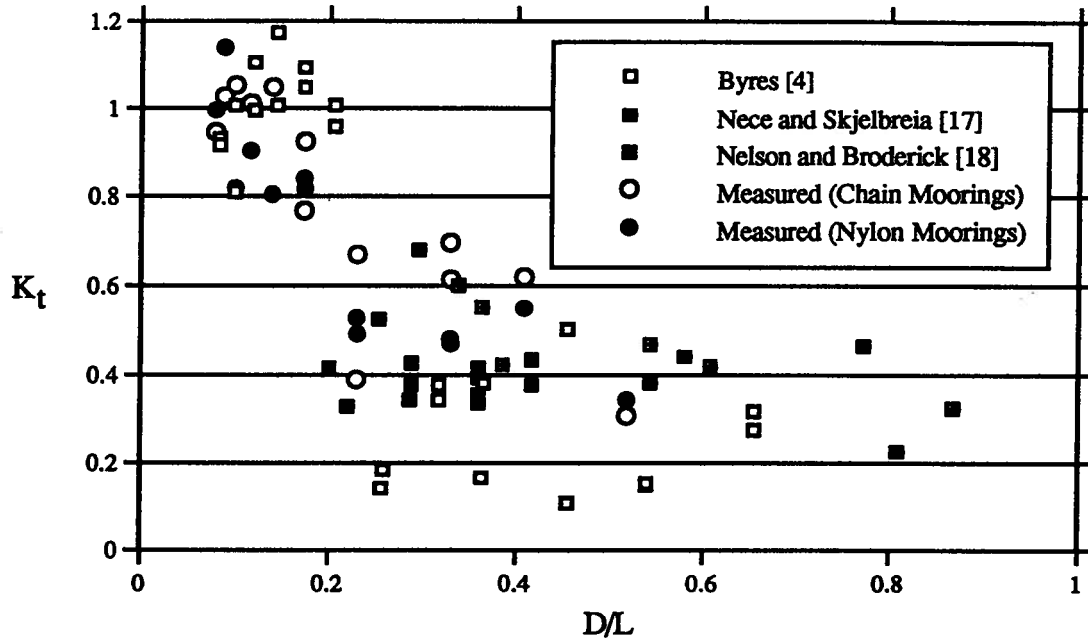


Fig. 5.11 Comparison of transmission coefficients between rectangular and circular caisson breakwaters.

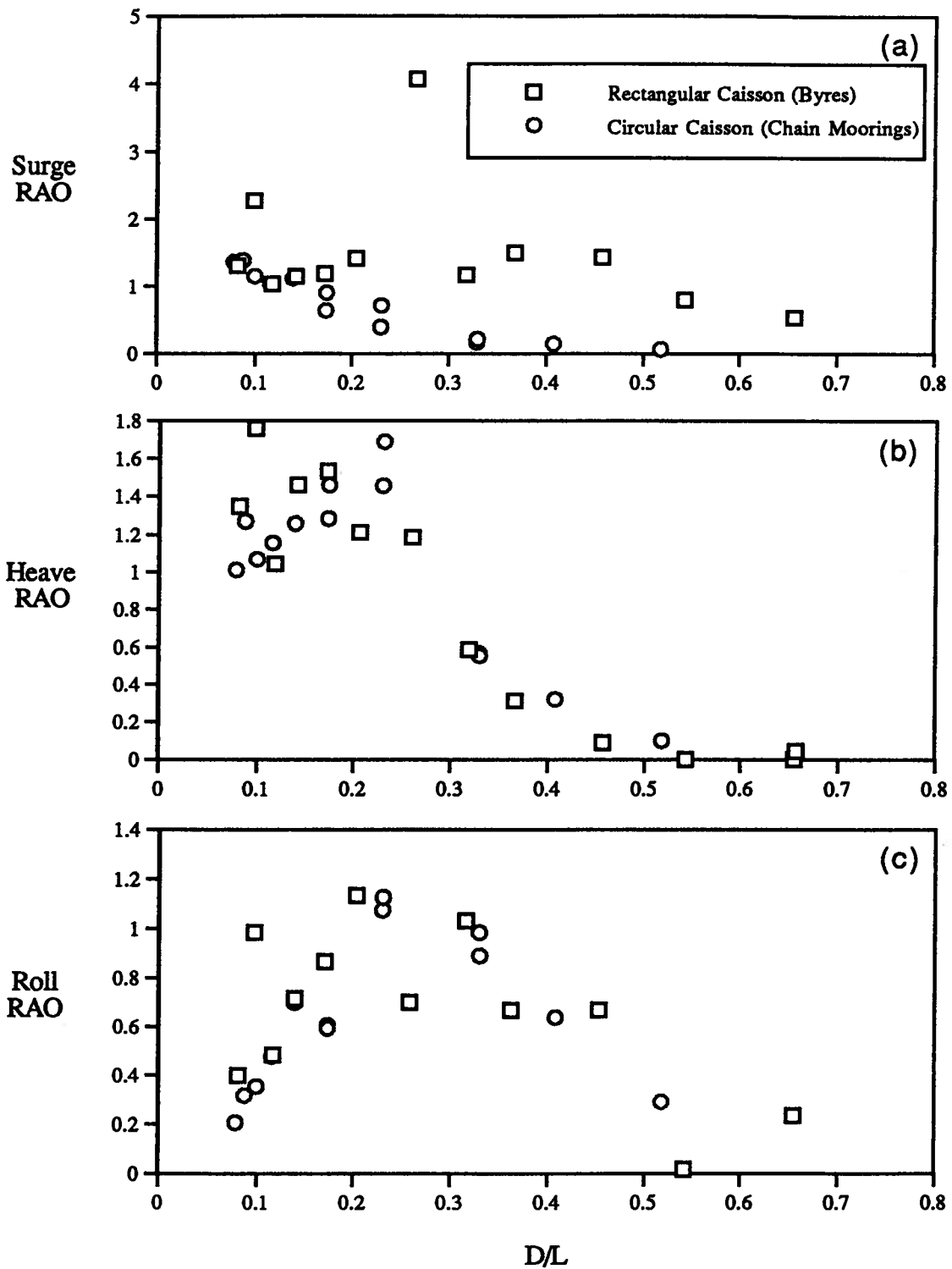


Fig. 5.12 Comparison of observed breakwater motions. (a) surge, (b) heave, and (c) roll.

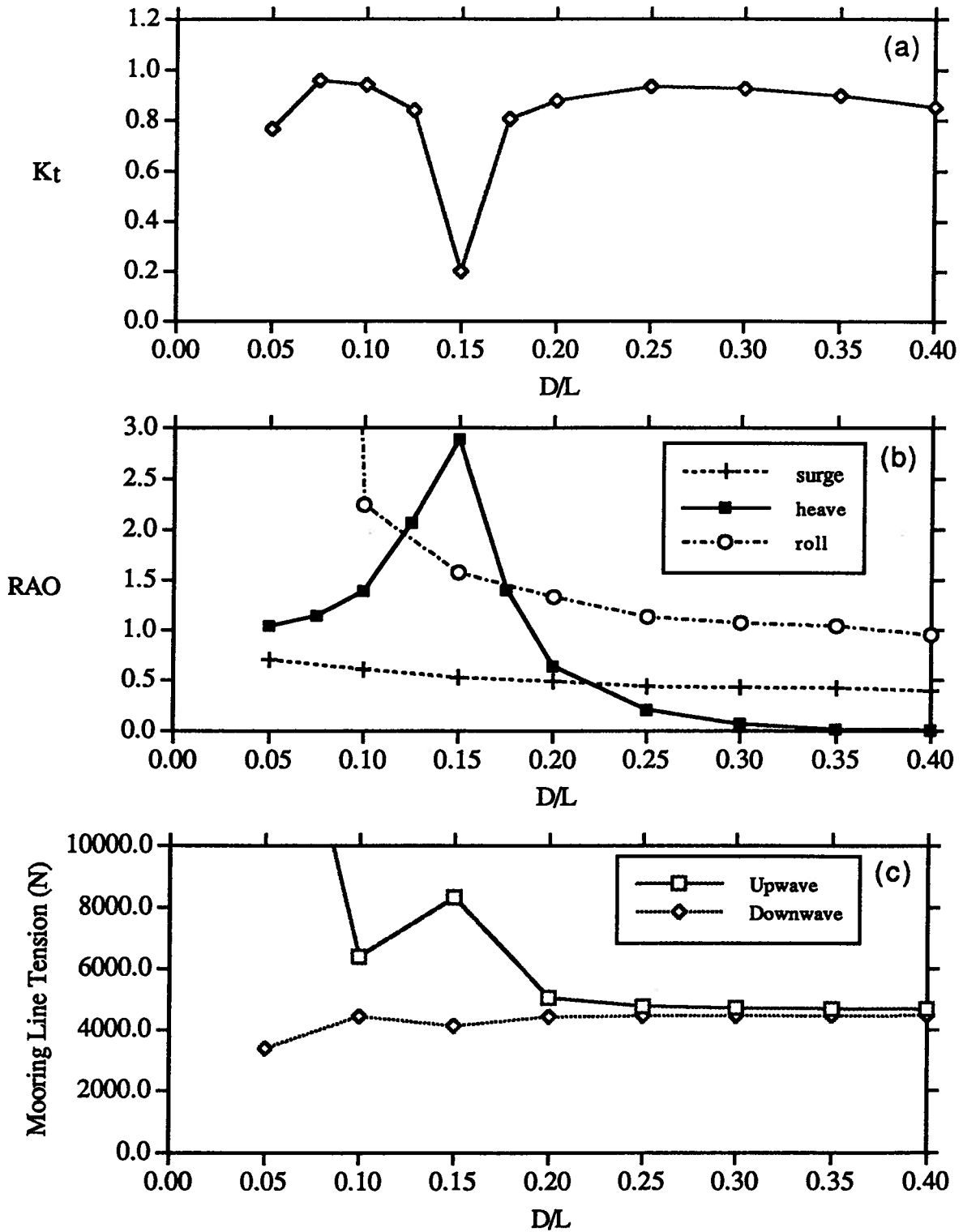


Fig. 6.1 Numerical results for base case with chain mooring lines. (a) transmission coefficient, (b) motion amplitudes, (c) mooring line forces.

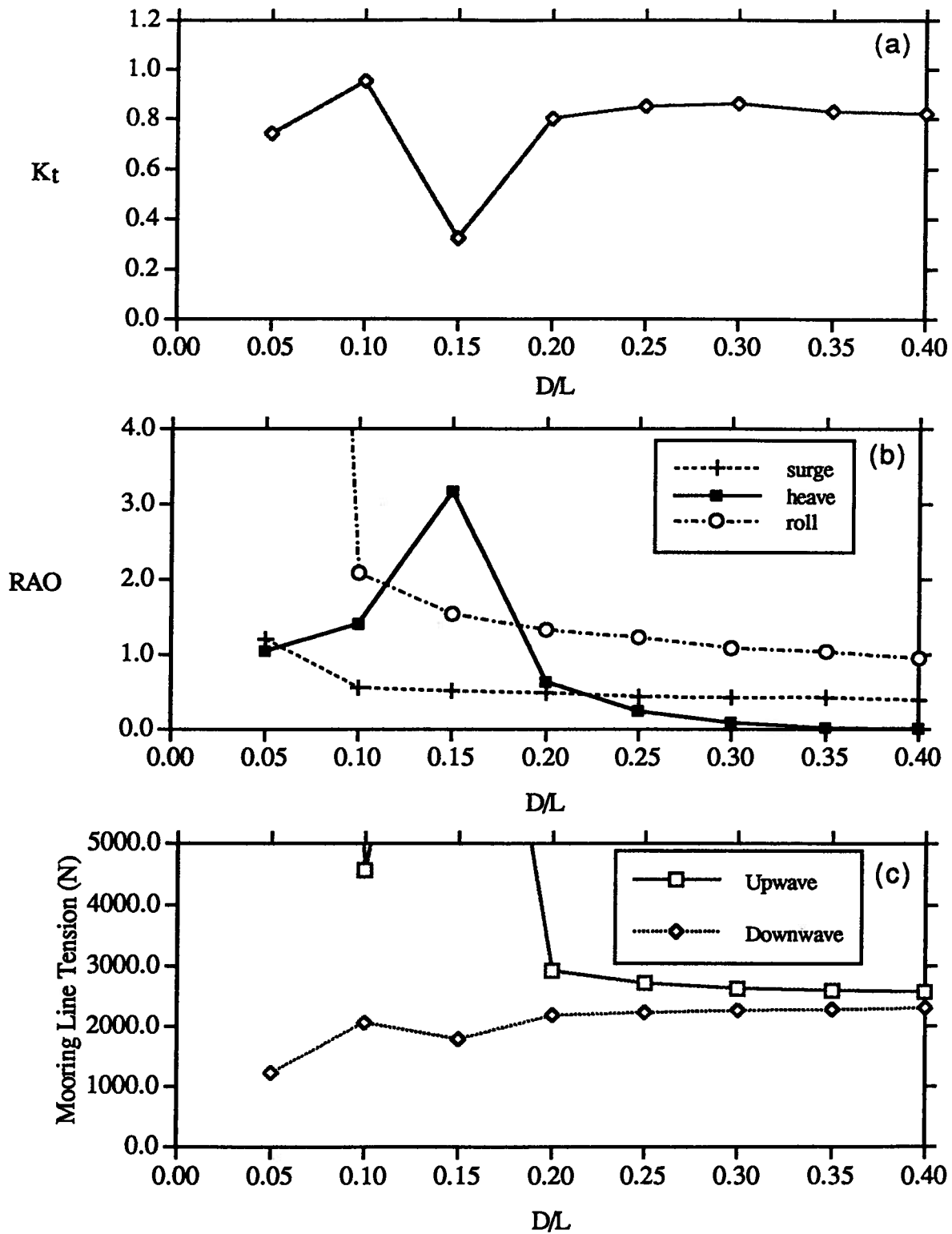


Fig. 6.2 Numerical results for base case with nylon mooring lines. (a) transmission coefficient, (b) motion amplitudes, (c) mooring line forces.

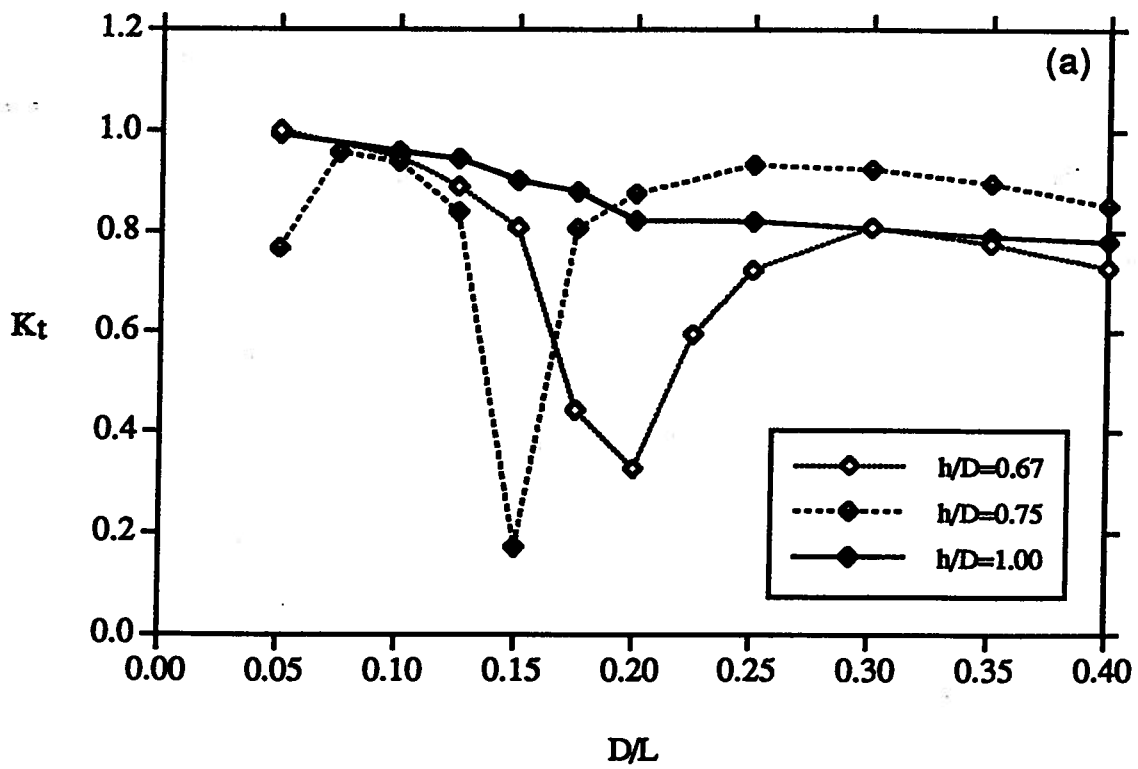


Fig. 6.3 Numerical results showing the influence of relative draft, h/D , for the case of chain mooring lines. (a) transmission coefficient.

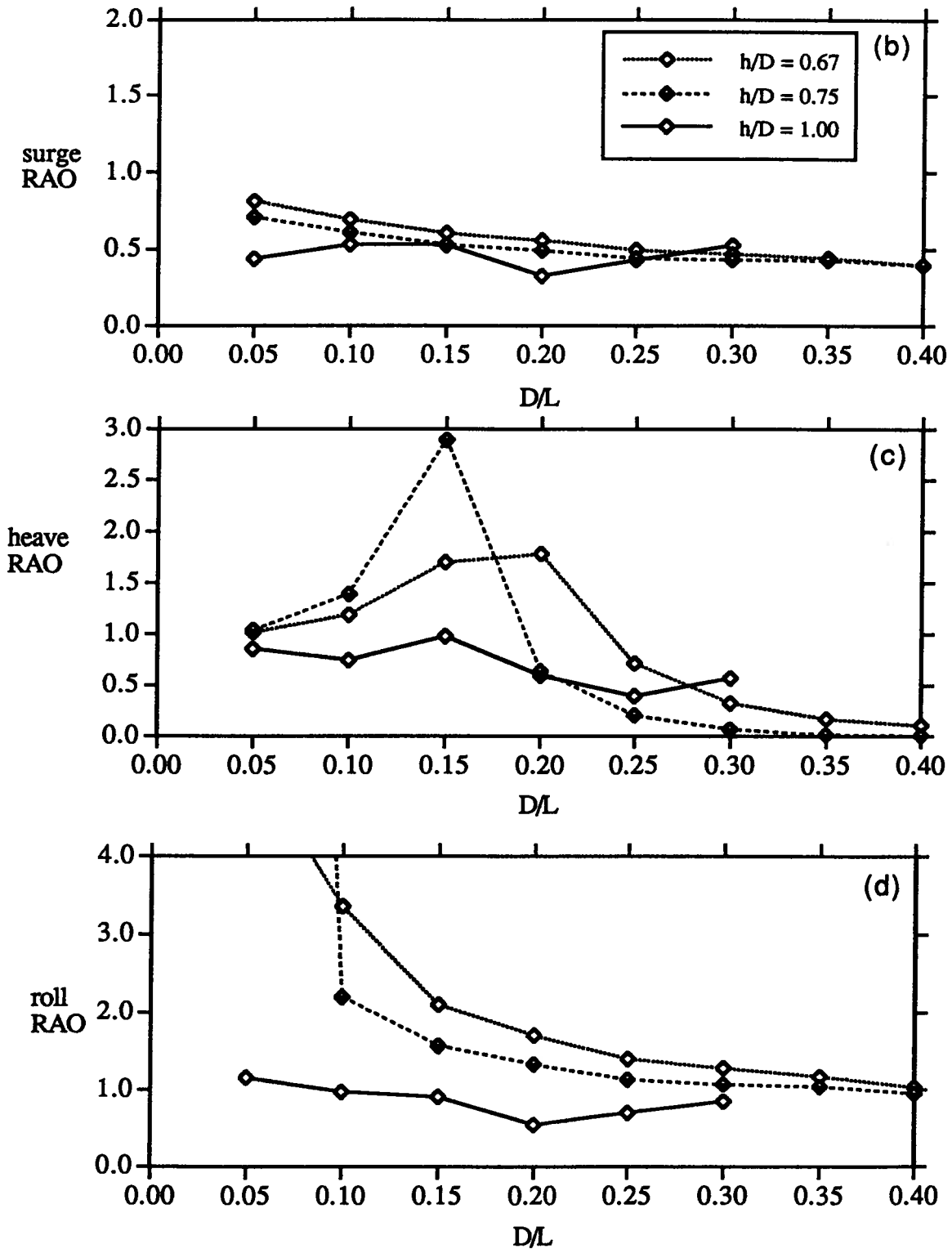


Fig. 6.3 Numerical results showing the influence of relative draft, h/D , for the case of chain mooring lines (cont.). (b) surge RAO, (c) heave RAO, (d) roll RAO.

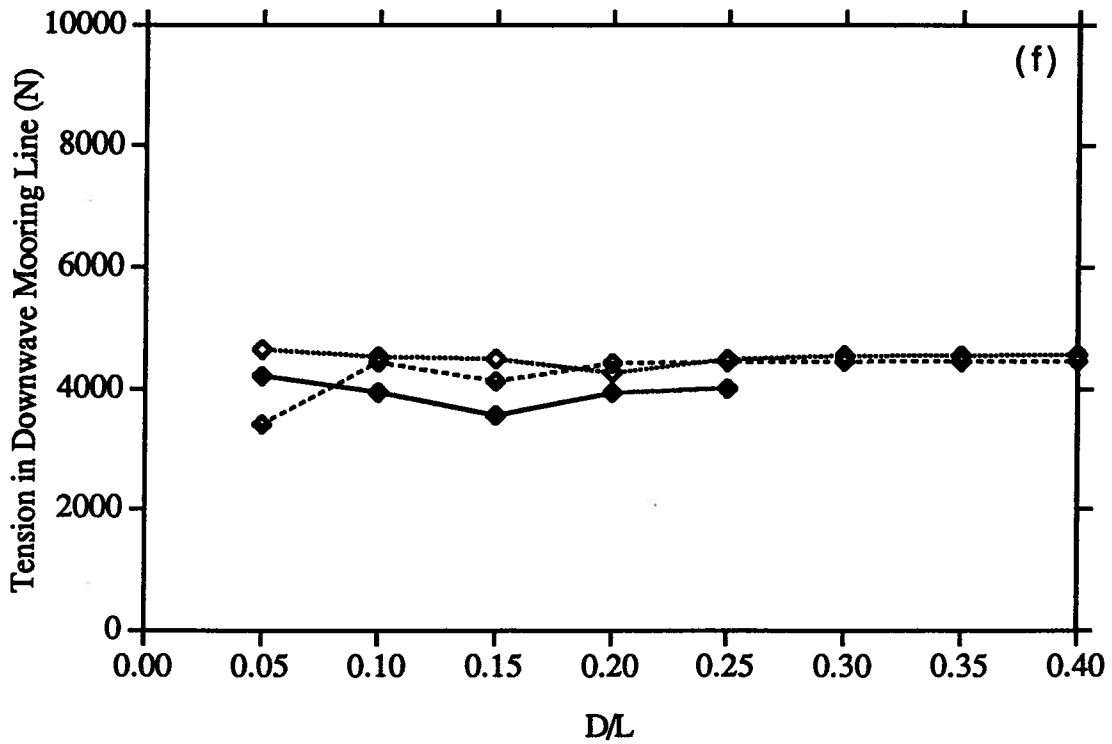
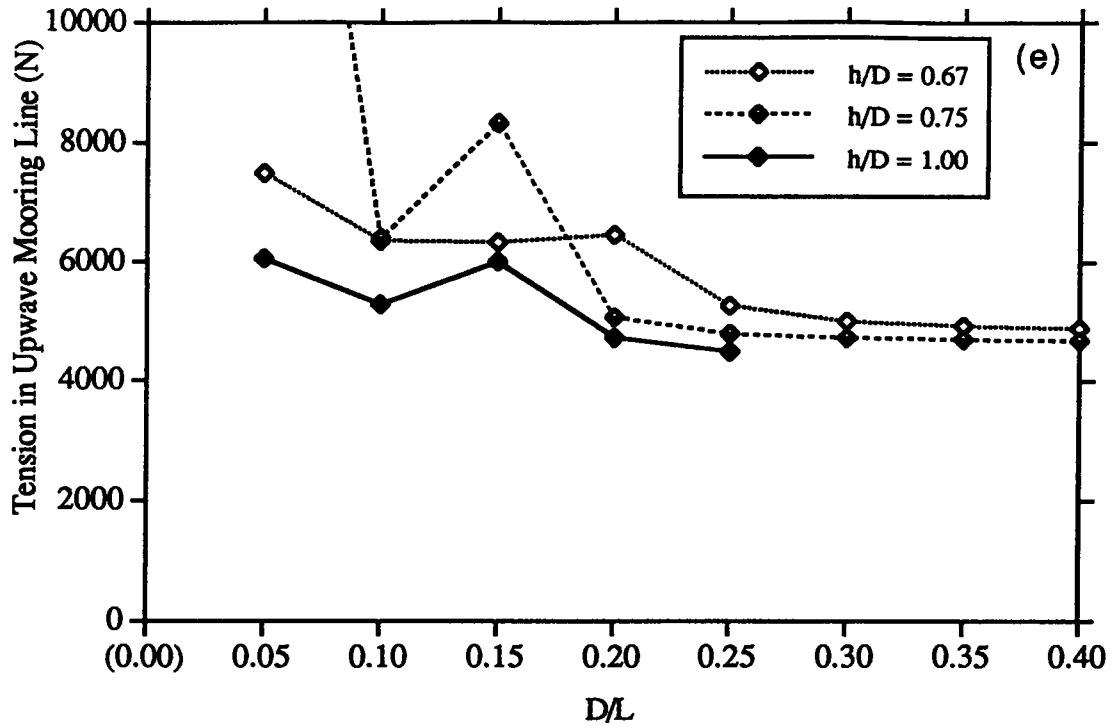


Fig. 6.3 Numerical results showing the influence of relative draft, h/D , for the case of chain mooring lines (cont.). (e) upwave mooring line force, (f) downwave mooring line force.

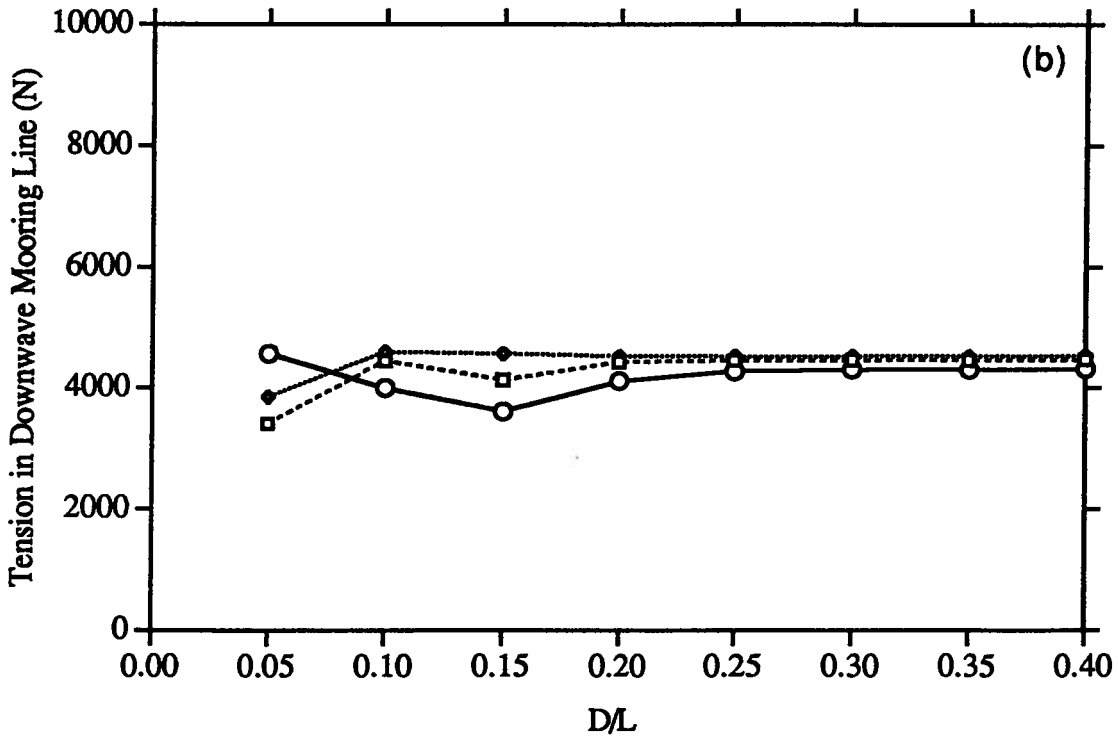
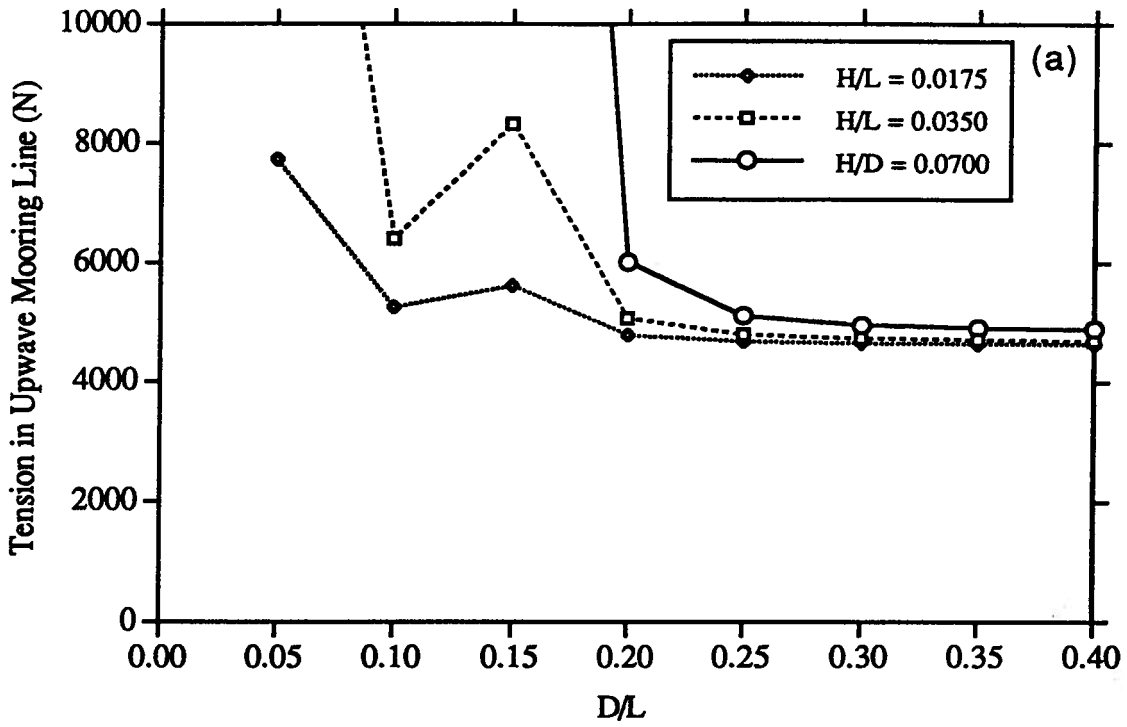


Fig. 6.4 Numerical results showing the influence of wave steepness, H/L , for the case of chain mooring lines. (a) upwave mooring line force, (b) downwave mooring line force.

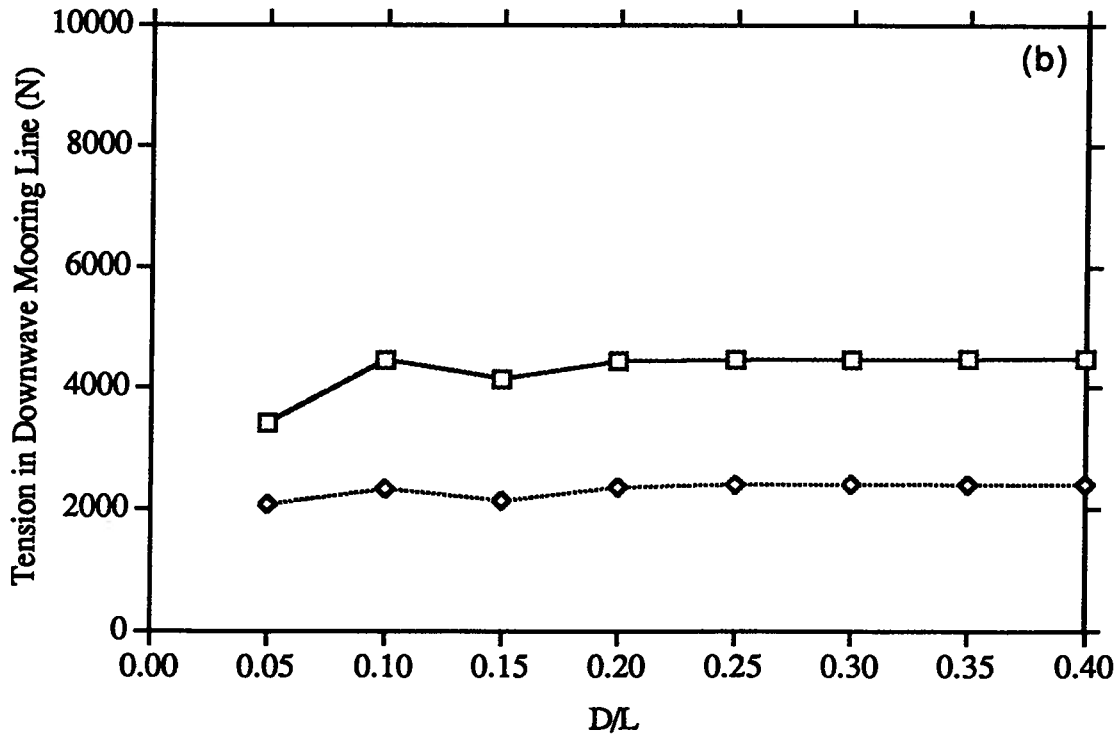
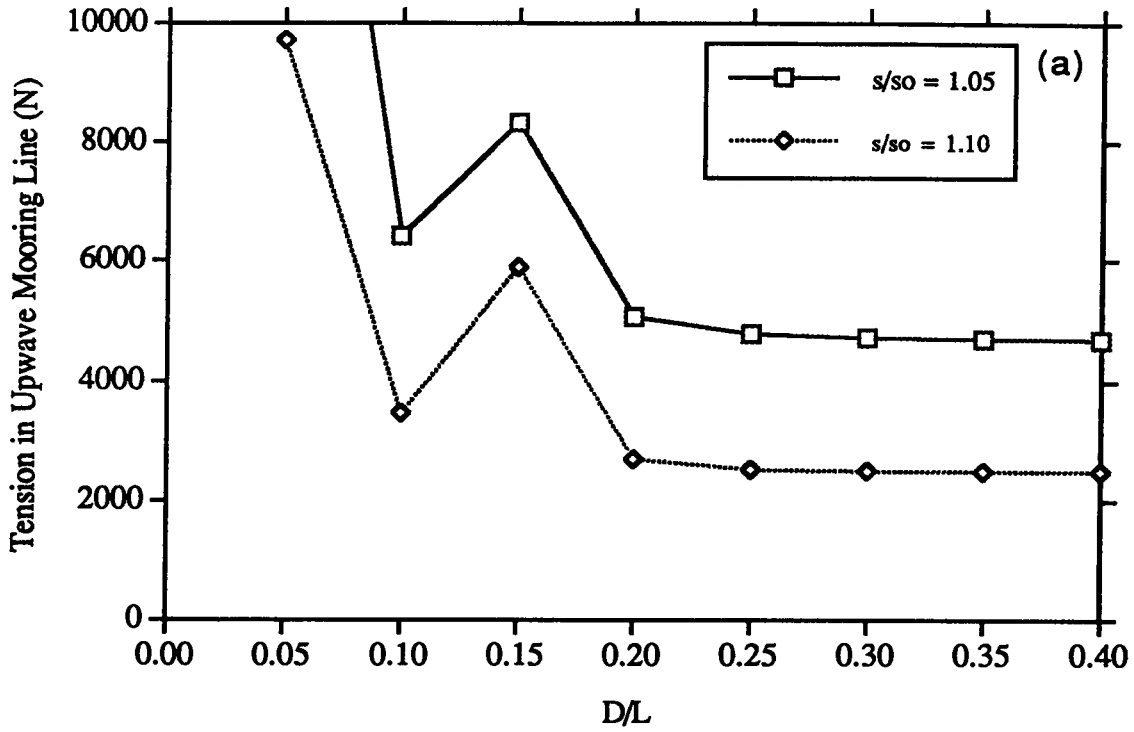


Fig. 6.5 Numerical results showing the influence of wave steepness, H/L , for the case of chain mooring lines. (a) upwave mooring line force, (b) downwave mooring line force.

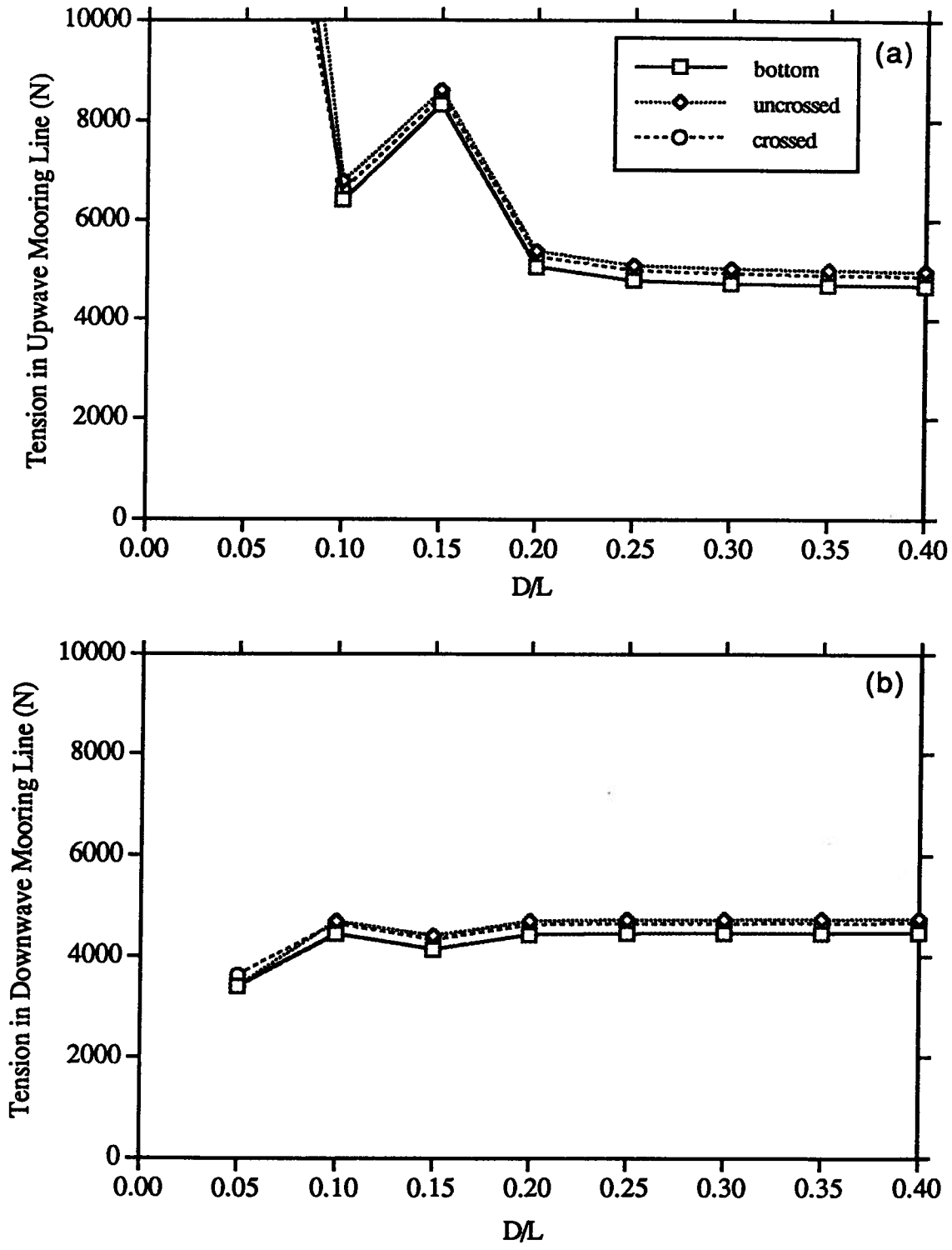


Fig. 6.6 Numerical results showing the influence of mooring line attachment point for the case of chain mooring lines. (a) upwave mooring line force, (b) downwave mooring line force.

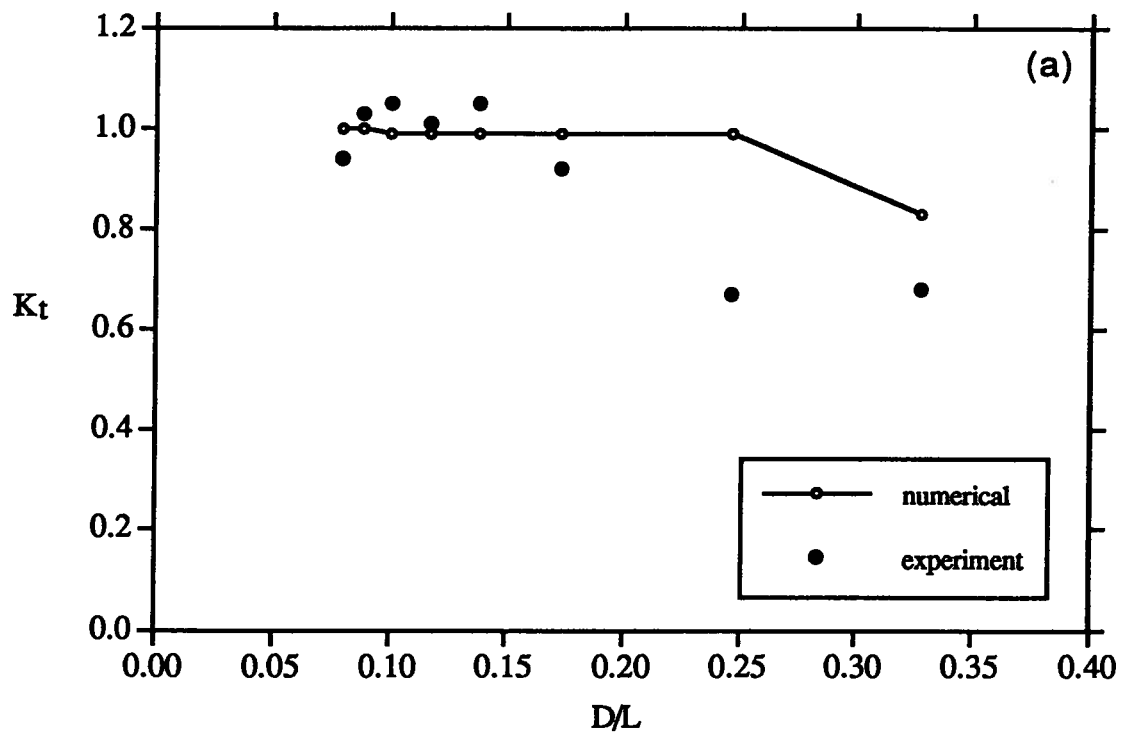


Fig. 6.7 Wave flume test results compared with numerical results for base case with chain. (a) transmission coefficient.

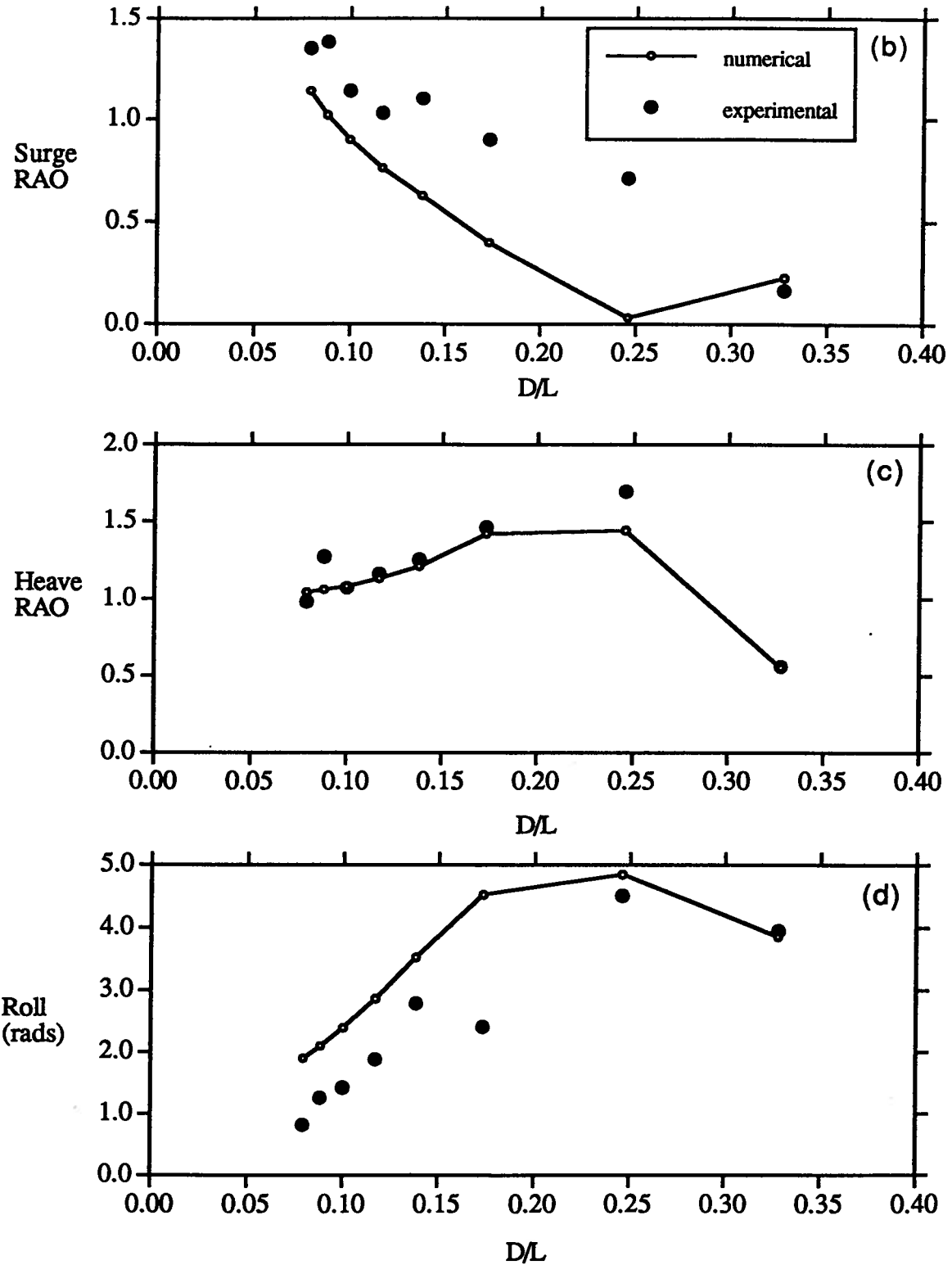


Fig. 6.7 Wave flume test results compared with numerical results for base case with chain (cont.). (b) surge RAO, (c) heave RAO, (d) roll (rads).

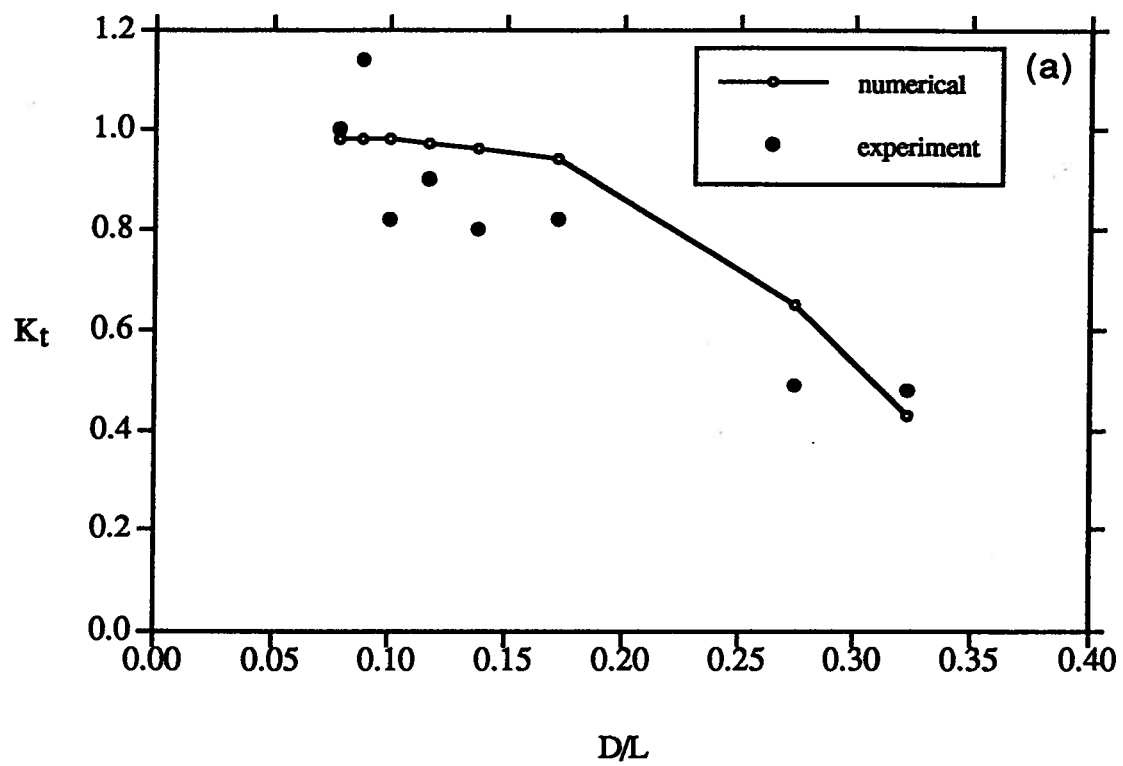


Fig. 6.8 Wave flume test results compared with numerical results for base case with nylon. (a) transmission coefficient.

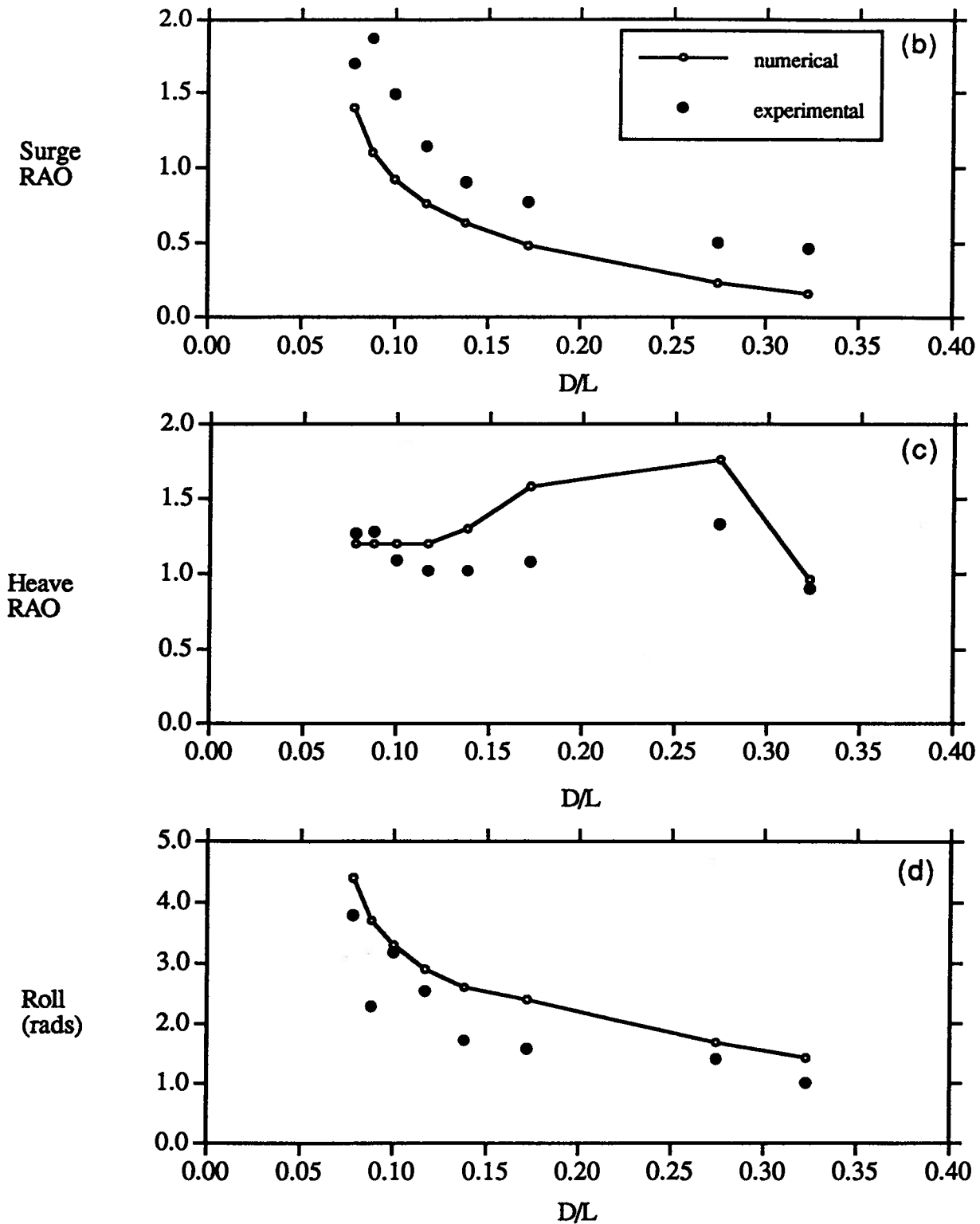


Fig. 6.8 Wave flume test results compared with numerical results for base case with nylon (cont.). (b) surge RAO, (c) heave RAO, (d) roll (rads).